Plains CO_2 Reduction (PCOR) Partnership
Energy & Environmental Research Center (EERC)

BELL CREEK TEST SITE – SIMULATION REPORT

Plains CO_2 Reduction (PCOR) Partnership Phase III
Task 9 – Deliverable D66, Update 6

Originally Submitted: August 2011; Update 1 Submitted: August 2012; Update 2 Submitted: August 2013; Update 3 Submitted: August 2014; Update 4 Submitted: August 2015 Update 5 Submitted: August 2016

Prepared for:

Andrea M. Dunn

National Energy Technology Laboratory
U.S. Department of Energy
626 Cochrans Mill Road
PO Box 10940
Pittsburgh, PA 15236-0940

DOE Cooperative Agreement No. DE-FC26-05NT42592

Prepared by:

Lu Jin
Kyle J. Peterson
Nicholas W. Bosshart
Lawrence J. Pekot
Olarinre Salako
Shaughn A. Burnison
Steven A. Smith
Blaise A.F. Mibeck
Benjamin S. Oster
Jun He
Wesley D. Peck
John A. Hamling
Scott C. Ayash
Charles D. Gorecki

Energy & Environmental Research Center
University of North Dakota
15 North 23rd Street, Stop 9018
Grand Forks, ND 58202-9018

October 2017
Approved

2019-EERC-10-21

EERC DISCLAIMER

LEGAL NOTICE This research report was prepared by the Energy & Environmental Research Center (EERC), an agency of the University of North Dakota, as an account of work sponsored by the U.S. Department of Energy (DOE) National Energy Technology Laboratory (NETL). Because of the research nature of the work performed, neither the EERC nor any of its employees makes any warranty, express or implied, or assumes any legal liability or responsibility for the accuracy, completeness, or usefulness of any information, apparatus, product, or process disclosed or represents that its use would not infringe privately owned rights. Reference herein to any specific commercial product, process, or service by trade name, trademark, manufacturer, or otherwise does not necessarily constitute or imply its endorsement or recommendation by the EERC.

ACKNOWLEDGMENTS

This work was performed under DOE NETL Cooperative Agreement No. DE-FC26-05NT42592. The EERC would like to thank Denbury Resources Inc. (Denbury) for providing necessary data to perform this work. Special thanks go to the members of Denbury's Bell Creek team for their valuable input and fruitful discussions.

DOE DISCLAIMER

This report was prepared as an account of work sponsored by an agency of the United States Government. Neither the United States Government, nor any agency thereof, nor any of their employees, makes any warranty, express or implied, or assumes any legal liability or responsibility for the accuracy, completeness, or usefulness of any information, apparatus, product, or process disclosed, or represents that its use would not infringe privately owned rights. Reference herein to any specific commercial product, process, or service by trade name, trademark, manufacturer, or otherwise does not necessarily constitute or imply its endorsement, recommendation, or favoring by the United States Government or any agency thereof. The views and opinions of authors expressed herein do not necessarily state or reflect those of the United States Government or any agency thereof.

TABLE OF CONTENTS

LIST OF FIGURES

Continued . . .

LIST OF FIGURES (continued)

LIST OF TABLES

BELL CREEK TEST SITE – SIMULATION REPORT

EXECUTIVE SUMMARY

The Plains CO_2 Reduction (PCOR) Partnership is working with Denbury Resources Inc. (Denbury) to evaluate the effectiveness of carbon dioxide (CO_2) enhanced oil recovery (EOR) and study CO_2 storage associated with commercial EOR in the Bell Creek Field. This report discusses modeling and simulation activities conducted since August 2016.

Specific modeling and simulation activities discussed in this report include 1) updating the Bell Creek reference model with 11 new repeat/monitor pulsed-neutron logs (PNLs) and InSAR (interferometric synthetic aperture radar) data, 2) completing the Version 3 (V3) geologic model, 3) developing a dynamic simulation model for the Phase 4 area, 4) conducting production/injection performance analyses for individual wells, 5) conducting history matching and predictive simulations with different injection/production constraints, 6) analyzing possible CO_2 transport and trapping mechanisms in the reservoir, 7) comparing simulation results with 4-D seismic monitoring and predicting long-term CO_2 trapping behavior, and 8) determining CO_2 relative permeability hysteresis curves and integrating them into a five-spot model.

A full-field V3 geologic model was completed based on a revised depositional interpretation,[1] enabled by the integration of 3-D and 4-D seismic data, PNLs, legacy well logs, and core analysis. The model was developed by 1) partitioning the reservoir into seven areas for focused facies distributions, each area having distinct geologic characteristics; 2) determining the vertical and lateral facies associations within each of these areas through interpretation of well logs and seismic attributes; 3) creating facies logs for wells to serve as control points; 4) creating training images from interpreted facies associations; 5) using multiple point statistics to interpolate the distribution of facies in interwell areas, drawing upon measurable relationships provided by the training images while honoring control points; and 6) conditioning petrophysical properties (porosity, permeability, and fluid saturations) to the facies model using variogram-based geostatistical methods. These efforts were conducted to enable better simulation history matching and increased accuracy of predictive forecasts.

A simulation model of the Phase 4 area was created from the V3 geologic model. A history match was achieved for 49 years of field records, including primary production, waterflooding, and CO_2 EOR stages. Individual-well production performance in the Phase 4 development area was analyzed to evaluate boundary conditions and water saturation in the reservoir. Water

[1] Jin, L., Bosshart, N.W., Oster, B.S., Hawthorne, S.B., Peterson, K.J., Burton-Kelly, M.E., Feole, I.K., Jiang, T., Pekot, L.J., Peck, W.D., Ayash, S.C., and Gorecki, C.D., 2016, Bell Creek test site – simulation report: Plains CO_2 Reduction (PCOR) Partnership Phase III draft Task 9 – Deliverable D66 (Update 5) for U.S. Department of Energy National Energy Technology Laboratory Cooperative Agreement No. DE-FC26-05NT42592, Grand Forks, North Dakota, Energy & Environmental Research Center, August.

alternating gas (WAG) and continuous CO_2 injection (CCI) predictive simulations with different pressure settings were conducted for the Phase 4 area to assess oil recovery and associated CO_2 storage performance. Compared to development Phases 1 and 2, Phase 4 has a higher ratio of production wells to injection wells (nearly a 1:1 ratio in Phases 1 and 2 versus 1.8:1 in Phase 4) and a historically lower average CO_2 injection rate per injection well (54.8 Mscf/day/injector in Phases 1 and 2 versus 24.6 Mscf/day/injector in Phase 4). The production/injection activities of this development phase have resulted in a lower predicted sweep efficiency and oil recovery factor (13%–14% OOIP [original oil in place] in Phases 1 and 2 versus 6.5%–7% OOIP in Phase 4) when compared to prior development phases.

Steady-state relative permeability tests were performed using a clean sandstone core sample collected from Well 05-06 OW to derive gas-phase relative permeability curves. A hysteretic effect was identified from the drainage and imbibition CO_2 relative permeability curves. The curves were integrated in simulation models, and simulations were conducted to investigate the effects of CO_2-trapping mechanisms, including residual, solubility, and structural/stratigraphic trapping. The effectiveness of residual and solubility trapping mechanisms is continually changing because WAG injection causes fluid saturations within the reservoir to change continually, ultimately affecting associated CO_2 storage. The effects of both structural and stratigraphic trapping are widespread in the Bell Creek Field because of the complex geologic characteristics of the reservoir. A five-spot model and a model of Phases 1 and 2 combined were used to investigate the effects of these trapping mechanisms on CO_2 EOR and associated storage performance.

Simulation results from a five-spot model, taking into account Bell Creek fluid properties and reservoir conditions, predicted that residual trapping may not have a significant effect on oil recovery factor, but it may yield increased associated CO_2 storage up to 20% with an assumed residual CO_2 saturation of 0.3. Solubility trapping also plays an important role in associated CO_2 storage performance. The simulation results suggest CO_2 solubility in Bell Creek oil is much greater ($\geq$5 times) than in water.

A series of seismic monitoring activities have been conducted to monitor CO_2 saturation and pressure changes. 4-D seismic amplitude differencing identified no evidence of out-of-zone CO_2 migration, supporting effective containment of injected CO_2 within the reservoir. Time-lapse seismic analysis enabled detailed interpretation of fluid and pressure communication pathways in the reservoir. Amplitude difference maps were used to calibrate the geologic and simulation models to improve long-term performance forecasts for the injected CO_2 in development Phases 1 and 2.[2] Based on predictive reservoir simulation, 1000 years after injection operations cease, all of the injected CO_2 is expected to remain in the reservoir.

[2] Salako, O., Livers, A.J., Burnison, S.A., Hamling, J.A., Wildgust, N., Gorecki, C.D., Glazewski, K.A., and Heebink, L.V., 2017, Analysis of expanded seismic campaign: Plains CO_2 Reduction Partnership Phase III Task 9 – Deliverable D104 for U.S. Department of Energy National Energy Technology Laboratory Cooperative Agreement No. DE-FC26-05NT42592, EERC Publication EERC-10-09, Grand Forks, North Dakota, Energy & Environmental Research Center, June.

BELL CREEK TEST SITE – SIMULATION REPORT

INTRODUCTION

The Bell Creek project is a collaboration between the Plains CO_2 Reduction (PCOR) Partnership and Denbury Onshore, LLC (Denbury) to study incidental CO_2 storage associated with a Denbury-operated commercial enhanced oil recovery (EOR) project. The PCOR Partnership is conducting site characterization; modeling and predictive simulation; PCOR Partnership project-focused risk assessment; and monitoring, verification, and accounting (MVA) to study the interrelationship of commercial CO_2 EOR operations and incidental CO_2 storage and to evaluate how various EOR injection strategies affect associated storage.

The Bell Creek Field in the northeastern Powder River Basin (PRB) (Figure 1) has been producing oil from the Muddy Formation for nearly 50 years. Denbury's employment of the tertiary technique of CO_2 EOR is progressing through nine phases of development (areas within the Bell Creek Field; Figure 2). The CO_2 used in Bell Creek is sourced from the ConocoPhillips-operated Lost Cabin natural gas-processing facility, which processes gas from the Madden Field in the Wind River Basin of Wyoming, and the ExxonMobil-operated Shute Creek gas-processing facility, which processes gas from the LaBarge Field in the Green River Basin of Wyoming. Denbury built and operates compression and recycle facilities and a 374-kilometer/232-mile-long pipeline (known as the Greencore CO_2 pipeline), which connects the Lost Cabin facility with the Bell Creek oil field. The Greencore CO_2 pipeline interconnects with the Anadarko CO_2 pipeline originating at the Shute Creek Facility near LaBarge, Wyoming. Together, the Greencore and Anadarko CO_2 pipelines connect multiple regional CO_2 sources with several regional EOR fields. From May 2013 to June 2017, approximately 3.94 million tons of CO_2 has been delivered to Bell Creek Field for EOR operations.

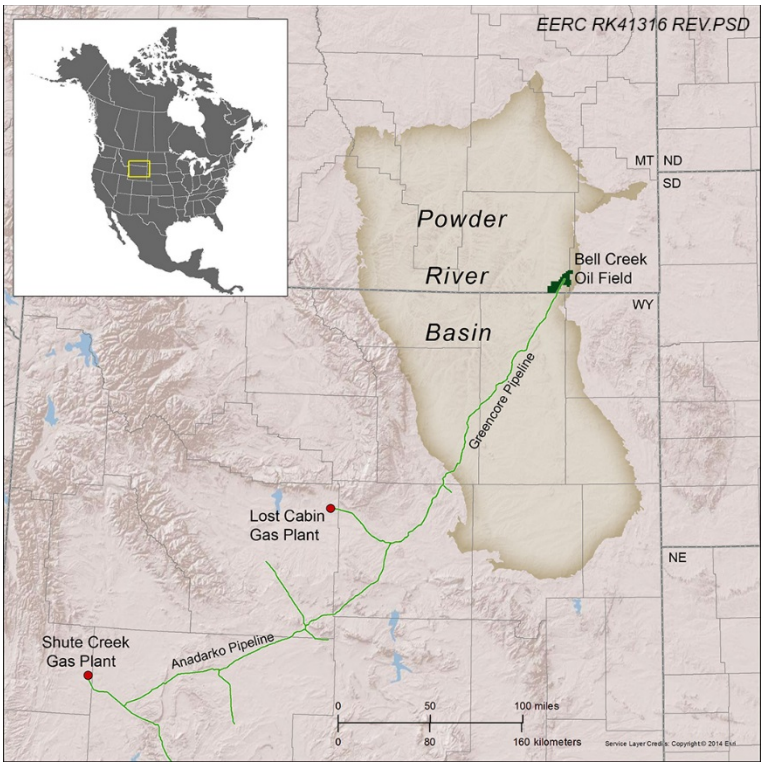

Figure 1. Map of the Bell Creek Field in relation to the PRB and the pipeline from the Lost Cabin and Shute Creek gas plants (Burnison and others, 2017).

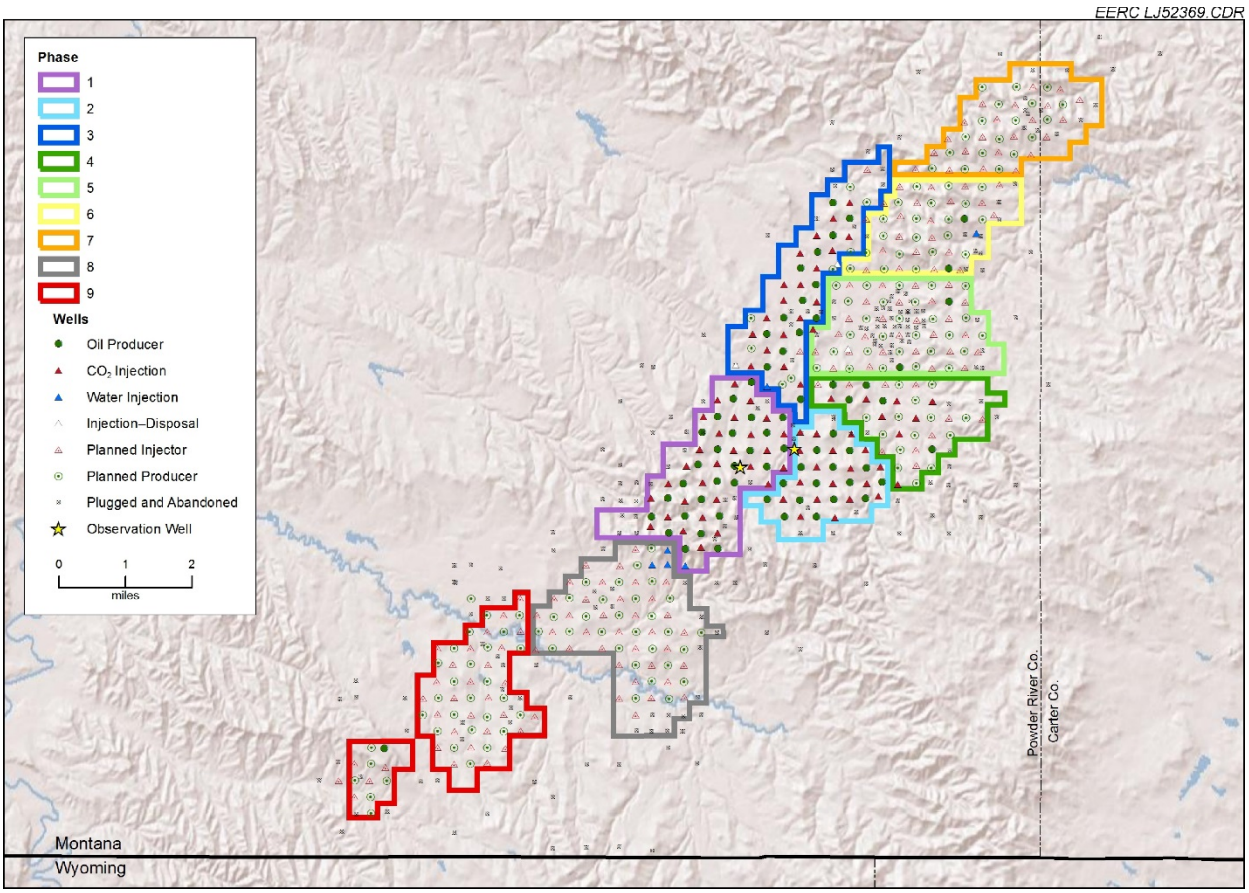

Figure 2. The Bell Creek Field showing the nine CO_2 EOR development phase areas of the Bell Creek Field (Jin and others, 2016a).

PURPOSE

Interactive modeling and simulation activities improve the understanding of EOR and associated storage performance. Modeling and simulation activities are among four main components being employed by the PCOR Partnership as part of an adaptive management approach (AMA) (Ayash and others, 2017; Figure 3) for monitoring, forecasting, and informing operations for EOR and associated storage performance.

The EERC's geocellular modeling of the subsurface enables increased understanding and prediction of the behavior of injected CO_2 and reservoir fluids over the injection and postinjection periods. History matching is performed on a numerically tuned dynamic reservoir model (constructed from a static geologic model) for validation and increased accuracy in predictive simulations. This history-matching process is followed by the simulation of multiple scenarios pertaining to production/pressure response and fluid migration within the reservoir. Additionally, these simulation activities provide a means to evaluate the sweep and storage efficiency and the applicability of various monitoring activities related to CO_2 injection.

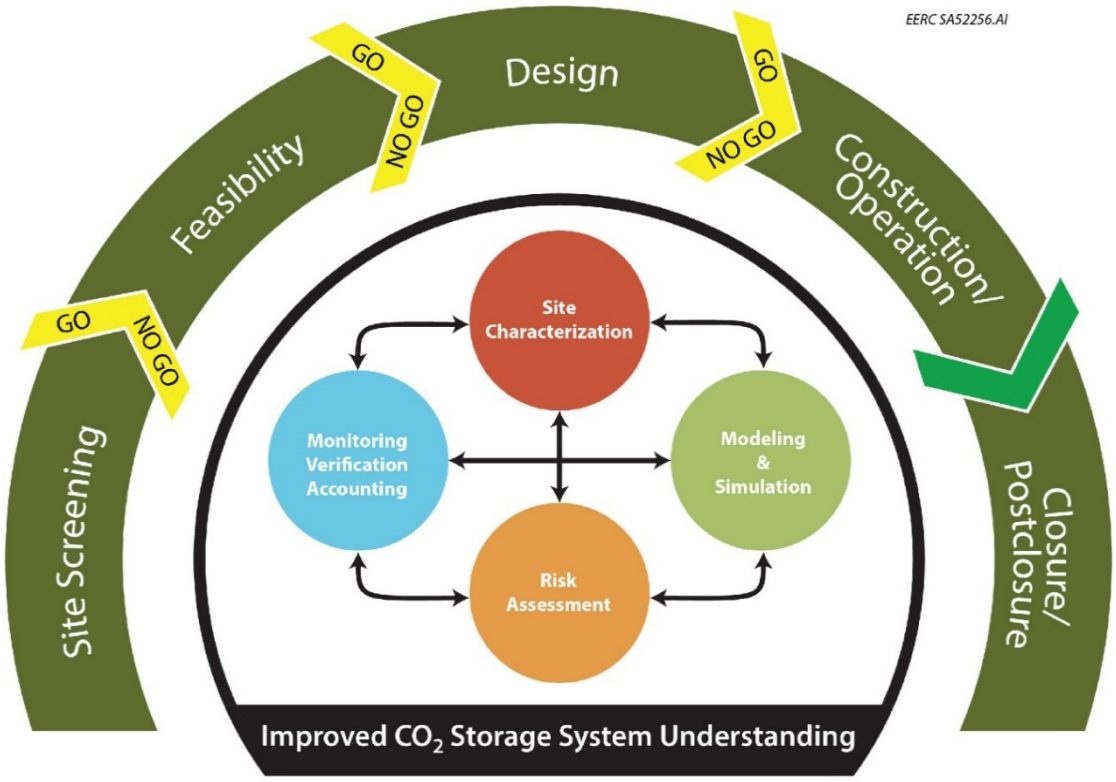

Figure 3. PCOR Partnership AMA for CO_2 storage project development (Ayash and others, 2017).

Geologic characterization, geocellular modeling, and numerical simulation are essential inputs for MVA techniques. This approach lays the foundation for a project's site-specific, goal-oriented MVA plan to effectively monitor the behavior of injected CO_2 and reservoir fluids as the project progresses. Predictive simulations assist with targeted deployment of MVA data acquisitions at optimal surface and subsurface locations in relevant temporal context for increased (time and cost) efficiency in EOR operations and associated storage of CO_2. The results and experience gained at the Bell Creek oil field will provide insight and knowledge that can be directly and readily applied to similar projects within the PCOR Partnership region and throughout the world (Steadman and others, 2011; Hamling and others, 2013).

The Bell Creek Field is currently in the injection/operation phase, where most of the PCOR Partnership's monitoring efforts are part of the MVA plan to demonstrate techniques and to develop viable monitoring strategies for injected CO_2. This includes the ability to account for CO_2 during EOR operations (i.e., injected, recycled, and incidentally stored), improved abilities to evaluate and forecast production performance, and the ability to verify that the incidentally stored CO_2 remains in the injection zone after EOR operations have ended. These monitoring efforts at the Bell Creek are conducted through modeling simulation activities, as well as intermittent acquisition of key monitoring data sets (such as seismic surveys and pulsed-neutron well logging [PNL] campaigns).

BACKGROUND

Following the adaptive management philosophy developed by the PCOR Partnership (Figure 3), Bell Creek modeling and simulation activities have been updated annually based on available site characterization data and field injection/production records to improve the MVA plan. All elements have been integrated into an iterative process to produce meaningful results for large-scale EOR projects and the associated storage of CO_2. To date, six versions of the modeling and simulation reports have been produced to cover the highlights of activities since 2011. A brief description of each report follows:

- **Bell Creek Test Site Simulation Report: PCOR Partnership Phase III Task 9 Deliverable D66, 2011, approved (Pu and others, 2011)**
  The Version 1 (V1) 3-D geologic model was developed based on the available site characterization data and focused on the Phase 1 area. A generalized lithology and stratigraphic framework in the Bell Creek oil field was interpreted that includes four lithofacies in the Muddy interval: Springen Ranch shale, Coastal Plain sand, Bell Creek sand, and Rozet shale. The structure and properties were populated based on the 154 wells within the study boundary. Available data were analyzed, interpreted, and incorporated into the 3-D static geologic and dynamic reservoir models to represent geologic and reservoir properties to provide a solid groundwork for simulation activities.

  The PVT (pressure, volume, and temperature) data from three fluid samples were analyzed and lumped together as seven components that matched the laboratory data. The results indicate that miscibility for oil samples can be achieved at the designed flooding pressure (2500–3000 psi) because the measured minimum miscibility pressure (MMP) is around 1430 psi using both slim-tube and vanishing interfacial tension tests.

- **Bell Creek Test Site Simulation Report: PCOR Partnership Phase III Task 9 Deliverable D66, 2012, approved (Saini and others, 2012)**
  A 1-D compositional simulation of experimental slim-tube tests was performed to ensure the accuracy of simulation results using a seven-component fluid model applied in the Peng–Robinson (PR) equation of state (EOS). MMP estimated from slim-tube simulation agrees with the experimental results.

  The constructed geologic model was validated through history matchng of oil rate, water cut, and gas/oil ratio (GOR) and was used for various predictive simulation scenarios for the Phase 1 area. Twelve cases, based on a five-spot, a quarter five-spot, and the entire Phase 1 pattern, were designed to address associated CO_2 storage and CO_2 breakthrough at monitoring well 05-06 OW (observation well) from a CO_2 water alternating gas (WAG) injection scenario.

- **Bell Creek Test Site Simulation Report: PCOR Partnership Phase III Task 9 Deliverable D66, 2013, approved (Braunberger and others, 2013)**
  A revised and more detailed 3-D static geocellular model of the Bell Creek oil field area (V2 model) was constructed using pertinent reservoir characterization data gathered in an extensive literature review and existing core analysis work for the entire Bell Creek oil

field and surrounding area. Seven hundred forty-eight wells with wireline logs and many with core data were analyzed, interpreted, and incorporated into the 3-D static geocellular and dynamic reservoir models to represent stratigraphy, petrophysical facies, and reservoir properties for simulation activities.

The seven-component PR EOS model was tuned and matched to both original oil and depleted oil from slim-tube test and laboratory data. This produced an acceptable EOS for both matching historic production/injection and for performing predictive simulations.

The Phase 1 area and immediately adjacent area (minor portions of Phases 2, 3, and 8) were clipped from the V2 model and matched to 46 years of production and injection records to validate the model and to get an estimate of the current saturations and pressures in the reservoir. Five predictive simulation cases were run to evaluate WAG and continuous CO_2 injection (CCI) at two injection bottomhole pressure (BHP) constraints and varying WAG cycle lengths.

- **Bell Creek Test Site Simulation Report: PCOR Partnership Phase III Task 9 Deliverable D66, 2014, approved (Liu and others, 2014)**
  Thirty-three baseline PNLs and seven repeat PNLs were used to discern formation top depths and thicknesses from the reservoir to the surface throughout the V2 geologic model. Changes in fluid saturations for CO_2, water, and oil were identified through the repeat logs and incorporated into the model. In addition, a reference model was created to serve as a repository for all relevant Bell Creek data used in the modeling and simulation activities. The existing V1 and V2 models, PNLs, historic and newly acquired logs, and core data were included in the reference model.

  A Phase 2 area simulation model was created from the fieldwide 3-D geologic model and validated by history-matching oil, water, and gas production; water injection; and reservoir pressure data. The history-matched Phase 1 and 2 models were used to conduct predictive simulations to estimate the CO_2 storage potential of the Bell Creek Field as well as better understand sweep efficiency, recovery factors, and CO_2 utilization. Five simulation cases for Phases 1 and 2 (ten cases total) were performed to investigate WAG and CCI for two injection BHP constraints and varying WAG cycle lengths. Results indicated that WAG yields faster oil recovery and better sweep efficiency than CCI in Phases 1 and 2 because of the vertical heterogeneity in the reservoir. The water injection cycle can recover a part of the bypassed oil during the CO_2 injection cycle in the WAG process. Findings also showed that CCI results in more CO_2 being stored.

- **Bell Creek Test Site Simulation Report: PCOR Partnership Phase III Task 9 Deliverable D66, 2015, approved (Bosshart and others, 2015)**
  The Bell Creek reference model was updated with new PNL and seismic data to complement existing Bell Creek data (field and processed logs, core analyses, structural tops, cultural/political boundaries, completed simulation results, and ground surface elevation from lidar measurements).

Previously developed Phase 1 and 2 simulation models were combined to simulate fluid migration between the phases. Field records of primary production, waterflooding, and CO_2 injection were history-matched. The distributions of fluid saturations within the model were analyzed. Fluid flow between Phases 1 and 2 was identified. Predictive simulations of CCI and WAG were used to estimate oil recovery, CO_2 storage, and CO_2 utilization. It was concluded that, in the EOR process, WAG operations exhibit a higher sweep efficiency and can utilize CO_2 better than CCI. In terms of storage, CCI can store approximately double the amount of CO_2 in comparison to WAG.

Previously developed geologic models (V1 and V2) were constructed in support of the established Bell Creek depositional interpretation (Galveston Island-style barrier bar deposits with depositional strike oriented northeast–southwest). Investigations discussed by this report (history-matching results, interpretation of 3-D and 4-D seismic surveys, and comparison of PNL data) warranted the construction of a V3 model based upon a new geological interpretation. The V3 model, under construction at the time of this report, was supported by a depositional model that included a local, transgressive barrier bar in Phases 1 and 2. This interpretation resulted in a 90° shift in the orientation of the paleo shoreline from previous interpretations.

- **Bell Creek Test Site Simulation Report: PCOR Partnership Phase III Task 9 Deliverable D66, 2016, pending approval (Jin and others, 2016a)**
  Seventeen PNLs were acquired late in 2015, providing both baseline characterization data and (for those wells with existing baseline PNLs) repeat/monitor data used to delineate fluid saturation changes. Seismic data also acquired in 2015 allowed further geologic characterization in the northeastern development phases, confirmed data consistency with previous 3-D seismic surveys, and allowed further delineation of permeability barriers and compartmentalization of the reservoir through time-lapse images of seismic amplitude difference volumes.

  Regional- and basin-scale reservoir models were developed to determine long-term CO_2 migration potential. A near-surface (shallow aquifer) model was constructed to investigate the potential for CO_2 migration into shallow aquifers above the reservoir. A simulation model of the Phase 3–7 area was constructed to investigate long-term CO_2 migration due to buoyancy within the reservoir formation. Simulations only considering migration because of buoyancy indicated CO_2 could migrate at approximately 3 ft/year to the east-southeast (updip). Additional factors not considered in these simulations, including mineral trapping, change in reservoir quality, and natural hydrodynamics, would likely further hinder and slow CO_2 migration.

  Three simulation models and a nine-component PVT model were developed to simulate the impact of impurities on recycled gas EOR and CO_2 storage performance. Analysis of Bell Creek produced gas showed methane (CH_4) to be the main impurity and also showed that the quantity of impurities decreased as the CO_2 flood continued. A series of minimum miscibility pressure (MMP) measurements were conducted on the Bell Creek oil which showed that as the mol% of CH_4 increased, the MMP increased, indicating a range of

impurities (up to 30 mol%) can be tolerated in the recycled gas without significant impairment of EOR efficiency or CO_2 storage performance.

SCOPE OF WORK

To evaluate the efficiency of large-scale CO_2 injection for EOR and to monitor the associated CO_2 storage in the Muddy Formation at the Bell Creek Field, several iterations of 3-D geologic modeling coupled with dynamic simulation work were completed as submitted in the previous six D66 reports (Pu and others, 2011; Saini and others, 2012; Braunberger and others, 2013; Liu and others, 2014; Bosshart and others, 2015; Jin and others, 2016a). This report documents the modeling and simulation activities completed since August 2016.

The updates pertaining to static modeling include 1) updating of the Bell Creek reference model with recently acquired PNL and InSAR data; 2) integration of the revised geological interpretation (Bosshart and others, 2015; Jin and others, 2016a), based on the newly acquired PNL, seismic, and legacy well log and core data, into the V3 geologic model; 3) completion of the V3 geologic model that has more accurately captured the reservoir heterogeneity, allowed for a better history match, and provided geologically more realistic predictive simulations.

The reservoir engineering and simulation activity updates for this reporting period pertain to 1) developing a dynamic simulation model for the Phase 4 area based on the V3 geologic model, 2) performing production/injection performance analysis for individual wells to improve the understanding of the reservoir and provide data for seismic interpretation, 3) conducting history matching and predictive simulations (CCI and WAG) with different injection/production constraints to assess oil recovery and associated CO_2 storage performance in Phase 4, 4) analyzing possible transport and trapping mechanisms of CO_2 to identify the most important trapping mechanisms for associated CO_2 storage in the reservoir, 5) comparing the simulation results with 4-D seismic monitoring results in the Phase 1 and 2 areas and predicting long-term CO_2 trapping behavior focusing on structural/stratigraphic trapping, 6) measuring CO_2 relative permeability hysteresis curves and integrating them into a five-spot model for a residual trapping study, and 7) investigating the effects of solubility trapping on associated CO_2 storage using the five-spot model.

Bell Creek Field Geology, New Data, and 3-D Geologic Modeling

The Lower Cretaceous Mowry Formation overlies the Muddy Formation (reservoir and CO_2 injection target formation) and provides the primary seal, preventing the migration of fluid to overlying aquifers and to the surface (Figure 4). Overlying the Mowry, several thousand feet of low-permeability strata (Belle Fourche, Greenhorn, Niobrara, and Pierre Formations) provide secondary seals that will retard, if not prevent, upward fluid migration in the unlikely event that the primary seal fails.

Deposited in nearshore marine environments (Bosshart and others, 2015), high-porosity (25%–35%), high-permeability (150–1175 mD) sandstones dominate the Muddy Formation reservoir within the Bell Creek oil field. The initial reservoir pressure, approximately 1200 psi, is significantly lower than the regional hydrostatic pressure regime of 2100 psi at 4500 feet (Burt and

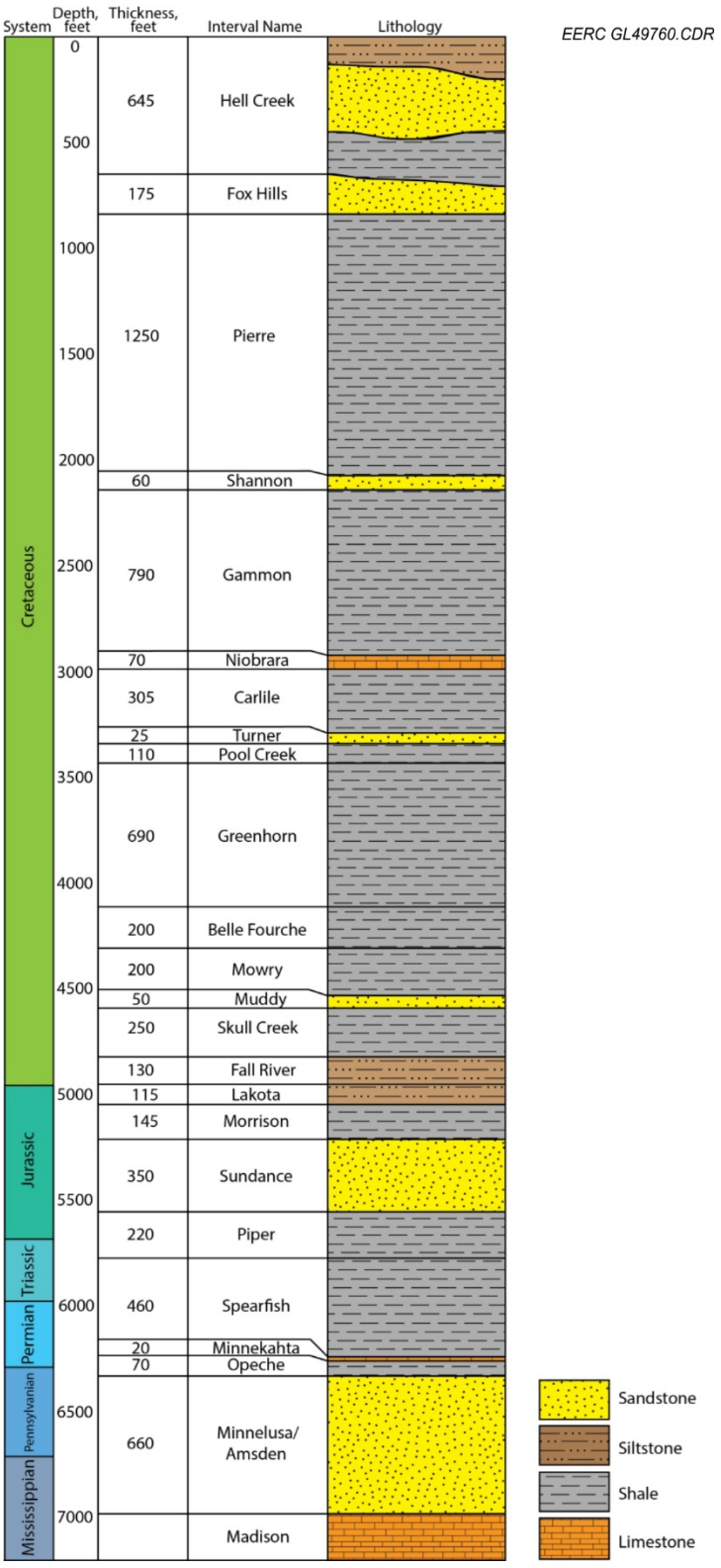

Figure 4. Regional stratigraphy of the eastern Powder River Basin. The Early Cretaceous Muddy Formation is the producing interval in the Bell Creek Field (Liu and others, 2014).

others, 1975). Structurally, the field is on a shallow monocline dipping less than 2° to the northwest with a strike trending southwest to northeast. Stratigraphically, the Bell Creek sand interval pinches out in the updip direction against the overlying Springen Ranch Member and the underlying Rozet Member of the Muddy Formation.

The Muddy Formation in the Bell Creek Field can be subdivided into four intervals/members based on well log and core analysis (in ascending order): the Rozet Member (lowermost silty interval overlying the Skull Creek shale), overlain by the Bell Creek Sand interval (reservoir), overlain by (if present) the Coastal Plain interval (included as the uppermost strata of the Bell Creek Sand interval in this study), and the Springen Ranch Member (estuarine and shallow marine siltstone/shale, Figure 5).

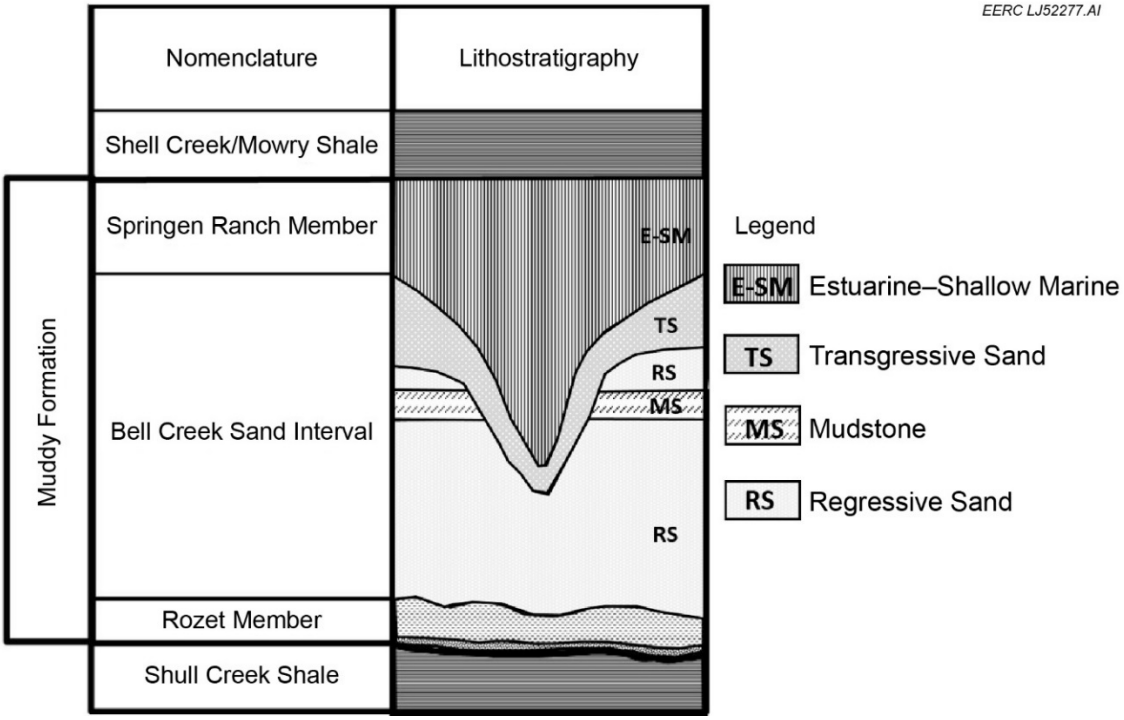

Figure 5. Muddy Formation reservoir stratigraphy (Jin and others, 2016a).

New Data Acquired

Since August 2016, new data have been acquired from a PNL campaign (January 2017) and interferometric synthetic aperture radar (InSAR) surveys. All newly acquired data, along with previous data (e.g., well logs, core analysis, structural tops, etc.), are stored in the Bell Creek reference model (Liu and others, 2014; Bosshart and others, 2015; Jin and others, 2016a).

PNL Data

During the 2017 PNL campaign, 11 wells were chosen for repeat/monitor logging in Development Phases 1 and 3 (Figure 6). Within the Phase 1 area, eight repeat/monitor PNL logs were acquired in production wells to 1) investigate oil, water, and CO_2 saturations associated with WAG injection; 2) monitor the vertical and horizontal uniformity of the WAG flood front as it was propagating through the Bell Creek reservoir; 3) increase understanding of CO_2 recycle, CO_2 trapping, and oil mobilization within geologically distinct areas; and 4) compare with and validate changes in seismic amplitude (4-D seismic) associated with CO_2 saturation and pressure increase. Within the Phase 3 area, three repeat/monitor PNL logs were acquired in production wells (or planned production wells) to determine changes in CO_2 saturation since 2015 (baseline PNLs were acquired in 2015, before CO_2 breakthrough) and to produce results that could be compared with differences seen in 4-D seismic data. Figure 7 displays the changes in saturation for Production Well 29-10.

Since 2013, 92 baseline and repeat/monitor PNL surveys have been acquired in 45 wells in Bell Creek Field (Figure 8). These PNL campaigns contributed large amounts of data to various investigations, such as monitoring CO_2 breakthrough between production and injection wells, improving the Bell Creek MVA program by monitoring saturations in overlying formations (Bosshart and others, 2015), calibrating history-matching efforts during dynamic simulation, and updating reservoir properties.

InSAR Data

InSAR provides a technique for mapping relative ground deformation from sequential radar images of Earth's surface obtained from orbiting satellites. The change in ground surface elevation over time may be the result of changing reservoir pressure within Bell Creek Field.

Two phases of InSAR analysis have been completed. The first phase consisted of processing of lower-resolution ground elevation measurements from the Advanced Land Observing Satellite (ALOS). The data were collected before injection, spanning the period from January 13, 2007, through January 24, 2011. These data were processed and analyzed to determine the naturally occurring ground surface deformation of the Bell Creek Field before injection. The second phase of InSAR satellite imagery consists of higher resolution COSMO-SkyMed (CSK) data that were obtained for the time interval from September 11, 2015, to May 8, 2016, during the operational phase, both during and after injection and pressurization.

Based on the results of this work, it was decided to continue collection of CSK data at least through December 2016 and, potentially, through June 2017 if continued promise is shown. Additional work will be undertaken to verify findings and integrate these data within modeling and simulation activities.

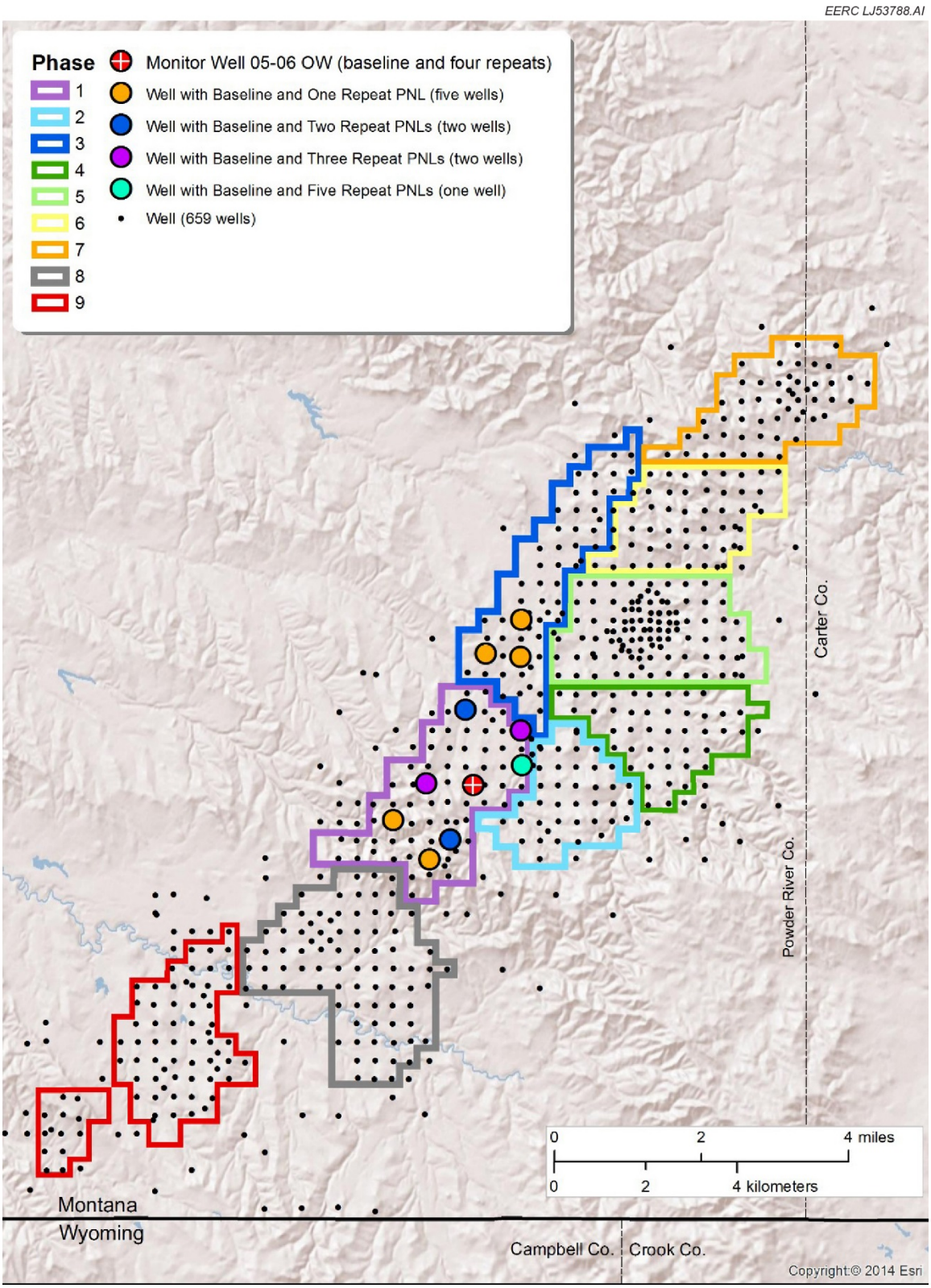

Figure 6. Map showing the distribution of wells logged during the 2017 PNL campaign.

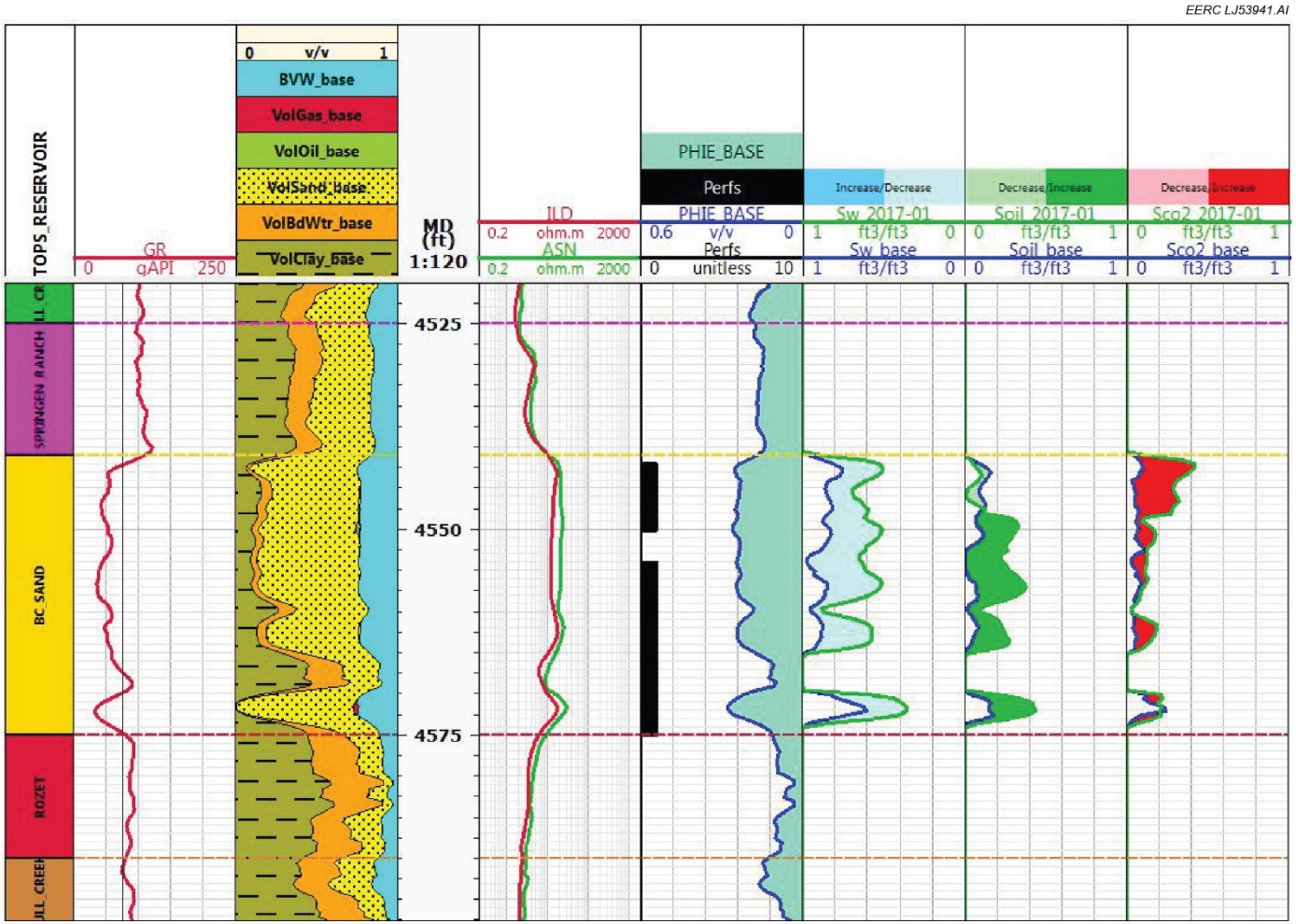

Figure 7. PNL display of Phase 3 Production Well 29-10 within the Muddy Formation. Track descriptions are (from left to right) Muddy Formation subintervals (members), gamma ray (GR), component volumes, measured depth reference track (feet), resistivity, perforated intervals and effective porosity, water saturation, oil saturation, and CO_2 saturation. Regarding the saturations, color fill is indicative of increase or decrease in PNL measurement from baseline (October 2015) to repeat/monitor (January 2017). Interval tops shown are (from bottom to top) Skull Creek, Rozet, Bell Creek Sand, Springen Ranch, and Shell Creek.

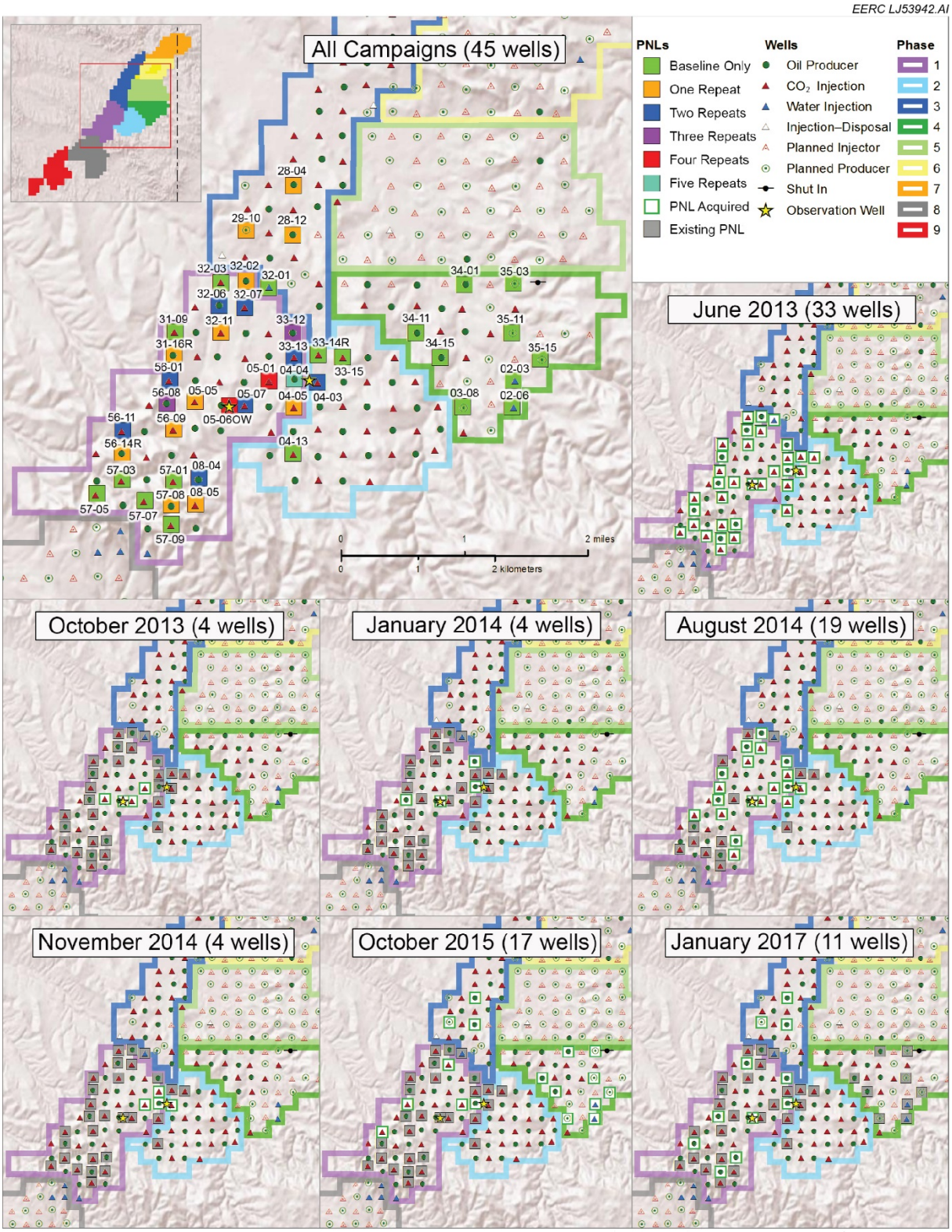

Figure 8. Bell Creek Field map showing where baseline and repeat/monitor pass PNLs have been collected since 2013 and also which wells were logged in each campaign.

3-D Geologic Modeling

To date, three versions of a static geologic model have been created. Version 1 and 2 models were developed based on the previous depositional environment interpretation of the Bell Creek Field, which characterized the Muddy sands as being part of a large, Galveston Island-style barrier bar along a shoreline trending approximately northeast to southwest. The history match provided a diagnostic that indicated improvements to the simulation and geologic model were necessary to improve prediction and to better replicate the reality of the system. Integration of 3-D and 4-D seismic data and PNLs along with legacy well logs and core analysis resulted in a revised geologic interpretation (Bosshart and others, 2015; Jin and others, 2016a), which was incorporated within the V3 reservoir model.

The V3 model's stratigraphic framework contains a facies model that was created based on the revised geologic interpretation of Bosshart and others (2015) and Jin and others (2016a). The facies model was used to further constrain petrophysical properties (porosity, permeability, and fluid saturations), along with temperature and pressure properties. History-matching of the simulation using the new static model has provided insight into the validity of petrophysical property distributions and has indicated areas where accuracy could be improved. Multiple iterations of property distribution refinement based on history-matching results have increased the confidence in the capture of the complex geologic heterogeneity of the Bell Creek reservoir. This has yielded a higher degree of certainty in the predictive simulation results of long-term CO_2 plume and pressure behaviors and the ultimate fate of injected CO_2.

Stratigraphic Framework

The V3 geologic model contained four Muddy Formation stratigraphic zones (informal members) from the Shell Creek Member to the Rozet Member that were correlated across 799 wells in the Bell Creek Field and surrounding areas. These zone tops were picked from vintage well logs, including gamma ray, spontaneous potential, sonic travel time, shallow and deep resistivity, and bulk density. From the base of the interval, the Rozet Member is the lower confining layer, which is overlain by the Bell Creek Sand Member (reservoir interval), which is confined above by the Springen Ranch and Shell Creek Members. The Bell Creek Sand member was further divided into 20 layers to better capture the lithologic heterogeneity in the field. The confining layers were each modeled as a single layer to keep simulation cell count as low as possible. The resulting model contained approximately 25 million cells at a cell size of 41.25 by 41.25 feet, which corresponds to four times the areal seismic data resolution. The overall average cell thickness was 3.4 feet, with an average cell thickness of 1.4 feet within the reservoir.

Facies Model

Two-point, variogram-based modeling techniques are limited in their ability to represent complex lateral and vertical lithological relationships, and object-based modeling techniques are limited in their capability of including large amounts of conditioning data (well logs, seismic data, core analysis, etc.) to guide distribution (Strebelle and Journel, 2001). Multiple-point statistics is a pixel-based modeling technique that allows the use of large amounts of conditioning data to capture complex relationships between multiple facies. The variogram of classic two-point

statistics is replaced by a conceptual geological pattern or training image that is used to describe the relative position of multiple facies to one another (Caers and Zhang, 2004). The use of multiple-point statistics in the Bell Creek modeling efforts has allowed a geologically more realistic representation of connectivity and compartmentalization of sand bodies to better explain and predict the migration and associated storage of CO_2 in the field.

Following Bosshart and others (2015) and Jin and others (2016a), the inclusion of 3-D and 4-D seismic data has allowed the identification of seven geobodies (geologically similar areas) within the Bell Creek Sand Member (Figure 9). Vertical and lateral facies associations within each geobody were determined from the interpretation of well logs. Fifteen facies were used to capture the complex geologic heterogeneity of the field. Facies logs were created for each well and upscaled into the stratigraphic framework as control points to guide facies distributions. Facies were distributed using multiple-point statistics, employing training images that were created based on type logs representative of the vertical facies associations in each geobody. In conjunction with type logs, seismic attributes and well log cross sections were used to capture the lateral facies association in each geobody. The final facies distribution was used to guide the distribution of petrophysical properties.

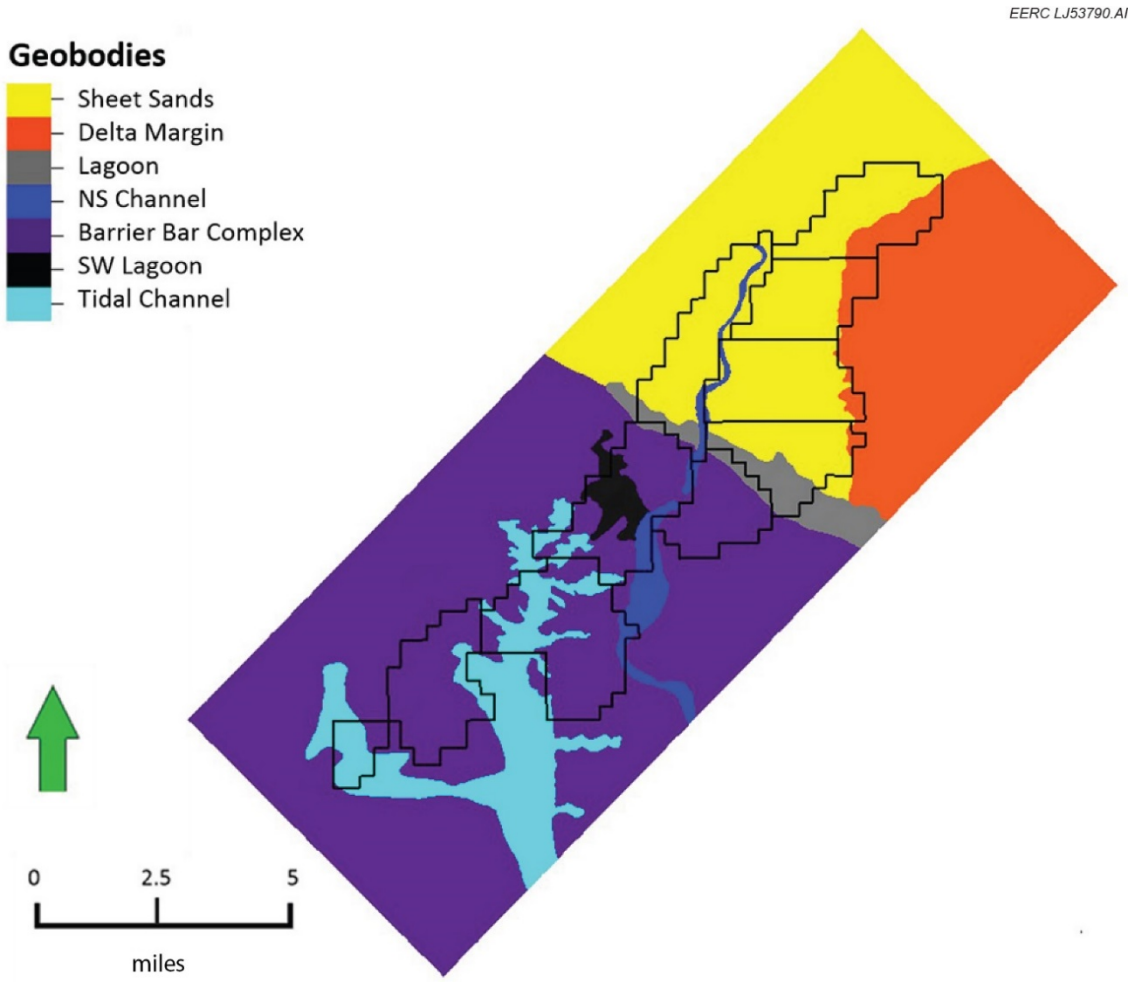

Figure 9. Map view of the modeled geobody regions within Bell Creek Field.

Petrophysical Model

Petrophysical properties were conditioned to the facies model using variogram-based geostatistical methods. Variograms were calculated for each facies based on lateral and vertical variance in upscaled property values. Petrophysical logs were calculated using results from core data along with log-derived porosity and permeability values. A water saturation property was distributed based on a J-function approach using vintage core analysis and high-pressure mercury injection data. Temperature and pressure properties were calculated from gradients derived from drillstem tests recorded within the field.

Porosity and Permeability Distribution

Total and effective porosity logs were made for each well in the study area based on the method described in detail in Braunberger and others (2013). Bulk density-derived porosity was compared to core measured porosity using crossplots. For those wells without bulk density logs, synthetic bulk density logs were created via a neural network using a combination of log curves within each well's log suite. Total porosity was then calculated from bulk density porosity for each well within the field. Effective porosity was calculated using a combination of total porosity, bulk density, and shale volume well logs. Effective porosity was calculated as the total porosity of the matrix minus the product of total shale porosity and volume of shale. Porosity logs were upscaled into the structural framework. Normal distribution parameters (minimum, maximum, mean, and standard deviation) were calculated for each facies to guide sequential Gaussian simulation distributions.

Permeability logs were created for each well in the study area via a neural network that compared core porosity and permeability and bulk density logs (Braunberger and others, 2013). A minimum and maximum value of permeability was calculated for each facies, and permeability was bivariately distributed into the stratigraphic framework based on a unique porosity/ permeability crossplot for each facies.

Porosity and permeability were distributed into the stratigraphic framework using variograms that were calculated for each facies. Variograms calculated within the reservoir facies show the major direction trending from northwest to southeast, perpendicular to the minor direction (Figure 10). These directions correlate well with the revised depositional interpretation with shoreline trending from northwest to southeast. The reservoir facies' lithologic and petrophysical properties change more rapidly in the variogram's minor direction, which is approximately parallel to the interpreted depositional dip (perpendicular to the interpreted shoreline). Lithologic and petrophysical properties do not change as rapidly in the major direction of the variogram, which is approximately parallel to the interpreted shoreline for the reservoir facies.

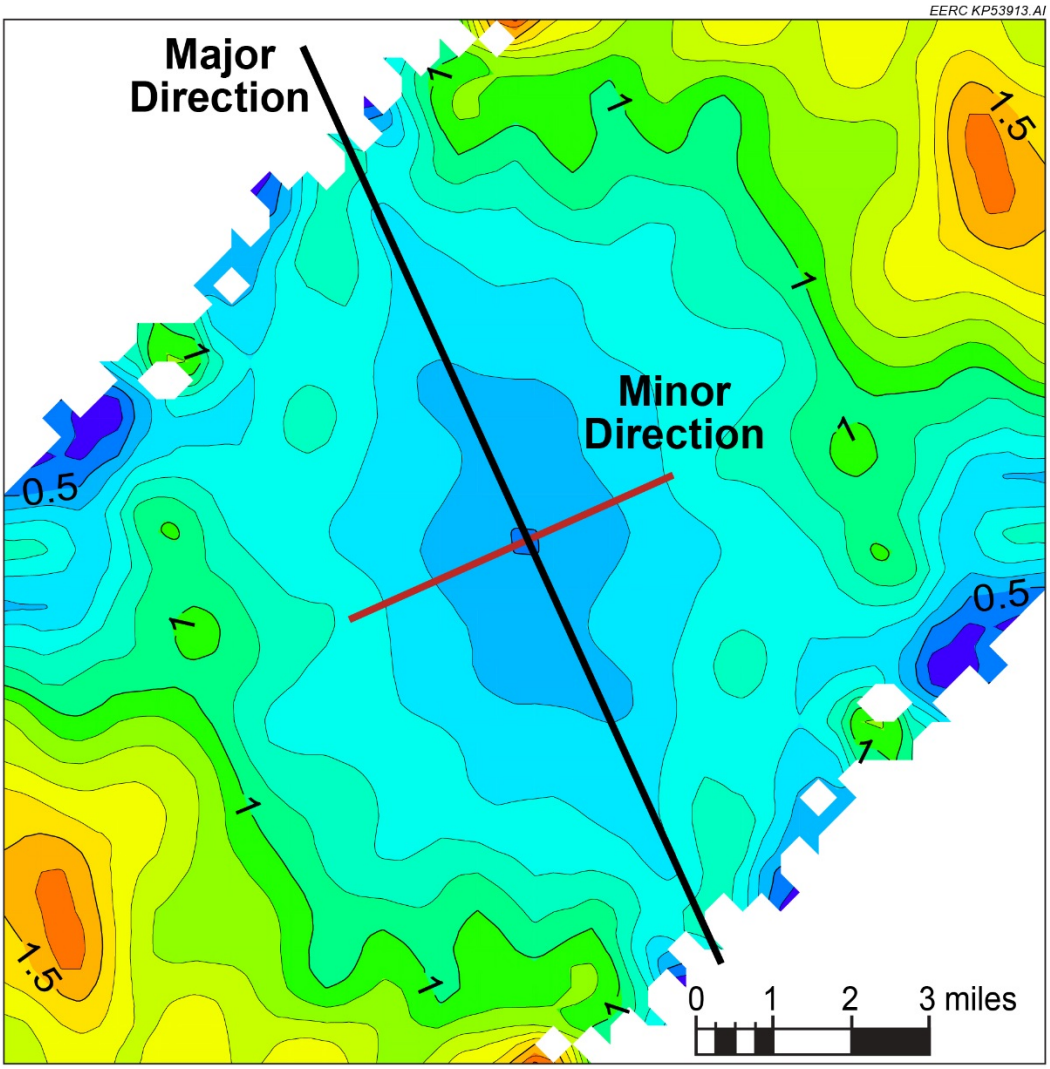

Figure 10. Variogram map of the effective porosity property for the prograding sand facies. The major direction (smaller variance per unit distance) is shown by a black line and trends approximately in the same direction as the interpreted shoreline (perpendicular to depositional dip). The minor direction (larger variance per unit distance) is shown by a red line and trends approximately parallel with depositional dip.

Water Saturation

Water saturation was distributed into the structural framework by first partitioning the reservoir into five separate flow units. The concept of a flow unit, first suggested by Amaefule and Mehmet (1993), is that rocks with similar petrophysical properties represent a basic element in the reservoir and have similar hydraulic properties. A critical factor in the determination of flow units is the pore structure which is defined by lithology and sedimentary features (bedding, laminations, etc.). Flow units are not necessarily confined by facies boundaries. Multiple flow units can be present within a single facies and, contrarily, a single flow unit can include several facies depending on the mineralogical and textural composition of the material (Svirsky and others,

2004). Defining flow units is based on the petrophysical parameters (porosity and permeability) and physics of flow at pore-scale (Svirsky and others, 2004). To partition the reservoir into flow units, a flow zone indicator value was calculated for each grid cell. The flow zone indicator value was used to assign a flow unit to each cell and was calculated as follows:

$$RQI = 0.0314\sqrt{\frac{k}{\emptyset}} \quad \text{[Eq. 1]}$$

Where *RQI* is reservoir quality index, k is permeability, and ∅ is porosity.

Normalized porosity ($\emptyset_z$):

$$\emptyset_Z = \frac{\emptyset}{1-\emptyset} \quad \text{[Eq. 2]}$$

Flow zone indicator (*FZI*):

$$FZI = \frac{\text{RQI}}{\emptyset_Z} \quad \text{[Eq. 3]}$$

When RQI is plotted versus normalized porosity on a log-log scale, all core samples with similar FZI values will lie on a straight line. Those core samples that lie on other parallel lines have different FZI values. Samples that lie on the same line (have similar FZI values) have similar pore structure and, therefore, make up a flow unit (Amaefule and Mehmet, 1993). Ranges in FZI values were used to group the Bell Creek reservoir into five flow units (Table 1).

Table 1. Classification of Flow Units Based on FZI Values

Flow Unit	FZI
Excellent-Quality Reservoir (EQR)	>6.5
Good-Quality Reservoir (GQR)	4.5–6.5
Medium-Quality Reservoir (MQR)	2.5–4.5
Low-Quality Reservoir (LQR)	1.0–2.5
Very Low Quality Reservoir (VLQR)	<1.0

A J-function approach, originally developed by Leverett (1941) as a method of relating water saturation and capillary pressure, was used to distribute the water saturation property into the structural framework. The J-function equation is as follows:

$$S_W = \frac{P_C}{\sigma \times cos\theta}\sqrt{\frac{k}{\Phi}} \quad \text{[Eq.4]}$$

Where S_W is fractional water saturation, P_C is capillary pressure, σ is surface tension, θ is the contact angle, k is permeability, and Φ is the fractional porosity of the rock.

A J-function for each flow unit was calibrated to core analysis data and high-pressure mercury injection data from the Muddy Formation in the Bell Creek Field (Braunberger and others, 2013). Lacking calibration data, the water saturation of the confining layers (Shell Creek, Springen Ranch, and Rozet Members of the Muddy Formation) was set to be 100% water-saturated.

Reservoir Engineering and Simulation

History Match for the Bell Creek Phase 4 Area

A simulation model based on the V3 geologic model was developed for the Bell Creek Phase 4 area (Figure 11) to provide the basis for predictive forecasts of field operations. The simulation model had 189 × 199 × 23 cells in the I, J, and K directions, respectively, resulting in 865,053 grid cells. Thirty-seven active wells were contained within the model, including 18 production wells, ten WAG injection wells, and nine water injection wells. The detailed well distribution is shown in Figure 12.

The Phase 4 area is located in the east-central region of the field. There is no evident edge water (aquifer support) connected to the pay zone. However, local water invasion has been identified from production performance analyses, especially for wells in the southwestern and middle areas of the phase. Figure 13 shows high initial water cut in wells along the southwestern boundary of the phase, indicating there was considerable water invasion or that initial water saturation was high in this part of the reservoir. Figure 14 illustrates the early water breakthrough, and relatively stable water cut following, in wells in the middle of Phase 4, which indicates the existence of movable water in this region before waterflooding.

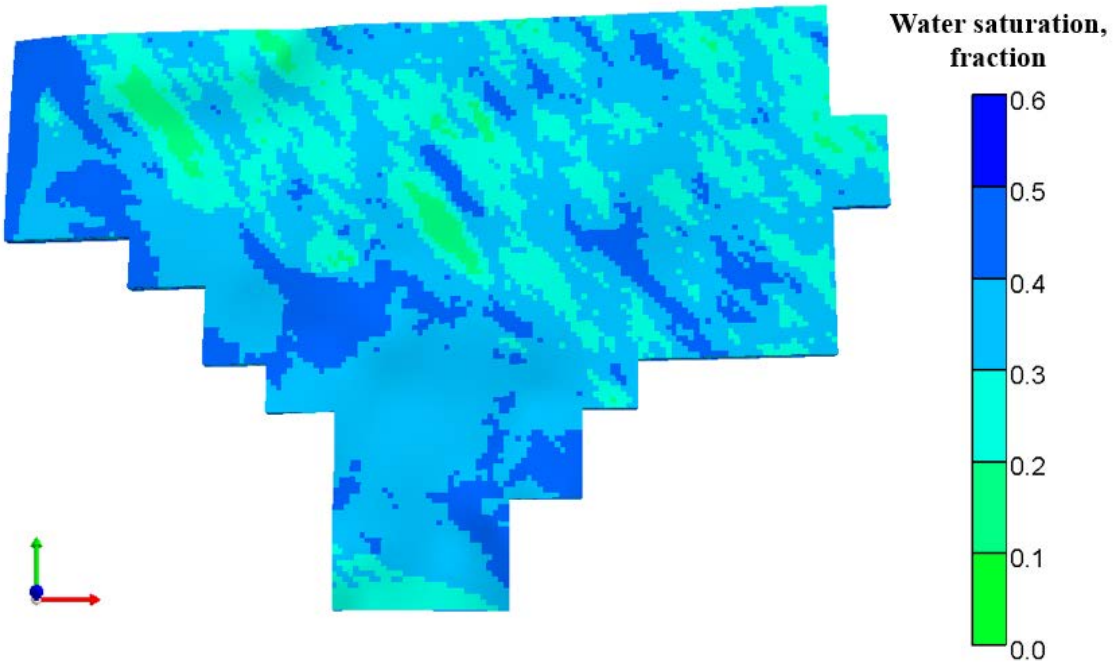

Figure 11. Schematic of the Bell Creek Phase 4 model.

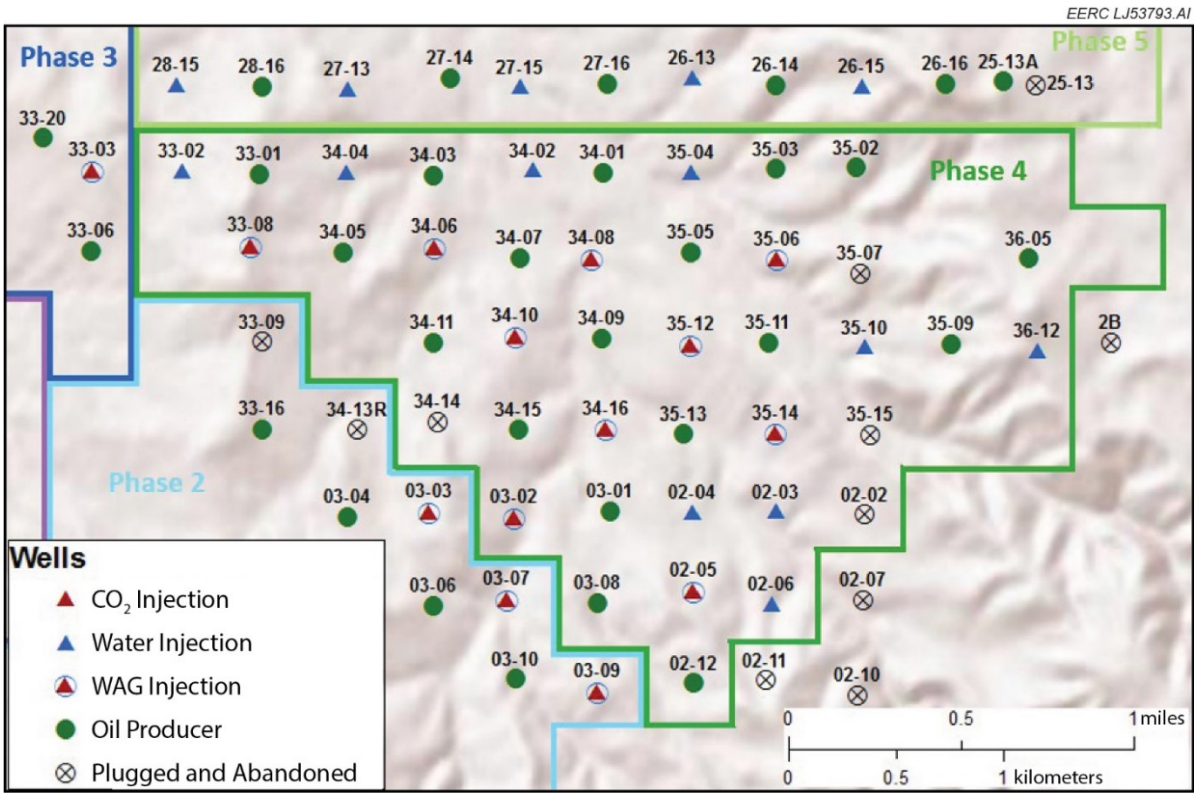

Figure 12. Well distribution in the Bell Creek Phase 4 and surrounding area (as of November 2016).

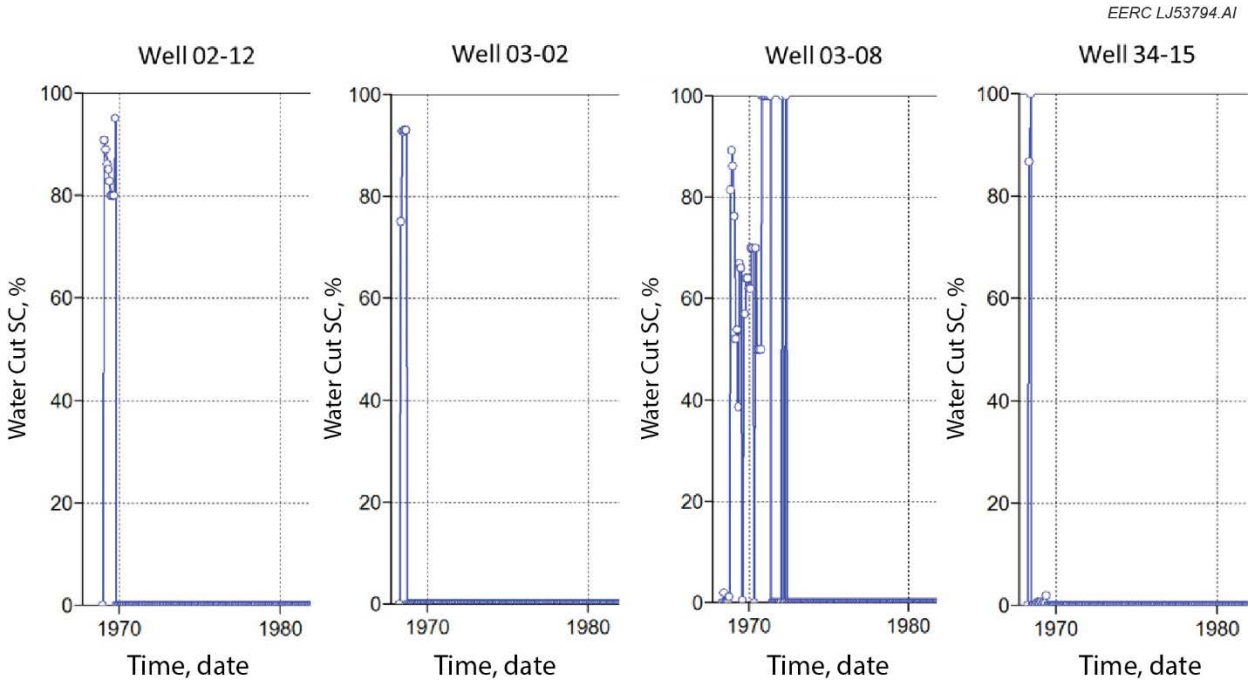

Figure 13. High initial water cut in the wells along the southwestern boundary of Phase 4 (SC: standard conditions).

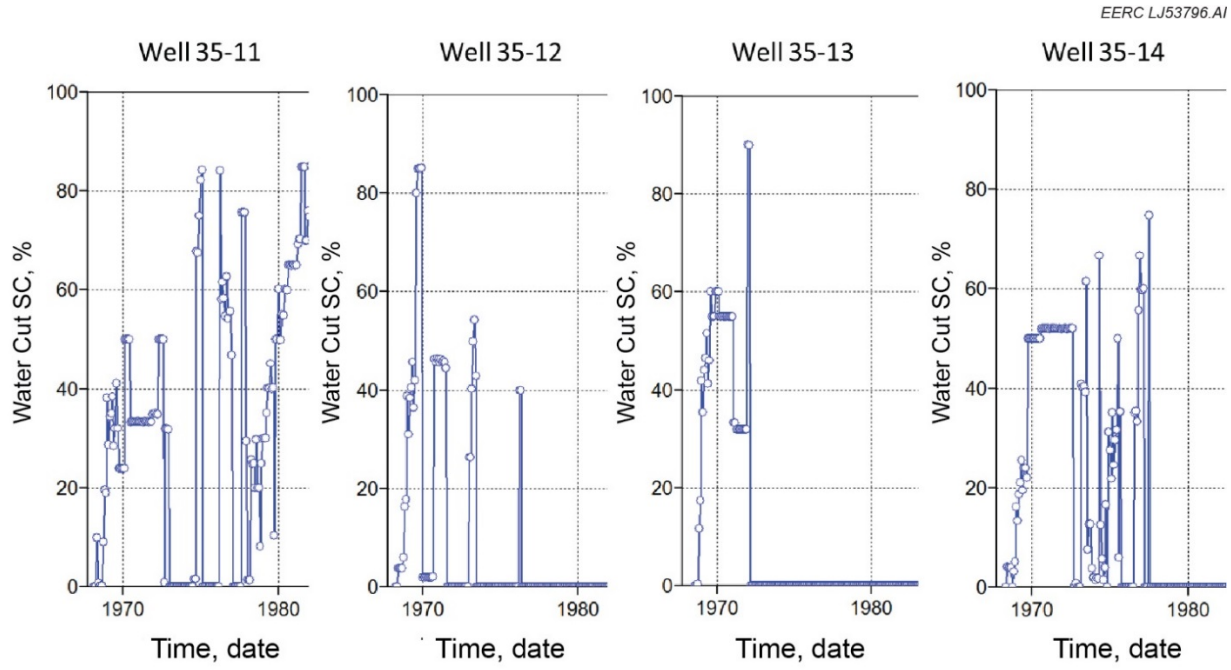

Figure 14. Early water breakthrough to wells in the middle of Phase 4.

Production performance analysis was also used to analyze fluid flow between phase regions, as this was an important factor for waterflood and CO_2 flood designs and operations. Production performance analyses indicated the reservoir was continuous across the boundary between Phases 4 and 5. Figures 13 and 15 show water cuts for wells located on both sides of the boundary between Phases 2 and 4. The wells in Phase 4 have high initial water cut, while the nearby wells in Phase 2 have water breakthrough after years of production, clearly indicating an absence of fluid flow across the boundary. The boundary between Phases 3 and 4 also appeared to be impermeable (permeability barrier interpreted as a fluvial incised valley), based upon the different well performance (Figure 16).

After the boundary conditions of the Phase 4 area were analyzed, a systematic history-matching process was conducted to reproduce the production data in this phase. Similar to the previously reported studies of Braunberger and others (2013), Liu and others (2014), Bosshart and others (2015), and Jin and others (2016a), liquid production and injection rates were used as primary constraints. Recorded oil, water, and gas production rates were used in comparison to the simulated results. In the primary production stage, local water saturation (especially for the southwestern and middle portions of the phase) was adjusted to match the water cut performance. In the water-flooding stage, petrophysical properties and out-of-boundary flow were adjusted to match the oil and water production rates. In the CO_2-flooding stage, relative permeability curves and end point saturations were tuned. A history match was achieved, and the results for liquids (oil and water combined), oil, water, and gas production are shown in Figures 17–20.

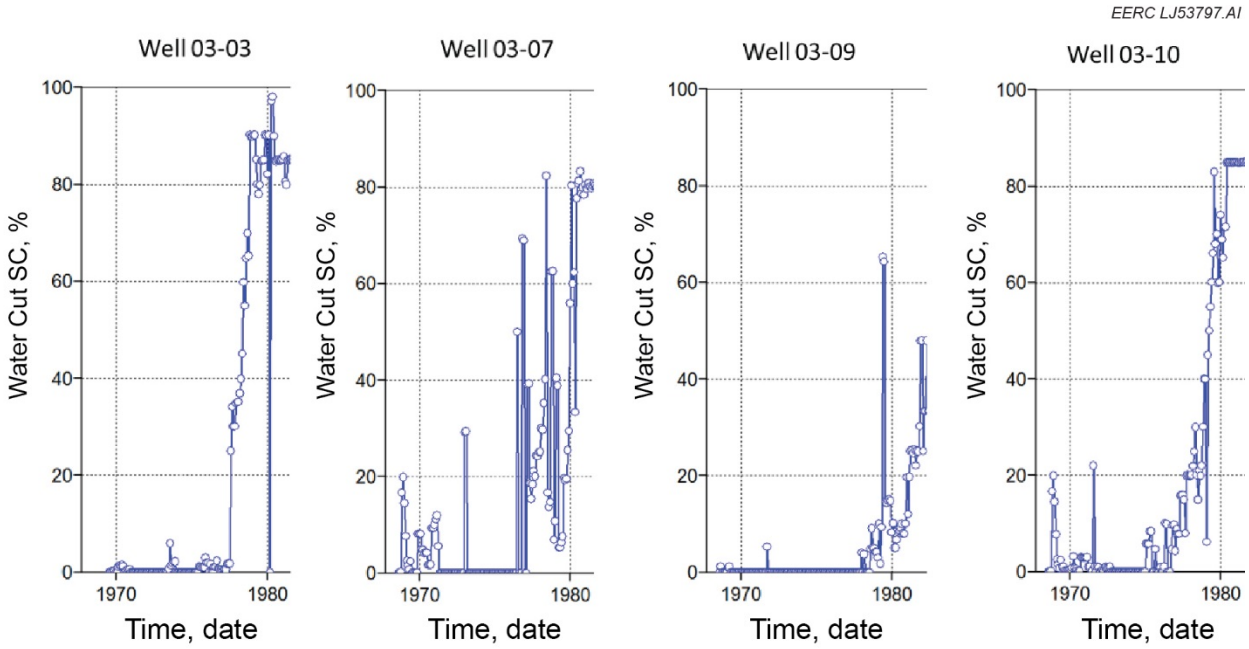

Figure 15. Low initial water cut in the wells along the northern boundary of Phase 2, indicating closed boundary conditions between Phases 2 and 4.

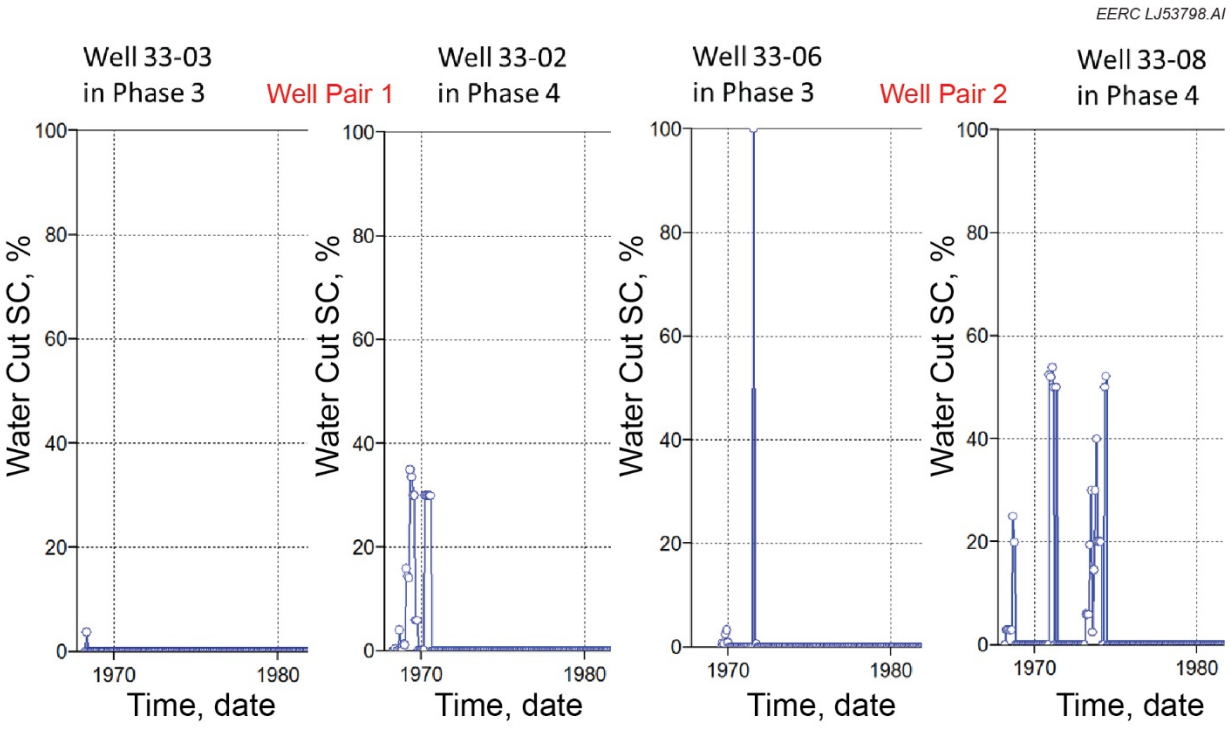

Figure 16. Comparison of water cut in wells along the boundary between Phases 3 and 4.

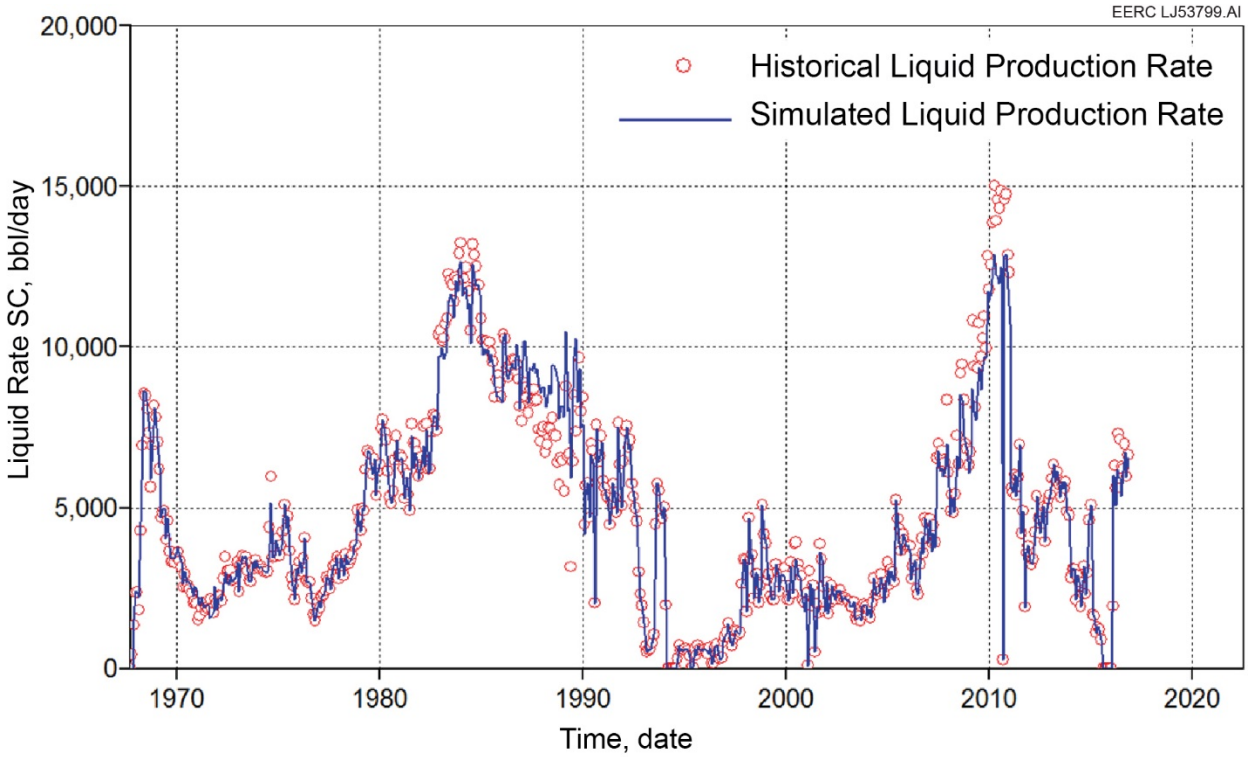

Figure 17. History-matched liquid production rate of the Bell Creek Phase 4 model.

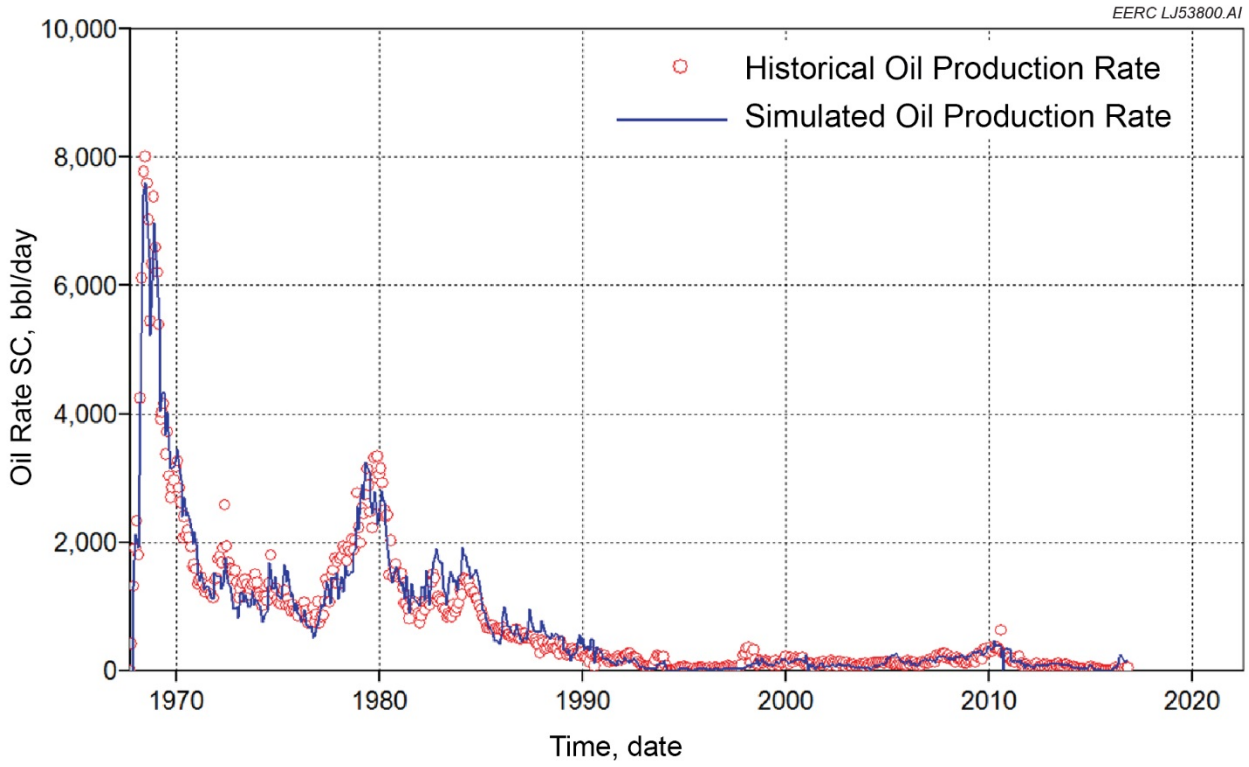

Figure 18. Bell Creek Phase 4 oil production rate history match results.

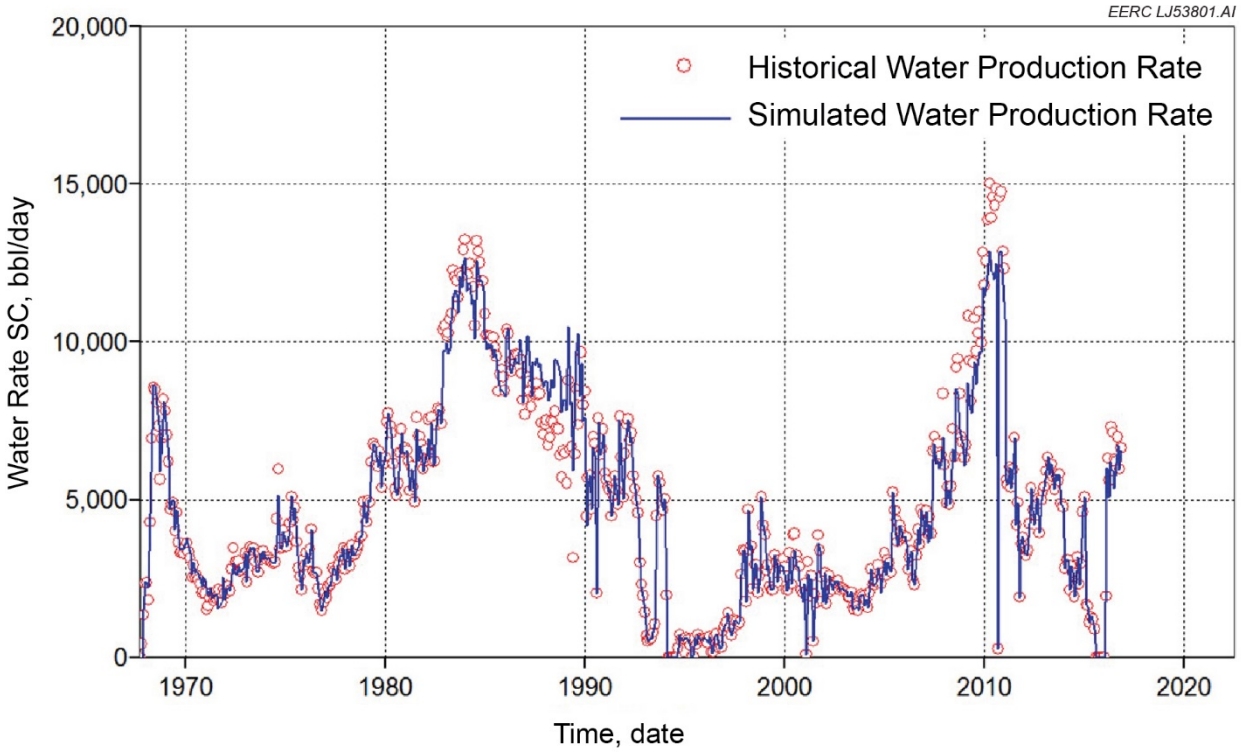

Figure 19. Bell Creek Phase 4 water production rate history match results.

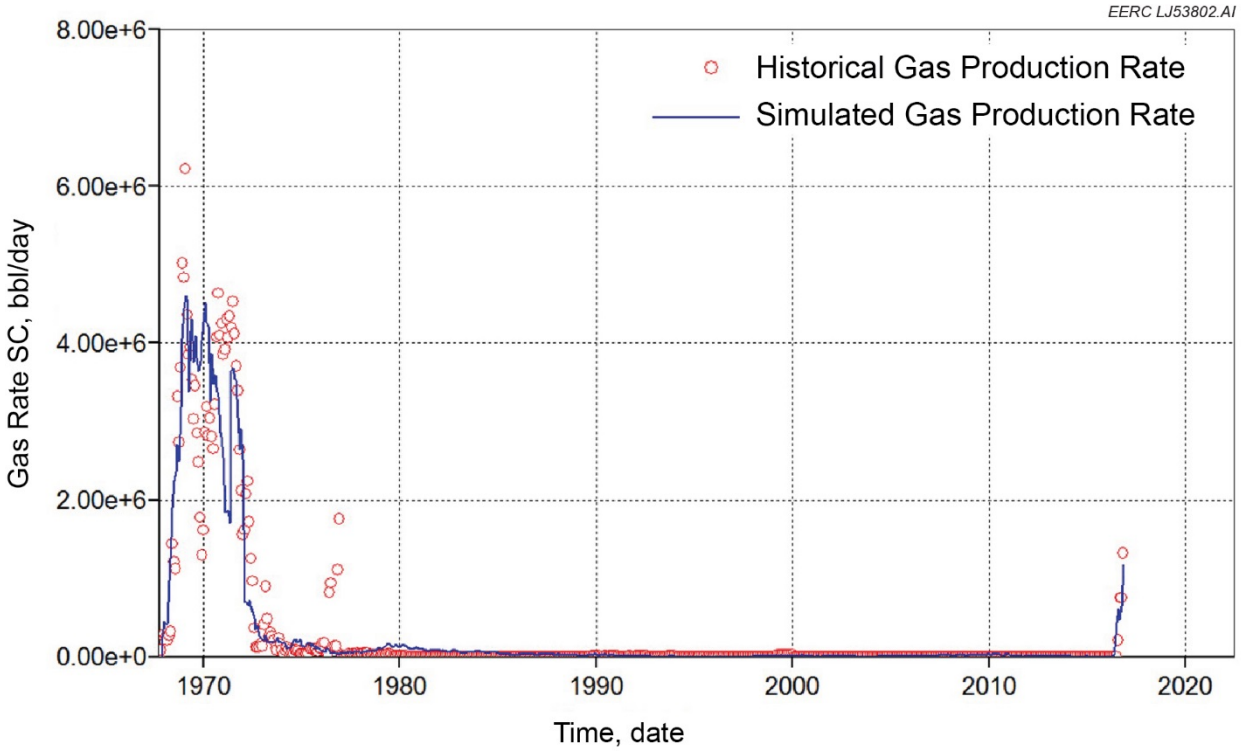

Figure 20. Bell Creek Phase 4 gas production rate history match results.

Predictive Simulation for the Bell Creek Phase 4 Area

Phase 4 shares an open boundary with Phase 5, where CO_2 flooding has not yet occurred (as of November 2016). Four water injection wells (Wells 33-02, 34-02, 34-04 and 35-04) lie along the Phase 4 and 5 boundary, preventing CO_2 injected in Phase 4 from migrating to Phase 5. Besides potential CO_2 migration across the model's open boundary to the north, complicated fluid saturation distributions and complex reservoir heterogeneity in the Phase 4 area posed additional challenges to determining an optimal CO_2 flood schedule. Thus it was necessary to carry out predictive simulations under different scenarios for performance evaluation. Four cases were simulated to observe reservoir response:

Case 1: CCI with injection BHP 2800 psi, producing BHP 2300 psi
Case 2: CCI with injection BHP 2800 psi, producing BHP 2600 psi
Case 3: WAG with injection BHP 2800 psi, producing BHP 2300 psi, 3-month cycle
Case 4: WAG with injection BHP 2800 psi, producing BHP 2600 psi, 3-month cycle

Based on the current operating schedule, CO_2 injection rate was set at 1 MMscf/day/injector for all CCI and WAG cases, and water injection rate was set at 1000 bbl/day/injector for WAG cases. BHP constraints were 2800 psi for all injectors and 2600 (or 2300) psi for all production wells, as indicated in the case descriptions.

Figure 21 shows hydrocarbon pore volume injected (HCPVI) for CCI and WAG cases over a simulated time frame from 2016 to 2080 with the production/injection settings described above. Smaller pressure drawdown between injection and production wells results in decreased HCPVI for the same injection modes. This is because injection rate is proportional to pressure drawdown; small pressure drawdown means the injection rate constraints may not be reached (especially water rate), ultimately resulting in decreased HCPVI. More pore volumes of CO_2 can be injected into the reservoir than water under the same pressure constraints because CO_2 has lower density and viscosity than water. Thus the WAG cases show decreased HCPVI than CCI for the same injection pressure settings.

Figures 22 and 23 show cumulative injected and stored CO_2 by CCI and WAG versus HCPVI, respectively. The CCI cases resulted in injection and associated storage of approximately twice the amount of CO_2 in comparison to the WAG cases with the same pressure settings. Although twice as much CO_2 was injected during CCI, incremental oil recovery was only slightly higher (< 1% OOIP) than that of WAG injection with the same pressure settings (Figure 24). Compared to the predictive performance of incremental oil recovery in the Phase 1 and 2 areas, the performance in the Phase 4 area is considerably lower after 45 years of EOR operations (13%–14% OOIP versus 6.5%–7% OOIP, respectively). Several factors account for less effective CO_2 flooding in Phase 4. First, the ratio of production wells to CO_2 injection wells in Phase 4 is 1.8:1, while it is nearly 1:1 in Phases 1 and 2, allowing the reservoir in Phases 1 and 2 to be swept more thoroughly than Phase 4. The comparison of CO_2 saturation distribution in these phases after 1 year of CO_2 flooding is demonstrated in Figure 25. The CO_2 saturations in Phases 1 and 2 are more extensive than in Phase 4. Second, the average actual CO_2 injection rate of each individual WAG injection well in Phases 1 and 2 is more than twice that of Phase 4 (54.8 Mscf/day/injector versus

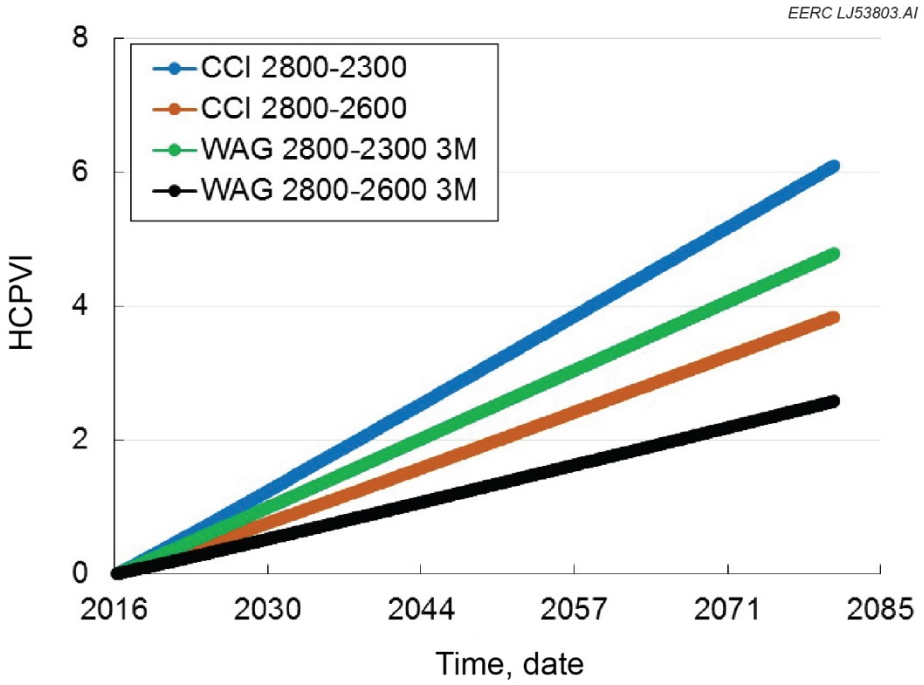

Figure 21. HCPVI for the simulated CCI and WAG cases.

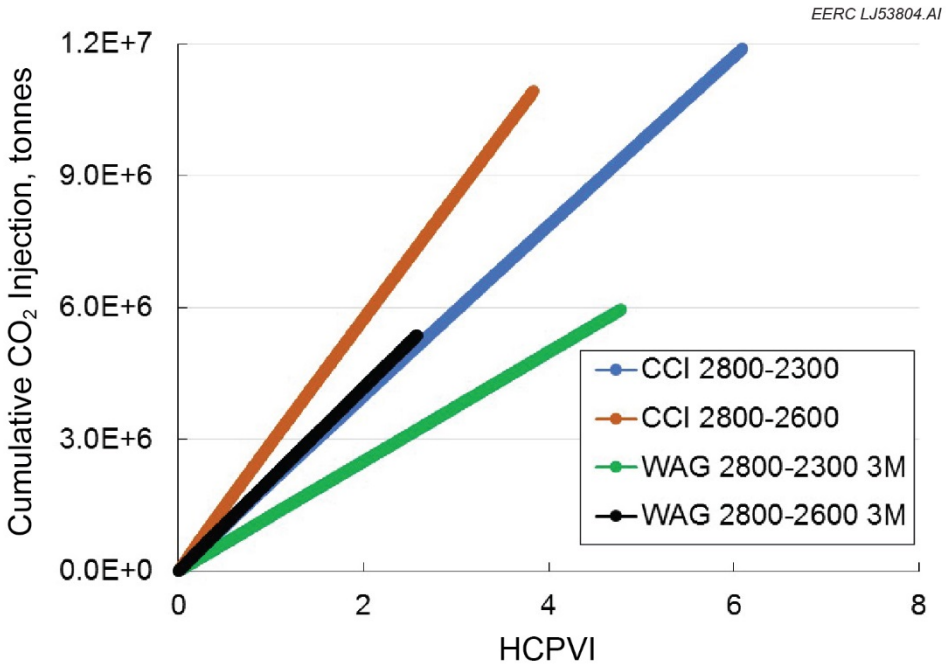

Figure 22. Cumulative CO_2 injected during CCI and WAG operations.

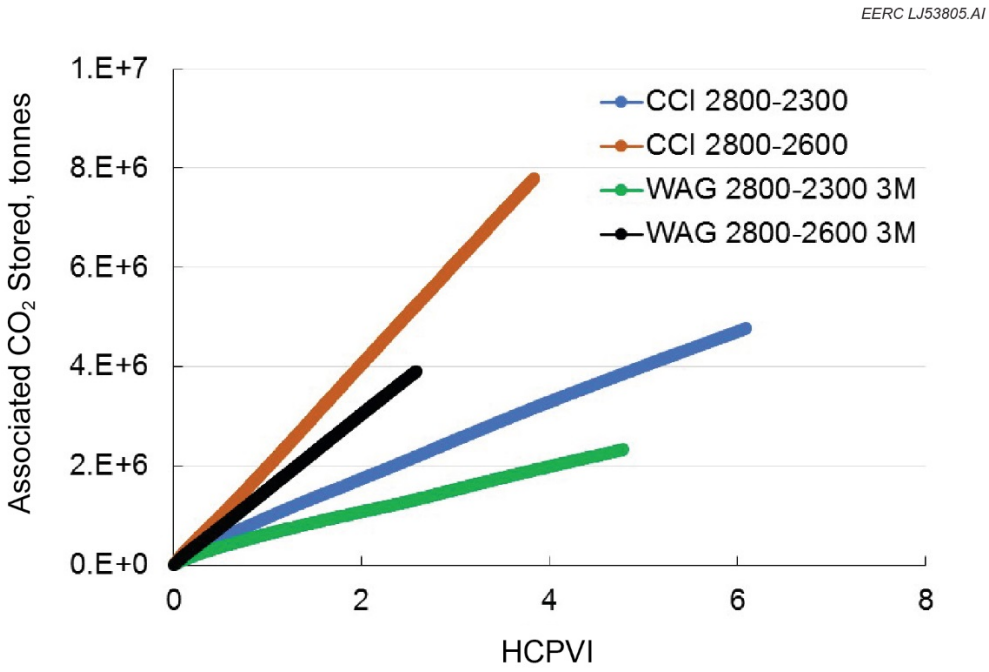

Figure 23. Cumulative CO_2 stored during CCI and WAG operations.

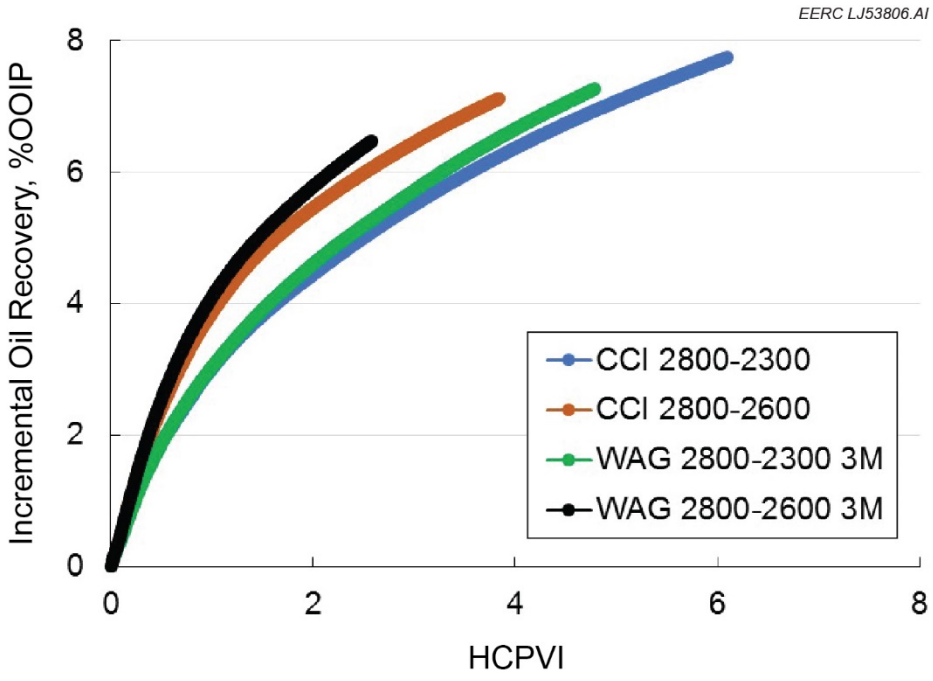

Figure 24. Incremental oil recovery by CCI and WAG operations.

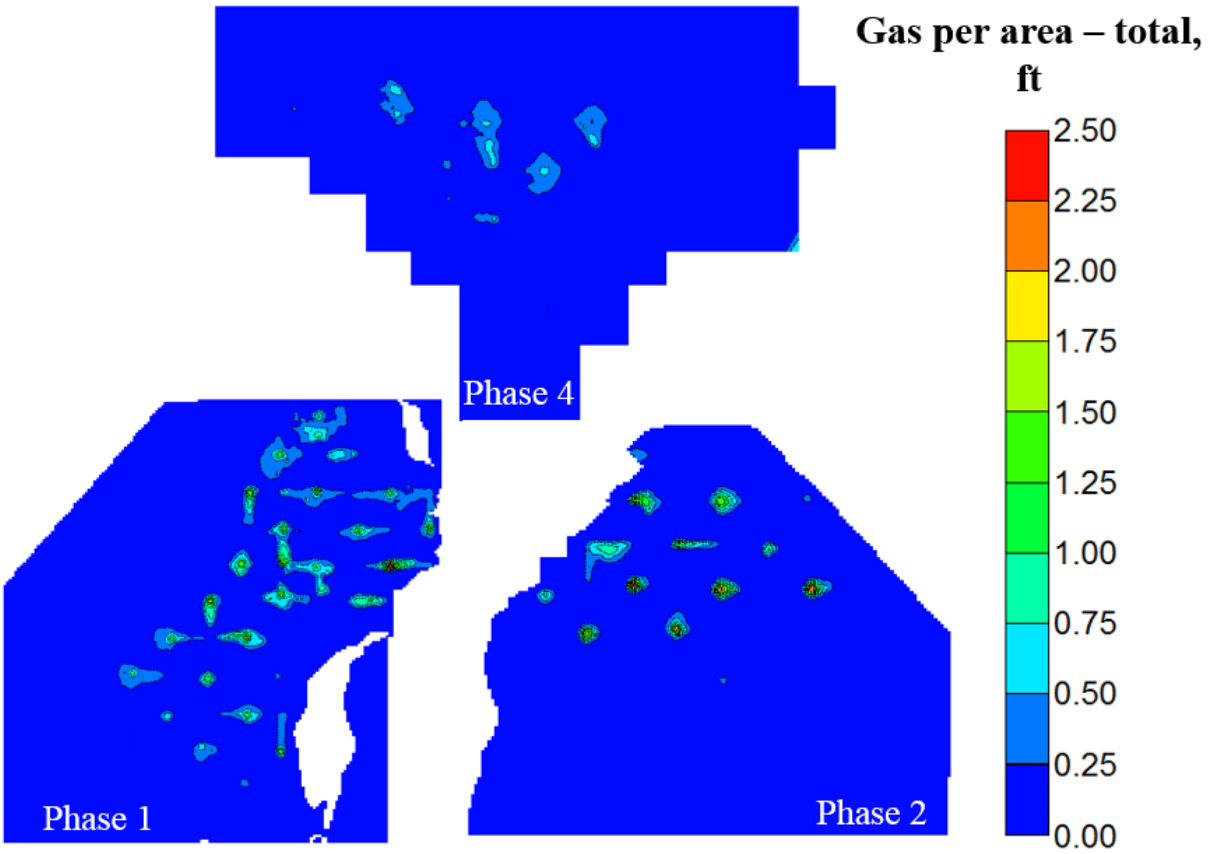

Figure 25. Comparison of CO_2 distribution in different phases after 1 year of CO_2 flooding.

24.6 Mscf/day/injector, respectively). Third, there are four temporary water injection wells along the boundary between Phases 4 and 5 to prevent CO_2 flow from Phase 4 to Phase 5. These water injection wells are close to the WAG injection wells in Phase 4. Therefore, part of the injected CO_2 is dissolving in the injected water, which decreases the amount of CO_2 available for sweeping oil in the Phase 4 area. However, these four water injectors were only temporary until Phase 5 is developed. There is no noticeable difference in recovery factor expected for this temporary setup when Phase 5 is fully developed.

Trapping of Injected CO_2 in Reservoirs with CO_2 EOR Operations

Effective trapping mechanisms ensure injected CO_2 will remain, in permanence, within the area of review (limited lateral migration) and contained within the zone of interest (limited vertical migration). The four primary CO_2 trapping mechanisms include structural/stratigraphic, residual, solubility, and mineral trapping. CO_2 trapping processes are important to EOR performance, as they can affect the CO_2 utilization factor. For instance, trapped CO_2 may lead to a higher CO_2 utilization factor since less CO_2 is available to contact oil and sweep it from the reservoir; therefore, more CO_2 needs to be injected for an equivalent oil recovery. Aside from oil recovery,

the trapping mechanisms determine associated CO_2 storage during and after CO_2 flooding. Figure 26 shows the increase of CO_2 trapping strength (or security) with time based upon previous studies (Metz and others, 2005). Of the four primary CO_2 trapping mechanisms, structural/stratigraphic, residual, and solubility trapping are important for the CO_2 flowing behavior in the Bell Creek Field and, therefore, were investigated and are discussed in the following sections. Mineral trapping, with the exception of a small number of documented instances of CO_2 storage in basalt formations (McGrail and others, 2006, 2016), are thought to occur over an extended time frame (hundreds to thousands of years). Thus this trapping mechanism is of decreased importance when immediate containment/conformity of injected CO_2 is considered and will likely have no impacts on operational activities in the Bell Creek Field. As such, CO_2 mineralization has not been a focus and will not be discussed further in this report.

Residual CO_2 Trapping

Residual trapping occurs under the effects of relative permeability, resulting in immobilization of gas in the pore space. Relative permeability is a concept used to describe individual fluid phase mobility when multiple fluid phases are present, while accounting for capillary pressure phenomena. CO_2 may be trapped within the pore space of a permeable reservoir because of capillary force when two or more fluids coexist in the rock (i.e., CO_2, oil, and/or water). Relative permeability can be measured directly from experiments with sufficient data points or generated from empirical correlations by fitting them to limited data (Spiteri and others, 2008).

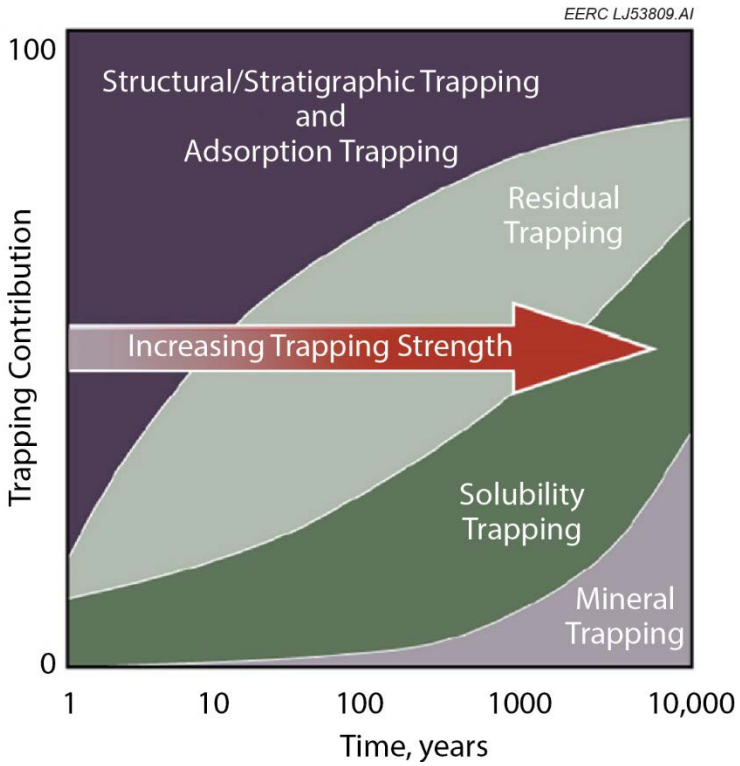

Figure 26. Increase of CO_2 trapping strength with time (modified from Intergovernmental Panel on Climate Change, 2005).

Injection of CO_2 results in increasing near-wellbore CO_2 saturation accompanied by a decrease in brine/oil saturation, in which case relative permeability of CO_2 increases (the fraction of the overall permeability available to CO_2 increases). During postinjection periods, CO_2 continues migrating farther from the injection point, and the CO_2 saturation will decrease (accompanied by an increase in brine/oil saturation), in which case the relative permeability of CO_2 decreases (the fraction of the overall permeability available to CO_2 decreases). As CO_2 saturation decreases, a "residual" saturation will eventually be reached at which CO_2 is effectively immobilized and, therefore, considered stabilized under the effects of residual CO_2 trapping. Thus predicting the extent of CO_2 migration within the reservoir under the effects of residual trapping requires an estimate of residual CO_2 saturation. Previous studies have shown that residual CO_2 saturation may be on the order of 5%–30%, varying with reservoir conditions (Ennis-King and Paterson, 2001; Zuo and Benson, 2014; Niu and others, 2015; Krevor and others, 2015; Al-Menhali and Krevor, 2016).

An additional complexity is that the shape of relative permeability curves may be different depending on the directionality of changing fluid saturations (imbibition versus drainage), termed relative permeability hysteresis. The replacement of in situ liquid by injected CO_2 is termed drainage (nonwetting gas phase replaces the wetting liquid phase). In the WAG injection process, the gas and liquid phases alternately displace each other, meaning the drainage and imbibition processes occur in cycles. Hysteresis occurs under the effects of wettability and the effects of capillary pressure when CO_2 is present. This is important to understand in investigations of CO_2 storage, as the effect is usually pronounced when liquid and gas occupy the same system and may have direct implications to CO_2 migration and the trapping of CO_2 in the pore space (Burnside and Naylor, 2014).

Assessment of Relative Permeability Hysteresis and Residual Trapping in Bell Creek

Relative permeability hysteresis was measured using a clean sandstone core sample, collected from Bell Creek's 05-06-OW at a depth of 4533 ft. Table 2 contains the measured physical properties of the core sample and the oil used in the procedure. Steady-state relative permeability tests were performed to derive the relative permeability curves of the gas phase. The experiments were conducted under reservoir conditions (2350 psi and 108°F for confining pressure and temperature, respectively). The pressure profile for the drainage (CO_2 injection) and imbibition (oil injection) processes are shown in Figures 27 and 28, respectively. The plots demonstrate that steady-state displacement was established in both drainage and imbibition processes after 1000 seconds. Following the procedure described by Fatemi and others, (2012) and Krevor and others, (2012), the relative permeability curves for the gas branch were estimated (Figure 29), which clearly shows a hysteretic effect between the CO_2 relative permeability curves during drainage and imbibition processes. The irreducible (or trapped) gas saturation increases from 0.07 in the drainage process to 0.19 in the imbibition process, which means a considerable amount of CO_2 was trapped in the core sample during the cycle.

Several relative permeability hysteresis models, including Land's trapping model, Carlson's hysteresis model, and Killough's hysteresis model are available to predict the effects of hysteresis on oil recovery and associated storage (Larsen and Skauge, 1998; Fatemi and others, 2012). In this

Table 2. Physical Properties of the Core Sample and Oil Used in Relative Permeability Hysteresis Measurements

Material	Parameter	Value	Unit
Core Sample	Diameter	0.97	in.
	Length	1.91	in.
	Weight	44.37	g
	Grain density	2.65	g/cm^3
	Porosity	0.26	fraction
	Permeability	1052	mD
Oil	Temperature	108	°F
	Viscosity	4.35	cP

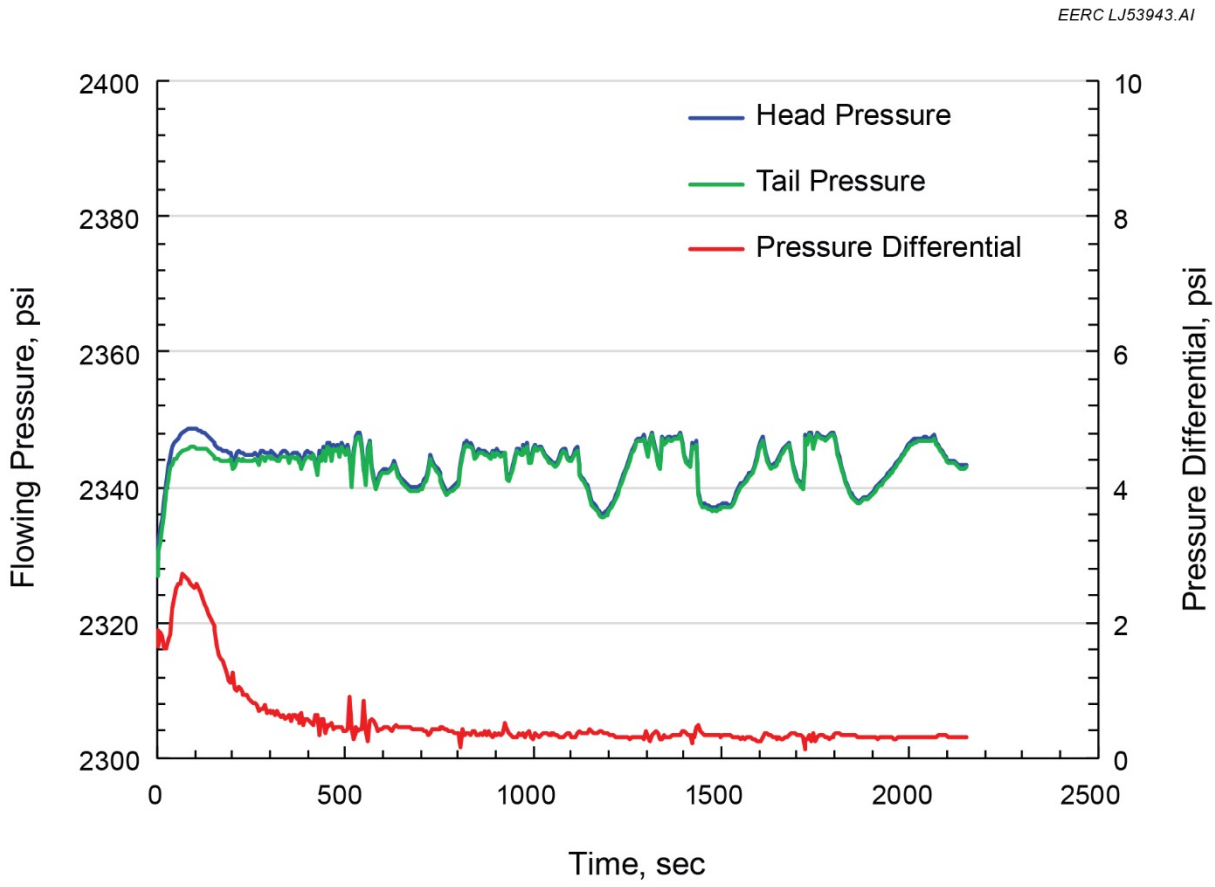

Figure 27. Pressure profile in the drainage process (CO_2 injection).

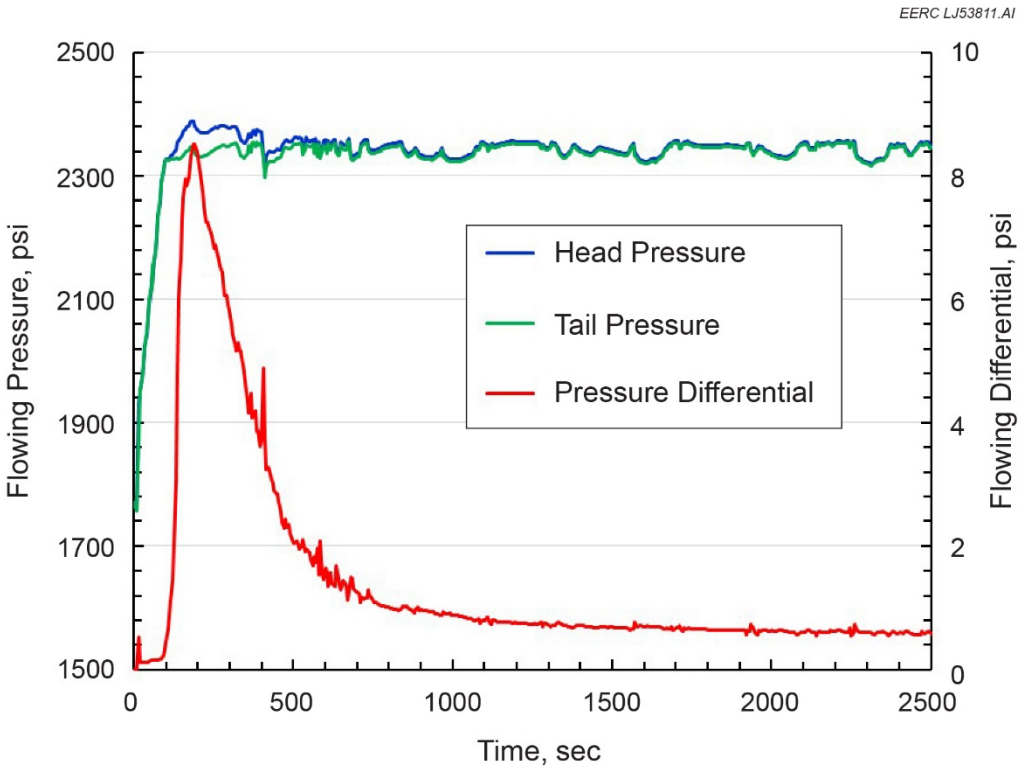

Figure 28. Pressure profile in the imbibition process (oil injection).

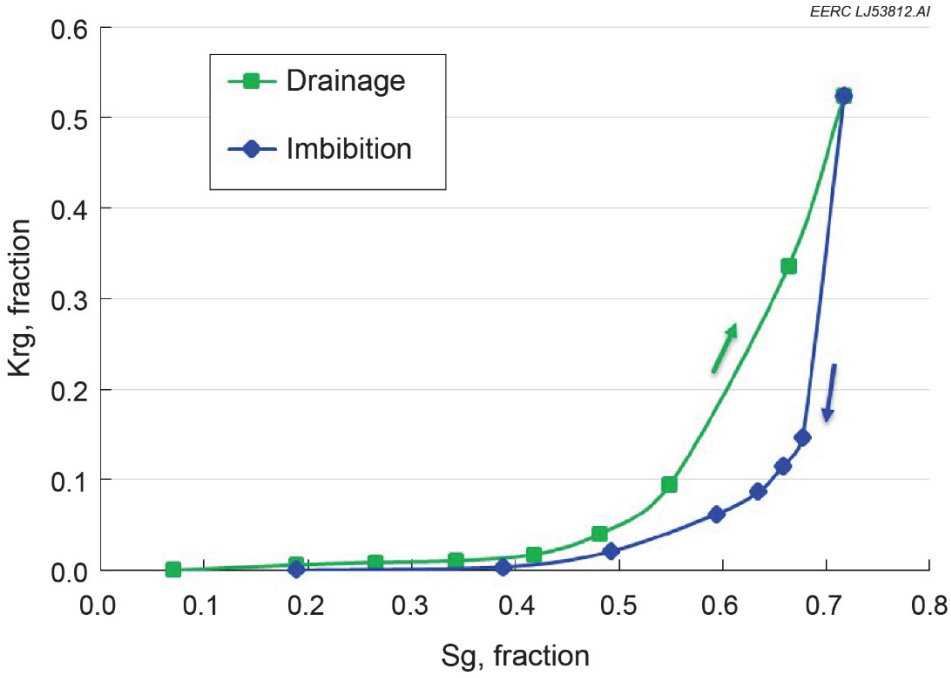

Figure 29. Relative permeability curves for CO_2 in the drainage and imbibition processes showing a clear hysteretic effect.

study, Land's model was used in simulation cases to evaluate the effect of hysteresis on CO_2 flood performance. Three different residual CO_2 saturations (0.1, 0.2, and 0.3) were considered in the study to span a range of possible CO_2-trapping scenarios. A previously developed five-spot simulation model, discussed by Jin and others (2016a), was used to conduct the simulation.

Figure 30 shows the comparison of incremental oil recovery for the five-spot model CO_2 EOR simulation cases with and without relative permeability hysteresis. The results indicate relative permeability hysteresis does not have a significant impact on oil recovery in this model. Oil recovery factor is slightly higher when the residual CO_2 saturation is 0.3, but the difference is negligible between other cases. However, the effect of relative permeability hysteresis on associated CO_2 storage is obvious (Figure 31). The results indicate more CO_2 is stored in the reservoir when residual CO_2 saturation is high, as is expected. Quantitatively, a difference of approximately 20% of trapped CO_2 was noted between a case without hysteresis applied and a case with hysteresis applied and an assumed residual CO_2 saturation of 0.3. The simulated associated CO_2 storage for different residual CO_2 saturations is shown in Figure 32.

Solubility Trapping of CO_2

CO_2 dissolves in other formation fluids when injected into a reservoir, the result of which is termed solubility trapping. Similar to the residual trapping, solubility trapping occurs rapidly as CO_2 contacts liquids. The primary benefit of solubility trapping is the negation of buoyant forces when free-phase CO_2 is converted to solute in brine or oil. The solubility of CO_2 depends on several

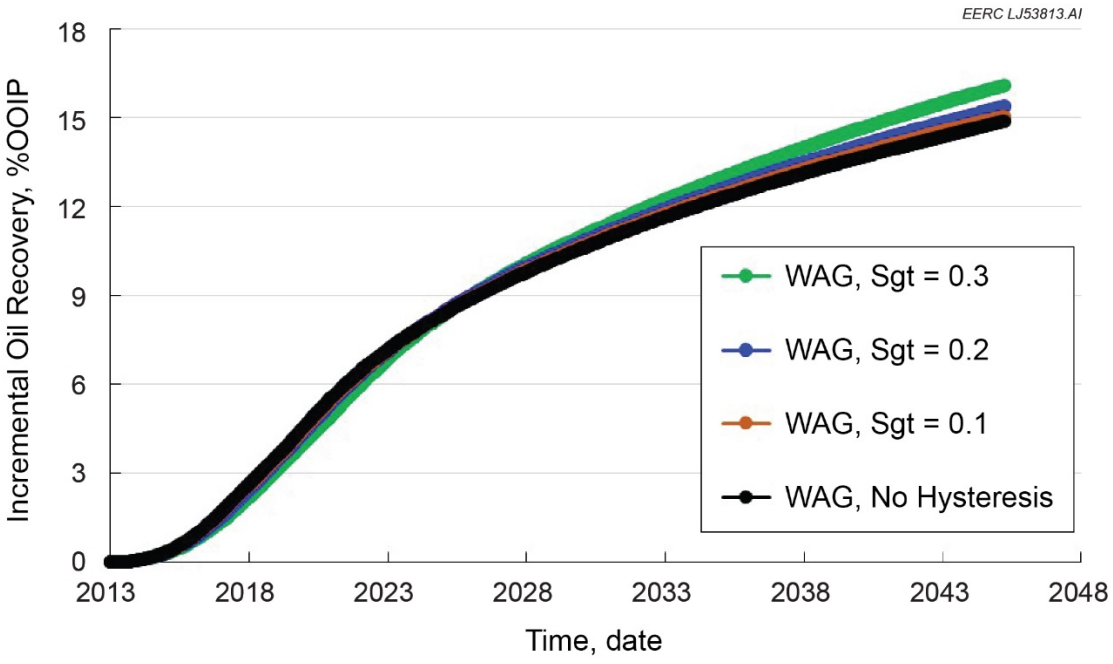

Figure 30. Comparison of incremental oil recovery for cases with different residual CO_2 saturations.

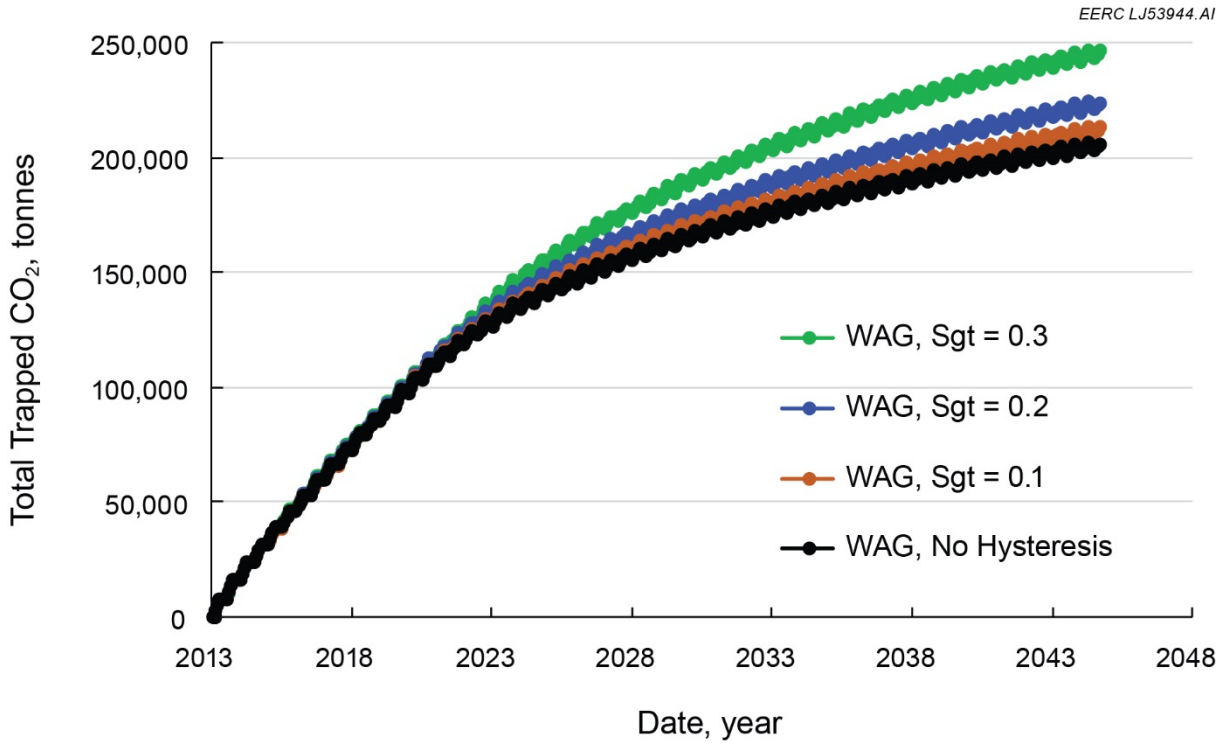

Figure 31. Comparison of CO_2 trapped for cases with different residual CO_2 saturations.

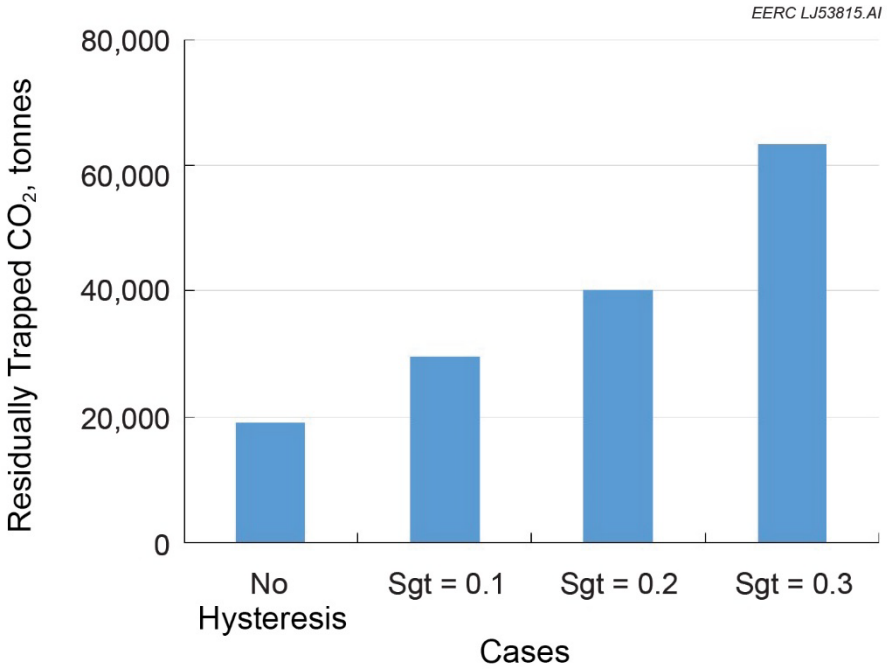

Figure 32. Comparison of CO_2 trapped by residual trapping for different residual CO_2 saturations.

factors, including temperature, pressure, salinity, and oil composition. The solubility of CO_2 in brine decreases with increasing temperature and salinity and increases with increasing pressure. Diffusion results in migration of dissolved CO_2 outward from the immediate contact zone, although this process is slow (Jin and others, 2016b).

The densities of oil and water increase when CO_2 is dissolved in the fluids, which may create gravitational instability in the reservoir leading to convective mixing of fluids. The mixing of fluids with differing dissolved CO_2 content will further enhance the dissolution process in the long run (Szulczewski and others, 2013). CO_2 dissolution is considered a significant trapping mechanism in deep saline formations, with potential to permanently store large amounts of CO_2 (Bachu and Adams, 2003; Metz and others, 2005; Bachu and Bennion, 2007; Ampomah and others, 2016).

CO_2–oil interaction has been studied extensively by the petroleum industry. CO_2 dissolution in oil is the primary mechanism for CO_2 EOR, in which dissolved CO_2 changes the oil's physical properties, yielding important benefits to recovery. Through this process, oil swells with CO_2 in solution, and oil viscosity is reduced, effectively increasing oil mobility (thus, oil recovery). However, the results of this process differ with changing pressure, oil composition, and impurities in the CO_2 stream. Additionally, injection gas composition and schedule may change over time through operational practices (e.g., recycled gas injection). Another complication is posed by changing fluid saturations within the reservoir (decreasing oil saturation relative to water saturation). Within the oil phase, specifically, the CO_2 EOR process preferentially mobilizes "lighter" hydrocarbon species (short-chain hydrocarbons) in comparison to "heavier" hydrocarbon species (long-chain hydrocarbons) (Hawthorne and others, 2014). This results in changing oil composition over time. Therefore, understanding CO_2 dissolution in oil is critical for successful CO_2-flooding projects. Several correlations have been developed to calculate CO_2 solubility in oil, including those of Simon and Graue (1965), Mehrotra and Svrcek (1982), Chung and others (1988), Emera and Sarma (2007), Al-Jarba and Al-Anazi (2009).

Simulating the Effects of Solubility Trapping

In reservoir simulation, the interactions between CO_2 and oil are computed by the cubic equations of state (EOS) because of the complex phase behavior involved in the simulation process. CO_2 solubility in the aqueous phase is calculated using Henry's Law (Mulliken and Sandler, 1980; Li and Nghiem, 1986; Computer Modelling Group, 2014).

Using the same five-spot model developed for Bell Creek (Jin and others, 2016), simulations accounting for CO_2 dissolution in water and oil were conducted. The results of cases assuming different residual CO_2 saturations are shown in Figure 33. The results indicate CO_2 solubility in oil is much greater ($\geq$5 times) than that of water. Residual oil saturation after waterflooding is usually 0.3 or greater in most conventional oil reservoirs. The simulation results also show that more CO_2 is dissolved when the trapped CO_2 saturation is higher, as more CO_2 is available to interact with oil and water in the pore space.

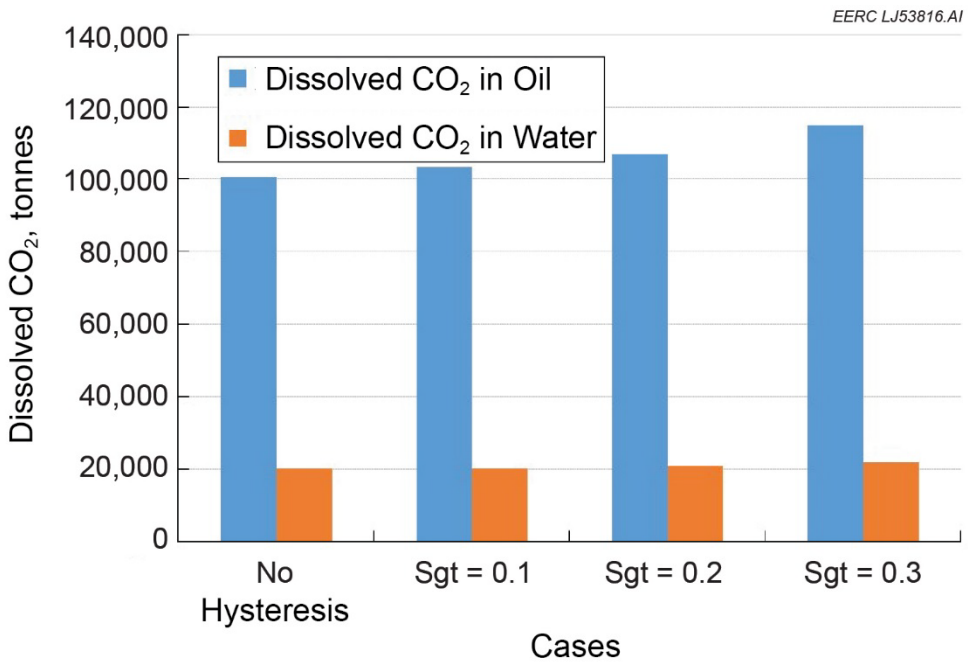

Figure 33. Comparison of simulated dissolved CO_2 for cases with different residual CO_2 saturations.

Structural/Stratigraphic Trapping of CO_2 in Bell Creek

Structural trapping occurs when buoyant forces immobilize injected CO_2 against low-permeability capping units within subsurface structures. CO_2 may migrate laterally through permeable strata below a sealing unit but vertical migration is inhibited, as CO_2 is not able to overcome capillary forces in tight, water-saturated sealing units (Zhou and others, 2008; Birkholzer and others, 2009; Cavanagh and Wildgust, 2011; Bachu, 2015).

The idea of stratigraphic trapping deals with heterogeneity, both vertical and lateral, in which reservoir-quality rock transitions to impermeable facies, such as a structural updip pinch-out of a sandstone bed against underlying and overlying shale units. Stratigraphic traps may be formed through lateral facies migration during deposition, erosional truncation, natural hydrodynamics, and diagenesis (Gerard, 2009).

Both stratigraphic and structural trapping mechanisms are important in the Bell Creek Field. The overlying Lower Cretaceous Mowry Shale provides the primary seal, preventing fluid migration to overlying aquifers and to the surface. The Muddy Formation within the field has gently dipping structure (Bell Creek sits on a shallow monocline with a 1°–2° dip to the northwest). An updip pinch-out of the Muddy sands against the overlying Springen Ranch shale and underlying Skull Creek shale occurs to the north and east of the field. Even within the field, local stratigraphic and structural traps are noted. Within the Muddy depositional framework, lateral facies changes and erosional processes have created permeability barriers resulting in compartmentalization. These characteristics have provided the trap for hydrocarbon accumulation in the field. Similarly, these characteristics are important for trapping CO_2 within the field.

Long-Term Simulation Assessment of Structural/Stratigraphic CO_2 Trapping

A history-matched simulation model encompassing both Phases 1 and 2, previously developed and calibrated with 3-D and 4-D seismic interpretations (discussed by Bosshart and others [2015] and Jin and others [2016a]) was used in numerical simulations to better predict reservoir performance and verify CO_2 containment. Figure 34 shows the extent of the model.

Based on the history-matched model, CCI and WAG cases (one each) were simulated to evaluate the long-term structural/stratigraphic CO_2 trapping in the reservoir. The minimum BHP constraint was set at 2300 psi for all production wells (both cases). The maximum injection pressure constraint was 2800 psi for all injection wells (both cases). The CO_2 injection rate for each well was set at the previous 6-month average value of that well. The water injection rate was set at 1675 barrels per day (bpd) and 1110 bpd for injection wells in the Phase 1 and 2 areas, respectively. The WAG case operational schedule was set as a 3-month, 1:1 cycle for water and CO_2 injection. Both CCI and WAG injection were simulated from 2016 to 2060, followed by a complete well shut-in and long-term monitoring simulation (1040 years) without fluid production and pressure depletion.

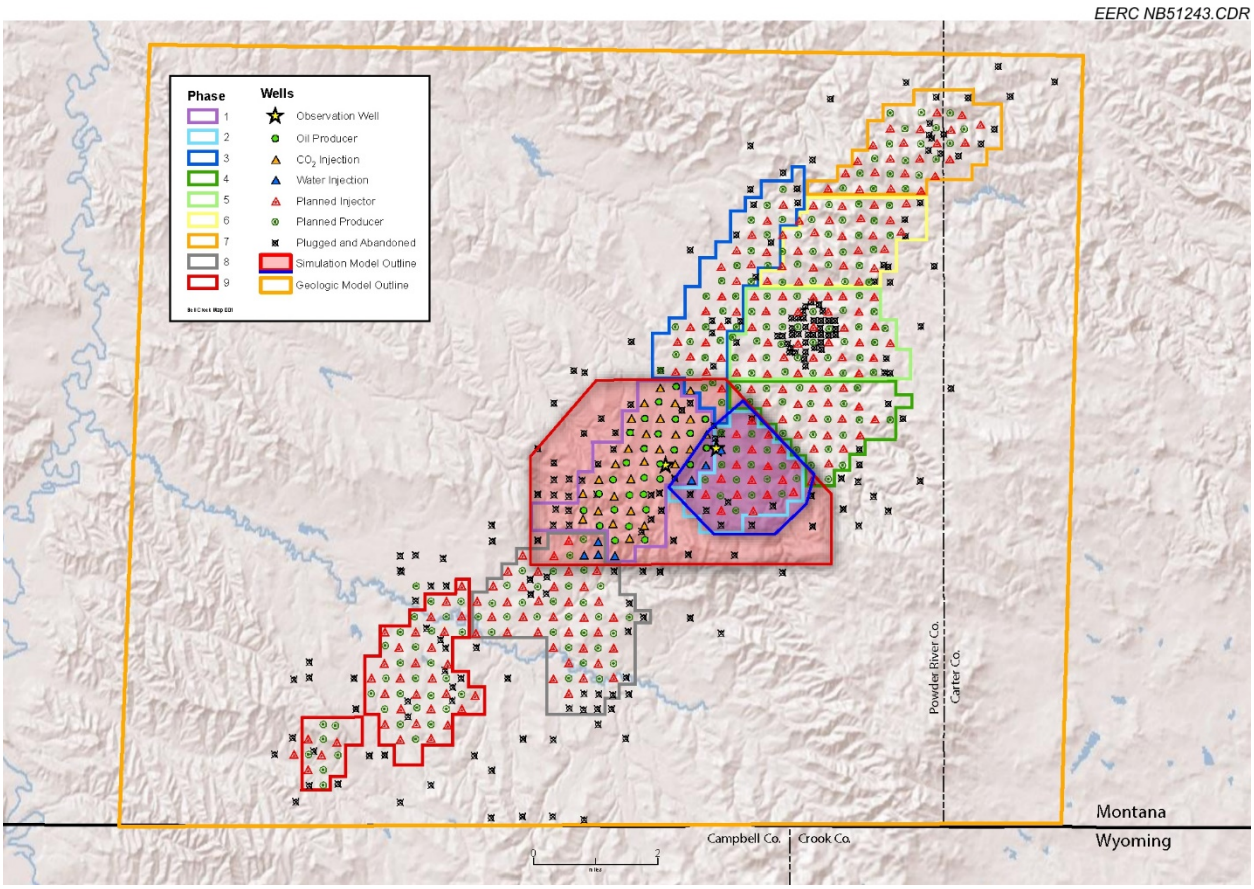

Figure 34. Schematic of the combined Phase 1 and 2 simulation model extent (the area shaded in red and blue; the area shaded in blue represents the extent of the previously developed individual Phase 2 simulation model).

Figures 35 and 36 show the distribution of injected CO_2 in the reservoir during the postinjection period for the CCI and WAG cases, respectively. These simulation results illustrate a prominent permeability barrier separating the two phases, with the exception of a small area where interphase fluid flow occurs. Simulation results indicated that, for this scenario, 12 million tonnes of CO_2 is predicted to be trapped in Phases 1 and 2 following CCI. The CO_2 in Phase 1 tended to move toward the eastern boundary of the phase over time, banking against the permeability barrier, as the reservoir has a 1°–2° dip to the northwest. A portion of the injected CO_2 flowed across the permeability barrier to the Phase 2 area. However, migration velocity was very slow (especially after 340 years), and the shape of the CO_2 saturation front did not change significantly from 700 to 1040 years. A similar result was observed in the WAG case, but with a smaller amount of trapped CO_2 (approximately 5 million tonnes of CO_2 was stored in the area). This also suggests that WAG is much more effective (by a factor of 2.4) for CO_2 EOR. The simulation results for both CCI and WAG cases clearly indicate the effectiveness of structural/stratigraphic trapping in the Phase 1 and 2 area, suggesting limited CO_2 migration potential exists (lateral or vertical) over a long postinjection time frame.

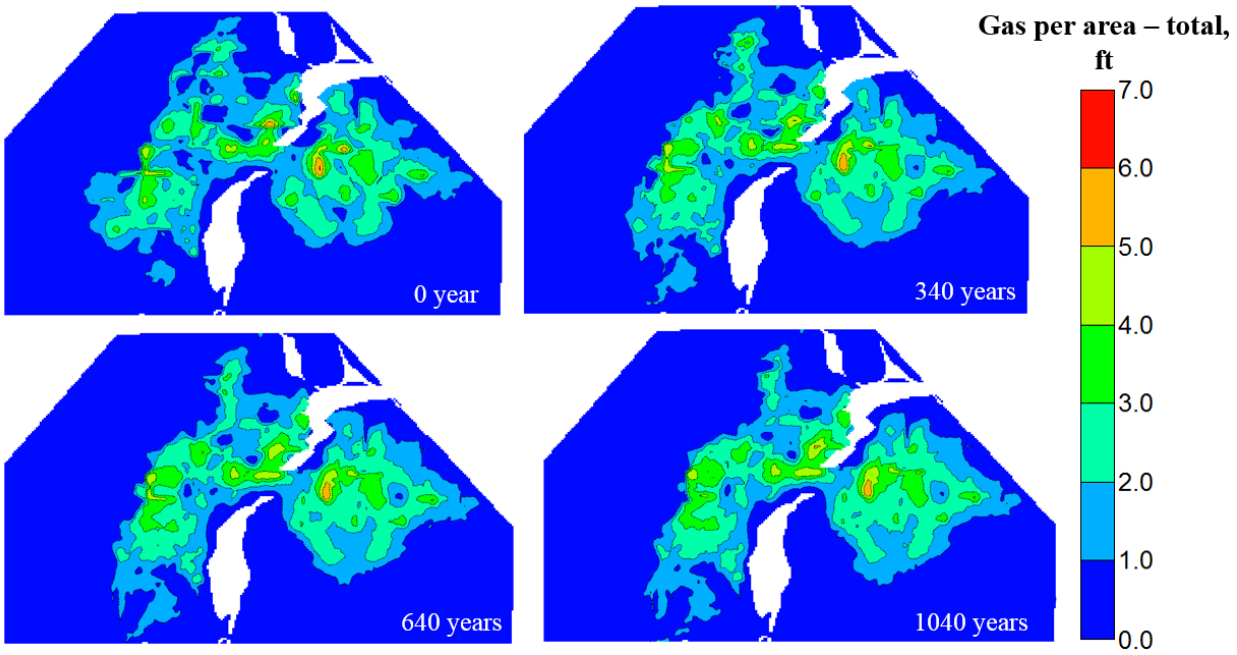

Figure 35. Post-CCI plume development in the Phase 1 and 2 areas.

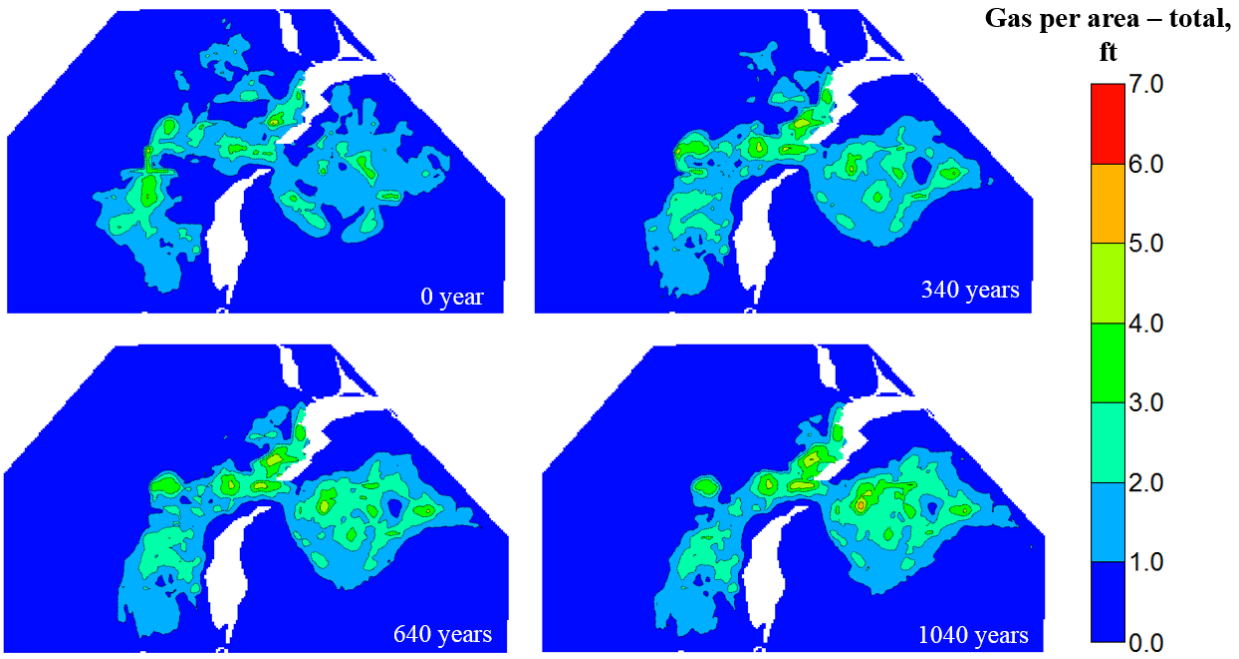

Figure 36. Post-WAG injection CO_2 plume development in the Phase 1 and 2 areas.

LIMITATIONS

The V3 model employed a complex, multiple-point statistics facies distribution using separate training images for different geobody regions. The training images created to guide facies distributions may have oversimplified lateral/vertical facies relationships. Additionally, areas of the model with limited data coverage (legacy well logs, seismic, core data, etc.) have greater uncertainty. Additional realizations of facies distributions (guided by history-matching results) may provide a better understanding of the geology in these areas.

Although meaningful simulation results have been presented here, a limited number of cases were conducted, and some case studies were based on small-scale models (e.g., the residual and solubility trapping evaluations). A more detailed sensitivity study for key parameters using a comprehensive simulation model will provide a better understanding of controlling factors for CO_2 EOR and associated storage in the field. Also, various field cases have shown that waterflooding may induce fractures within the reservoir, especially in the near-wellbore region. Such fractures may change flow patterns and impact sweep efficiency during CO_2 flooding. These factors may be investigated in future studies to better assist field operations.

SUMMARY

During the last year (August 2016 to August 2017), activities conducted for the Bell Creek Field and reported in this document included acquisition of new data (PNLs and InSAR data), completion of the V3 geologic model, history matching and predictive simulations in the Phase 4 area, integration of relative permeability hysteresis into the simulation models, and assessment of storage potential based on different CO_2 trapping mechanisms. Key highlights and results of the current modeling and simulation activities are summarized below:

- During the 2017 PNL campaign, 11 wells were chosen for repeat/monitor logging in Phases 1 and 3. The combination of baseline and repeat/monitor PNLs has aided in the monitoring of the WAG flood front and provided insight into the fluid saturation changes (CO_2, water, oil). A total of 92 PNLs have been acquired in 45 wells in the Bell Creek Field.

- Two phases of InSAR data analysis have been completed to date. The first phase, consisting of lower-resolution ALOS data, was conducted prior to CO_2 injection in the field. The second phase, consisting of higher-resolution CSK data, was conducted during the field's operational phase. Data from a third phase has been received, but analysis is not complete as of this report's development.

- Integration of 3-D and 4-D seismic data, PNLs, legacy well logs, and core analyses has resulted in a revised geologic interpretation (Bosshart and others, 2015; Jin and others, 2016a) which has provided the basis for the completion of the V3 geologic model.

- Seven geobody regions were identified from seismic data within the Bell Creek Field. Vertical and lateral facies associations within each geobody were determined from the interpretation of well logs. Facies were distributed throughout the field using multiple-point statistics, using training images informed by type logs for each geobody.

- Petrophysical properties were conditioned to the facies model using variogram-based geostatistical methods. Variograms calculated for each facies within the reservoir showed the most rapid variance in petrophysical properties occurring perpendicular to the interpreted shoreline (northwest to southeast), further strengthening the revised geologic interpretation.

- The reservoir was partitioned into five separate flow units based on modeled petrophysical properties. A J-function, calibrated to each flow unit by core analysis data and high-pressure mercury injection data, was used to distribute water saturation values throughout the field.

- A dynamic simulation model for the Phase 4 area was constructed from the V3 geologic model. A reasonable history match was achieved for 49 years of field records with primary production, waterflooding, and CO_2 EOR stages.

- Individual well production performance in the Phase 4 area was analyzed to evaluate boundary conditions and water saturation in the reservoir. Although there was no evident edge water (aquifer support) connected to the pay zone, local water invasion was obvious in some portions of the reservoir.

- CCI and WAG predictive simulations with different pressure settings were conducted for the Phase 4 area to assess oil recovery and associated CO_2 storage performance.

- CO_2-trapping mechanisms in the reservoir were analyzed. Three major CO_2-trapping mechanisms responsible for associated storage in the Bell Creek were identified: structural/stratigraphic trapping, residual trapping, and solubility trapping.

- Steady-state relative permeability tests were performed to derive the gas-phase relative permeability curves using a clean sandstone core sample collected from Well 05-06-OW. The effects of hysteresis were identified from the drainage and imbibition CO_2 relative permeability curves. The curves were integrated within a five-spot simulation model to investigate the effect of residual trapping on CO_2 EOR and storage performance. Results showed that residual trapping does not have a significant effect on oil recovery factor. Intuitively, higher trapped CO_2 saturation leads to more associated CO_2 storage.

- The five-spot simulation model was also used to investigate solubility trapping of CO_2 in the reservoir. Based on the fluid properties and reservoir conditions in the Bell Creek, CO_2 solubility in oil is much greater ($\geq$5 times) than that in water.

- A series of seismic monitoring activities have been conducted to detect/track the injected CO_2 and pressure distribution, ensuring safe associated CO_2 storage in the reservoir. Data collected from a 4-D seismic survey were used to calibrate the combined Phases 1 and 2 model, which was then used to predict the long-term CO_2 trapping (1040 years postinjection) in the area. Results showed that CO_2 was effectively trapped in the Phase 1 and 2 area under the effects of structural/stratigraphic trapping.

KEY ADVANCEMENTS

1. Version 3 geologic model – The integration of 3-D and 4-D seismic data and PNL logs with legacy well logs and core data has allowed a revised depositional interpretation to be incorporated into the V3 geologic model. The revised depositional interpretation and increased representation of compartmentalization through the modeling of a large number of facies in separate geobodies allowed for a more realistic representation of the geologic heterogeneity in the Bell Creek Field. This made areas in which petrophysical properties were apparently inaccurate (did not match with historic injection and production data) more easily identifiable. These apparently inaccurate properties could then be narrowed down to a particular facies within a defined geobody and be recalculated to better reflect the understanding gained from the history-matching process.

2. Evaluation of Associated CO_2 Storage in the Bell Creek Reservoir – Besides history matching of production/injection data and prediction of different EOR operational schemes, the performance of associated CO_2 storage in the Bell Creek Reservoir was also evaluated by considering three primary CO_2 trapping mechanisms: structural/stratigraphic, residual, and solubility trapping. The results showed that the Bell Creek reservoir is not only suitable for CO_2 EOR but also a good site for associated CO_2 storage.

3. Integration of Measured Relative Permeability Hysteresis Curves into Simulation – Because of the importance of relative permeability hysteresis on CO_2 flowing behavior in the reservoir, a set of CO_2 hysteretic curves were measured using a clean sandstone core sample collected from Bell Creek's 05-06OW (observation well) at a depth of 4533 ft. The curves were integrated into a five-spot model developed for Bell Creek. Results showed that significantly more CO_2 (up to 20%) could be trapped in the reservoir by considering the CO_2 hysteresis effect.

ONGOING AND FUTURE WORK

Areas of future research have been identified and are discussed below. However, the PCOR Partnership Program currently has no scheduled activities beyond the end of 2018, and the identified activities will only be conducted if deemed agreeable with the remaining PCOR Partnership Program time line and budget. This D66 – Bell Creek Simulation Report (Update 6) is currently the last simulation update report unless future activities are scheduled and supported under the PCOR Partnership Program.

Geologic Modeling and Reservoir Simulation

Although the PCOR Partnership currently has scope and budget through the end of 2018, the CO_2 EOR project in the Bell Creek Field will likely continue for many years. At present, CO_2 injection has taken place in four of the nine phase areas of the field (Phases 1 through 4), with plans to initiate injection in Phase 5 before the end of 2017. In the coming years, CO_2 injection is planned in Phases 6–9.

Seismic, PNL, injection/production, and core data have allowed for very thorough characterization, risk assessment, risk management, and MVA programs for CO_2 EOR and associated CO_2 storage in the Bell Creek Field. Additional data acquired before the scheduled end of the PCOR Partnership Program may be integrated in the V3 geologic model, and simulation models may be updated for better prediction of CO_2 distribution in the reservoir.

Effects of Heterogeneity on CO_2 Flooding

WAG injection technologies have been widely applied to improve CO_2 sweep efficiency and enhance oil recovery (Harpole and Hallenbeck, 1996; Zhou and others, 2012; Braunberger and others, 2013; Han and Gu, 2014). However, injectivity abnormalities caused by reservoir heterogeneity, especially in reservoirs with complex geologic conditions, can adversely affect the success and the economic feasibility of the CO_2-flooding processes (Saneifar and others, 2016). Bell Creek has complicated reservoir property and fluids saturation distributions, because of the

processes active during Muddy Formation deposition and a lengthy production history. Therefore, future efforts investigating and quantifying the effects of reservoir heterogeneity on CO_2 flooding and associated storage performance in the field would be appropriate.

Effects of Induced Fractures on CO_2 Flooding

Waterflooding has been conducted to improve oil production after primary production for more than 30 years in the Bell Creek. Large volumes of water injection may have created fractures in a limited area around injectors. These fractures may connect to the high-permeability paths in the reservoir, forming preferable flow channels between injectors and producers. Rapid increases in water production and changes in water cuts that vary with injection rates support an interpretation of induced fractures and high-conductivity flow paths between injection and production wells (Koning and Niko, 1985; Baker and others, 2016). However, water and CO_2 are cyclically injected in Bell Creek, and the cyclic injection may reduce the effective fluid mobility in all rock types, irrespective of their petrophysical properties and flow characteristics. Thus a greater fraction of fluids would flow through fractures, resulting in poor frontal advancement in rock with lower permeability, reduced overall injectivity, and loss of WAG operational efficiency. Therefore, it is beneficial to evaluate the effects of induced fractures on reservoir performance using a Bell Creek simulation model.

Asphaltene Deposition during CO_2 Flooding

Injected CO_2 (solvent) can induce flocculation and deposition of asphaltene and other heavy organic particles during the miscible displacement process (Srivastava and others, 1999; Zekri and others, 2009; Zhao and others, 2016). After precipitation, asphaltene can remain as a suspended solid in the oil or adhere to the rock, which may alter wettability (from water-wet to oil-wet) and/or plug pore throats. This process may create challenging production problems and detrimental effects on oil recovery. These aspects are well known from investigations in many other reservoirs and have been observed in Bell Creek Field/laboratory activities. Because wettability is strongly related to relative permeability and pore throat size is critical for the flow efficiency, an investigation of the effects of asphaltene deposition on CO_2 EOR and associated storage in the Bell Creek Field may provide important insight.

REFERENCES

Al-Jarba, M., and Al-Anazi, B.D., 2009, A comparison study of the of the CO_2-oil physical properties – literature correlations accuracy using visual basic modeling technique: Oil and Gas Business, May 30.

Al-Menhali, A.S., and Krevor, S., 2016, Capillary trapping of CO_2 in oil reservoirs—observations in a mixed-wet carbonate rock: Environmental Science & Technology, v. 50, no. 5, p. 2727–34.

Amaefule, J., and Mehmet, A., 1993, Enhanced reservoir description—using core and log data to identify hydraulic flow units and predict permeability in uncored intervals/wells: Presented at the 68th Annual Technical Conference and Exhibition, SPE 26436.

Amaefule, J.O., Altunbay, M., Tiab, D., Kersey, D.G., and Keelan, D.K., 1993, Enhanced reservoir description—using core and log data to identify hydraulic (flow) units and predict permeability in uncored intervals/wells: Presented in SPE Annual Technical Conference and Exhibition, Society of Petroleum Engineers, January 1.

Ampomah, W., Balch, R., Cather, M., Rose-Coss, D., Dai, Z., Heath, J., Dewers, T., and Mozley, P., 2016, Evaluation of CO_2 storage mechanisms in CO_2 enhanced oil recovery sites—application to Morrow sandstone reservoir: Energy & Fuels, v. 30, no. 10, p. 8545–55.

Ayash, S.C., Nakles, D.V., Wildgust, N., Peck, W.D., Sorensen, J.A., Glazewski, K.A., Aulich, T.R., Klapperich, R.J., Azzolina, N.A., and Gorecki, C.D., 2017, Best practice for the commercial deployment of carbon dioxide geologic storage—the adaptive management approach: Plains CO_2 Reduction (PCOR) Partnership Phase III Task 13 Deliverable D102/Milestone M59 for U.S. Department of Energy National Energy Technology Laboratory Cooperative Agreement No. DE-FC26-05NT42592, EERC Publication 2017-EERC-05-01, Grand Forks, North Dakota, Energy & Environmental Research Center, May.

Bachu, S., 2015, Review of CO_2 storage efficiency in deep saline aquifers: International Journal of Greenhouse Gas Control, v. 40, p. 188–202.

Bachu, S., and Adams, J.J., 2003, Sequestration of CO_2 in geological media in response to climate change—capacity of deep saline aquifers to sequester CO_2 in solution: Energy Conversion and Management, v. 44, no. 20, p. 3151–75.

Bachu, S., and Bennion, B., 2007, Effects of in-situ conditions on relative permeability characteristics of CO_2—brine systems: Environmental Geology, v. 54, no. 8.

Baker, R., Dieva, R., Jobling, R., and Lok, C., 2016, The myths of waterfloods, EOR floods and how to optimize real injection schemes: Presented in SPE Improved Oil Recovery Conference, Society of Petroleum Engineers, April 11.

Birkholzer, J.T., Zhou, Q., and Tsang, C.F., 2009, Large-scale impact of CO_2 storage in deep saline aquifers—a sensitivity study on pressure response in stratified systems: International Journal of Greenhouse Gas Control, v. 3, p. 181–194.

Bosshart, N.W., Jin, L., Dotzenrod, N.W., Burnison, S.A., Ge, J., He, J., Burton-Kelly, M.E., Ayash, S.C., Gorecki, C.D., Hamling, J.A., Steadman, E.N., and Harju, J.A., 2015, Bell Creek test site—simulation report: Plains CO_2 Reduction (PCOR) Partnership Phase III Task 9 Deliverable D66 (Update 4) for U.S. Department of Energy National Energy Technology Laboratory Cooperative Agreement No. DE-FC26-05NT42592, EERC Publication: EERC-10-09, Grand Forks, North Dakota, Energy & Environmental Research Center, August.

Braunberger, J.R., Pu, H., Gorecki, C.D., Bailey, T.P., Bremer, J.M., Peck, W.D., Gao, P., Ayash, S.C., Liu, G., Hamling, J.A., Steadman, E.N., and Harju, J.A., 2013, Bell Creek test site—simulation report: Plains CO_2 Reduction (PCOR) Partnership Phase III Task 9 Deliverable D66 Update 2 for U.S. Department of Energy National Energy Technology Laboratory Cooperative Agreement No. DE-FC26-05NT42592, August.

Burnison, S.A., Bosshart, N.W., Salako, O., Reed, S., Hamling, J.A., and Gorecki, C.D., 2017, 4-D seismic monitoring of injected CO_2 enhances geological interpretation, reservoir simulation, and production operations: Energy Procedia, v. 114, p. 2748–2759.

Burnside, N.M., and Naylor, M., 2014, Review and implications of relative permeability of CO_2/brine systems and residual trapping of CO_2: International Journal of Greenhouse Gas Control, v. 23, p. 1–1.

Burt, R.A., Haddenhorst, F.A., and Hartford, J.C., 1975, Review of Bell Creek waterflood performance—Powder River, Montana: Society of Petroleum Engineers (SPE) Paper 5670, Journal of Petroleum Technology, v. 27, no. 12.

Caers, J., and Zhang, T., 2004, Multiple point geostatistics: A quantitative vehicle for integrating geologic analogs into multiple reservoir models, *in* Integration of outcrop and modern analogs in reservoir modeling: AAPG Memoir, v. 80, p. 383–394.

Cavanagh, A.J., and Wildgust, N., 2011, Pressurization and brine displacement issues for deep saline formation CO_2 storage: Energy Procedia, v. 4, p. 4814–4821, DOI:10.1016/j.egypro. 2011.02.447.

Chung, F.T., Jones, R.A., and Nguyen, H.T., 1988, Measurements and correlations of the physical properties of CO_2-heavy crude oil mixtures: SPE Reservoir Engineering, v. 3, no. 3, p. 822–8.

Computer Modelling Group, 2014, WinProp. user guide—phase behavior & fluid property program, Version 2014.

Emera, M.K., and Sarma, H.K., 2007, Prediction of CO_2 solubility in oil and the effects on the oil physical properties: Energy Sources, Part A. v. 29, no. 13, p. 1233–42.

Ennis-King, J., Paterson, L.I., 2001, Reservoir engineering issues in the geological disposal of carbon dioxide, *in* Fifth International Conference on Greenhouse Gas Control Technologies: Cairns, v. 1, p. 290–295.

Farnham, F.E., and Haddenhorst, F.A., 1972, Four and one-half years—discovery to unitized operation of the major, multi-reservoir Bell Creek Field, *in* SPE Rocky Mountain Regional Meeting: Society of Petroleum Engineers, January 1.

Fatemi, S.M., Sohrabi, M., Jamiolahmady, M., and Ireland, S., 2012, Experimental and theoretical investigation of gas/oil relative permeability hysteresis under low oil/gas interfacial tension and mixed-wet conditions: Energy & Fuels, v. 26, no. 7, p. 4366–82.

Gerard, J., 2009, Stratigraphic traps—quantitative approach based upon a producing field database: American Association of Petroleum Geologists, Search and Discovery Article #40436, AAPG Annual Convention, Denver, Colorado, June 7–10.

Gorecki, C., Hamling, J., Klapperich, R., Steadman, E., and Harju, J., 2012, Integrating CO_2 EOR and CO_2 storage in the Bell Creek oil field: Presented at Carbon Management Technology Conference, Paper 151476.

Hamling, J.A., Gorecki, C.D., Klapperich, R.J., Saini, D., and Steadman, E.N., 2013, Overview of the Bell Creek combined CO_2 storage and CO_2 enhanced oil recovery project: Energy Procedia, v. 37, p. 6402–11.

Han, L., and Gu, Y., 2014, Optimization of miscible CO_2 water-alternating-gas injection in the Bakken Formation: Energy & Fuels, v. 28, no. 11, p. 6811–9.

Harpole, K.J., and Hallenbeck, L.D., 1996, East Vacuum Grayburg San Andres Unit CO_2 flood ten year performance review—evolution of a reservoir management strategy and results of WAG optimization, *in* SPE Annual Technical Conference and Exhibition: Society of Petroleum Engineers, January 1.

Hawthorne, S.B., Miller, D.J., Gorecki, C.D., Sorensen, J.A., Hamling, J.A., Roen, T.D., Harju, J.A., and Melzer, S., 2014, A rapid method for determining CO_2/Oil MMP and visual observations of CO_2/oil interactions at reservoir conditions: Energy Procedia, v. 63, p. 7724–7731.

Intergovernmental Panel on Climate Change, 2005, IPCC special report on carbon dioxide capture and storage: Prepared by Working Group III of the Intergovernmental Panel on Climate Change, Metz, B., Davidson, O., de Coninck, H.C., Loos, M., and Meyer, L.A., eds., Cambridge University Press, Cambridge, United Kingdom and New York, NY, USA, 442 p.

Jin, L., Bosshart, N.W., Oster, B.S., Hawthorne, S.B., Peterson, K.J., Burton-Kelly, M.E., Feole, I.K., Jiang, T., Pekot, L.J., Peck, W.D., Ayash, S.C., and Gorecki, C.D., 2016a, Bell Creek test site – simulation report: Plains CO_2 Reduction (PCOR) Partnership Phase III draft Task 9 Deliverable D66 (Update 5) executive summary for U.S. Department of Energy National Energy Technology Laboratory Cooperative Agreement No. DE-FC26-05NT42592, Grand Forks, North Dakota, Energy & Environmental Research Center, August.

Jin, L., Sorensen, J., Hawthorne, S., Smith, S., Pekot, L., Bosshart, N., Burton-Kelly, M., Miller, D., Grabanski, C., Gorecki, C., and Steadman, E., 2016b, Improving oil recovery by use of carbon dioxide in the Bakken Unconventional System—a laboratory investigation: SPE Reservoir Evaluation & Engineering, December 1.

Koning, E.J., and Niko, H., 1985, Fractured water-injection wells—a pressure falloff test for determining fracture dimensions: InSPE Annual Technical Conference and Exhibition, Society of Petroleum Engineers, January 1.

Krevor, S., Blunt, M.J., Benson, S.M., Pentland, C.H., Reynolds, C., Al-Menhali, A., and Niu, B., 2015, Capillary trapping for geologic carbon dioxide storage—from pore scale physics to field scale implications: International Journal of Greenhouse Gas Control, v. 40, p. 221–37.

Krevor, S., Pini, R., Zuo, L., and Benson, S.M., 2012, Relative permeability and trapping of CO_2 and water in sandstone rocks at reservoir conditions: Water Resources Research, v. 48, no. 2.

Kumar, N., and Sanders, J.E., 1974, Inlet sequence—a vertical succession of sedimentary structures and textures created by the lateral migration of tidal inlets: Sedimentology, v. 21, no. 4, p. 491–532.

Larsen, J.A., and Skauge, A., 1998, Methodology for numerical simulation with cycle-dependent relative permeabilities: SPE Journal, v. 3, no. 2, p. 163–73.

Leverett, M.C., 1941, Capillary behaviour in porous solids: Transactions of the AIME, v. 142, p. 159–172.

Li, Y.K., and Nghiem, L.X., 1986, Phase equilibria of oil, gas and water/brine mixtures from a cubic equation of state and Henry's law: The Canadian Journal of Chemical Engineering, v. 64, no. 3, p. 486–96.

Liu, G., Braunberger, J.R., Pu, H., Gao, P., Gorecki, C.D., Ge, J., Klenner, R.C.L., Bailey, T.P., Dotzenrod, N.W., Bosshart, N.W., Ayash, S.C., Hamling, J.A., Steadman, E.N., and Harju, J.A., 2014, Bell Creek test site – simulation report: Plains CO_2 Reduction (PCOR) Partnership Phase III Task 9 Deliverable D66 Update 4 for U.S. Department of Energy National Energy Technology Laboratory Cooperative Agreement No. DE-FC26-05NT42592, August.

McGrail, B.P., Schaef, H.T., Ho, A.M., Chien, Y.J., Dooley, J.J., and Davidson, C.L., 2006, Potential for carbon dioxide sequestration in flood basalts: Journal of Geophysical Research: Solid Earth, v. 111, no. B12.

McGrail, B.P., Schaef, H.T., Spane, F.A., Cliff, J.B., Qafoku, O., Horner, J.A., Thompson, C.J., Owen, A.T., and Sullivan, C.E., 2016, Field validation of supercritical CO_2 reactivity with basalts: Environmental Science & Technology Letters, v. 4, no. 1, p. 6–10.

Mehrotra, A.K., and Svrcek, W.Y., 1982, Correlations for properties of bitumen saturated with CO_2, CH_4 and N_2, and experiments with combustion gas mixtures: Journal of Canadian Petroleum Technology, v. 21, no. 06.

Metz, B., Davidson, O., De Coninck, H., Loos, M., and Meyer, L., 2005, IPCC special report on carbon dioxide capture and storage: Intergovernmental Panel on Climate Change, Geneva (Switzerland), Working Group III, July 1.

Molnar, P.S., 1990, Geologic reservoir study of the Bell Creek Field, Carter and Powder River Counties, Montana: Midland, Texas, Exxon Company.

Mulliken, C.A., and Sandler, S.I., 1980, The prediction of CO_2 solubility and swelling factors for enhanced oil recovery: Industrial & Engineering Chemistry Process Design and Development, v. 19, no. 4, p. 709–11.

Niu, B., Al-Menhali, A., and Krevor, S.C., 2015, The impact of reservoir conditions on the residual trapping of carbon dioxide in Berea sandstone: Water Resources Research, v. 51, no. 4, p. 2009–29.

Pu, H., Hamling, J.A., Bremer, J.M., Bailey, T.P., Braunberger, J.R., Ge, J., Saini, D., Sorensen, J.A., Gorecki, C.D., Steadman, E.N., and Harju, J.A., 2011, Bell Creek test site—simulation report: Plains CO_2 Reduction (PCOR) Partnership Phase III Task 9 Deliverable D66 for U.S. Department of Energy National Energy Technology Laboratory Cooperative Agreement No. DE-FC26-05NT42592, August.

Saini, D., Braunberger, J.R., Pu, H., Bailey, T.P., Ge, J., Crotty, C.M., Liu, G., Hamling, J.A., Gorecki, C.D., Steadman, E.N., and Harju, J.A., 2012, Bell Creek test site – simulation report: Plains CO_2 Reduction (PCOR) Partnership Phase III Task 9 Deliverable D66 Update 1 for U.S. Department of Energy National Energy Technology Laboratory Cooperative Agreement No. DE-FC26-05NT42592, August.

Saneifar, M., Heidari, Z., Linroth, M., and Purba, S.A., 2016, Effect of heterogeneity on fluid-injectivity loss during water-alternating-gas injection in the Scurry Area Canyon Reef Operators Committee Unit: SPE Reservoir Evaluation & Engineering, November 1.

Simon, R., and Graue, D.J., 1965, Generalized correlations for predicting solubility, swelling and viscosity behavior of CO_2-crude oil systems: Journal of Petroleum Technology, v. 17, no. 01, p. 102–6.

Spiteri, E.J., Juanes, R., Blunt, M.J., and Orr, F.M., 2008, A new model of trapping and relative permeability hysteresis for all wettability characteristics: SPE Journal, v. 13, no. 03, p. 277–88.

Srivastava, R.K., Huang, S.S., and Dong, M., 1999, Asphaltene deposition during CO_2 flooding: SPE Production & Facilities, v. 14, no. 04, p. 235–45.

Steadman, E.N., Anagnost, K.K., Botnen, B.W., Botnen, L.A., Daly, D.J., Gorecki, C.D., Harju, J.A., Jensen, M.D., Peck, W.D., Romuld, L., and Smith, S.A., 2011, The Plains CO_2 Reduction (PCOR) Partnership—developing carbon management options for the central interior of North America: Energy Procedia. v. 4, p. 6061–8.

Strebelle, S.B., and Journel, A.G., 2001, Reservoir modeling using multiple-point statistics, *in* SPE Annual Technical Conference and Exhibition: Society of Petroleum Engineers, January 1.

Svirsky, D., Ryazanov, A., Pankov, M., Corbett, P.W., and Posysoev, A., 2004, Hydraulic flow units resolve reservoir description challenges in a Siberian Oil Field, *in* SPE Asia Pacific Conference on Integrated Modelling for Asset Management: Society of Petroleum Engineers, January 1.

Szulczewski, M.L., Hesse, M.A., and Juanes, R., 2013, Carbon dioxide dissolution in structural and stratigraphic traps: Journal of Fluid Mechanics. v. 736, p. 287–315.

Zekri, A.Y., Shedid, S.A., and Almehaideb, R.A., 2009, Sulfur and asphaltene deposition during CO_2 flooding of carbonate reservoirs, *in* SPE Middle East Oil and Gas Show and Conference: Society of Petroleum Engineers, January 1.

Zhao, Y., Wang, T., Song, Y., Liu, Y., Dong, B., and Zhu, N., 2016, Visualization of asphaltene deposition effects on porosity and permeability during CO_2 flooding in porous media: Journal of Visualization, v. 19, no. 4, p. 603–14.

Zhou, D., Yan, M., and Calvin, W.M., 2012, Optimization of a mature CO_2 flood—from continuous injection to WAG, *in* SPE Improved Oil Recovery Symposium: Society of Petroleum Engineers, January 1.

Zhou, Q., Birkholzer, J.T., Tsang, C.-F., and Rutqvist, J., 2008, A method for quick assessment of CO_2 storage capacity in closed and semi-closed saline formations: International Journal of Greenhouse Gas Control, v. 2, no. 4, p. 626–639.

Zuo, L., and Benson, S.M., 2014, Process-dependent residual trapping of CO_2 in sandstone: Geophysical Research Letters, v. 41, no. 8, p. 2820–6.

APPENDIX A

GEOLOGIC INTERPRETATION INTEGRATED WITHIN THE BELL CREEK VERSION 3 (V3) MODEL

GEOLOGIC INTERPRETATION INTEGRATED WITHIN THE BELL CREEK VERSION 3 (V3) MODEL

Following the geologic interpretation of Bosshart and others (2015) and Jin and others (2016), vertical and lateral facies associations were interpreted from well logs within each geobody. Type logs that showed typical local stratigraphy were selected for each of seven geobodies (geologically similar areas) within the reservoir in the Bell Creek Field (Figure A-1).

Jin and others (2016) include discussion of a revised depositional interpretation for the field after integration of modern data sets (seismic data and well logs):

> "The Bell Creek sand within the Bell Creek Field appears to have been deposited as two stratigraphic units resulting from a regressive–transgressive sequence split by lowstand subaerial exposure and erosion.
>
> "The lower Bell Creek sand was deposited as deltaic/shoreline progradation (regression) from the northeast toward the southwest during a period of relative sea level fall. The higher seismic amplitude feature(s) on the eastern edge of the field in Phases 4, 5, and 6 likely represent the finer-grained material deposited at the margins of the prograding delta/shoreline during early Bell Creek sand deposition. Following relative sea level fall, there is evidence of a brief sea level rise producing a relatively thin, fine-grained (siltstone/mudstone) layer overlying the regressive/prograding deposits below. This layer can vary within the Bell Creek sand interval both in stratigraphic position and thickness (3 to 5 feet thick on average). A period of relative sea level fall and subaerial exposure is interpreted to follow, as evidenced in core as a thin layer of coarser sand, disrupted bedding, and (in some locations) the presence of thin coals (either intact or plant fragments).
>
> "Following relative sea level fall and the deposition of regressive sands, the seas began to transgress from the southwest, forming barrier bar and lagoonal environments in the southwest part of the field. The seas continued to rise, causing the barrier bar and lagoonal environments to migrate to the northeast, and a tidal channel complex was formed in the southwest lagoonal region. A brief stillstand allowed a local barrier bar to form in Phases 1 and 2 along with an associated lagoon to the northeast along the boundaries between Phases 1–3 and Phases 2–4. These features, as noted in the seismic data, suggest the shoreline orientation at this time to be approximately northwest–southeast.
>
> "Visible in the seismic is a high-amplitude feature with sinuous character trending generally north to south along the Phase 1 and 2 boundary, cross-cutting the Phase 1 and 2 barrier bar and lagoonal deposits in a perpendicular manner. This feature coincides with a previously inferred permeability barrier (interpreted from pressure compartmentalization effects; Farnham and Haddenhorst, 1972; Molnar, 1990). From well log analysis, this hydraulic disconnection is due to erosion of nearly all reservoir-quality sand. The shape and scale of this feature resembles a fluvial incised valley, which explains the erosion and decreased sand thickness (Bosshart and others, 2015).

"Fluvial sediment, transported to the shallow marine environment seaward of the barrier bar, was carried southeast by longshore currents, was draped into the incised channel (developed previously during lowstand subaerial exposure), and provided a hydraulic link between Phases 1 and 2. After the establishment of this Phase 1 and 2 hydraulic connection, relative sea level rise resumed, resulting in the deposition of (mostly continuous) transgressive sheet sands in the northern regions of the field. These transgressive sands of the upper Bell Creek sand interval vary in thickness but are typically between 5 and 10 feet thick. This final transgression appears to have occurred quickly, burying and preserving all of these features (before wave-reworking made them indiscernible) with the overlying estuarine–shallow marine Springen Ranch deposits."

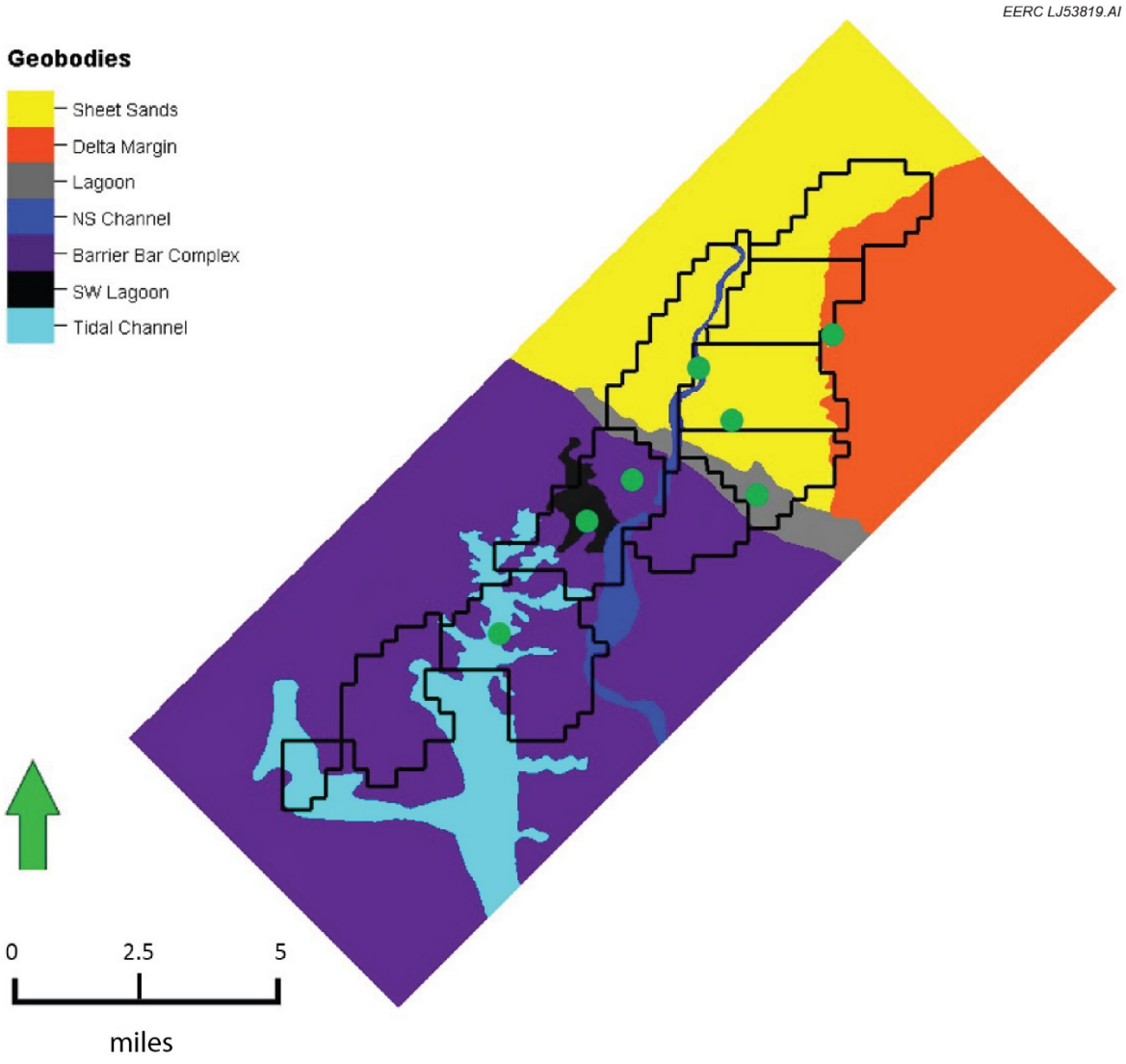

Figure A-1. Map view of V3 model study area showing spatial extent of each geobody and the location of the type log (green dots) used to generate training images for multiple-point statistics facies distribution in each geobody. Development phases are outlined in black.

Based on the interpretation of depositional environment outlined in Bosshart and others (2015) and Jin and others (2016), the lower Bell Creek Sand was deposited as a prograding delta front forced regression of the Western Interior Seaway. This sand unit is continuous across most of the study area, can range in thickness from approximately 5 to 15 feet, and is found in all geobodies except near the margin of the prograding delta (delta margin geobody).

The largest changes in the reservoir occur within the transgressive, upper Bell Creek Sand that overlies the regressive, lower Bell Creek Sand. Based on the revised depositional environment interpretation (Bosshart and others, 2015; Jin and others, 2016), the upper sand facies was deposited 1) as onlapping retrogradation occurred as the result of transgression or 2) through the formation of barrier bars in the southwest part of the field.

To better illustrate the geologic heterogeneity observed within differing geobodies in the Bell Creek Field, a series of "type logs" are contained in each of the following geobody interpretation sections.

Delta Margin Geobody

In the delta margin geobody (Figure A-2), the lower, prograding sand becomes silty and thins to the east. This change in lithology is represented by an increase in seismic amplitude, higher gamma ray signatures, and decreased resistivity readings. The silty prograding sand facies can be

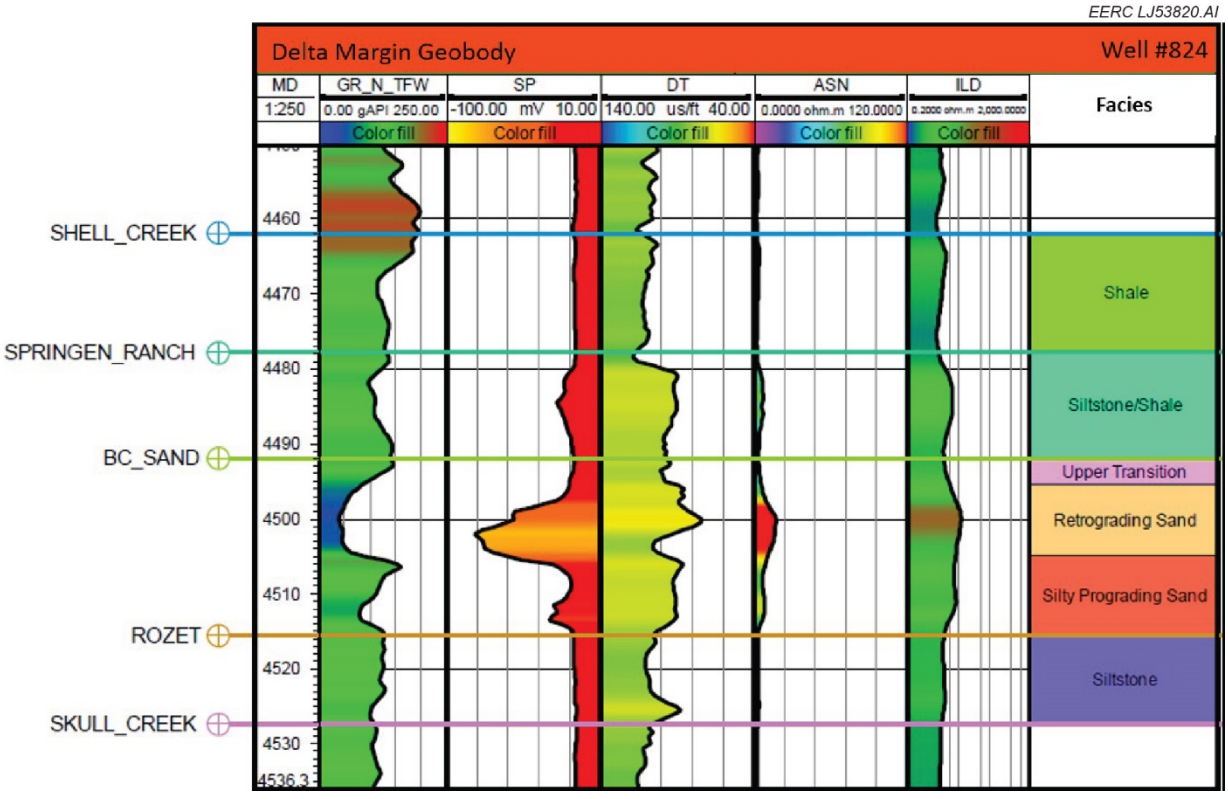

Figure A-2. Type log of the delta margin geobody.

overlain by approximately 1 to 3 feet of a laterally discontinuous mudstone that separates the lower, prograding deposits from the upper, retrograding deposits. The top of the reservoir is marked by a fining upward transition (upper transition facies) into the siltstones and shales above.

Barrier Bar Complex Geobody

Following relative sea level fall and the deposition of the lower, prograding sands, the Western Interior Seaway transgressed from the southwest, creating a barrier bar complex in the southwest part of the field. As noted in Bosshart and others (2015), these barrier bar deposits, in the transgressive, upper Bell Creek Sand interval, give strong indication of a paleoshoreline trending northwest to southeast. As made evident in 3-D seismic data and Bell Creek Sand interval isopach maps (Bosshart and others, 2015), multiple barrier bars were deposited in the southwest part of the field. At the onset of transgression, a barrier bar formed in the central portion of Phase 8. As the sea continued to transgress, additional barrier bars were deposited in Phase 9 and the Phase 1 and 2 areas. Using the trend of the barrier bar features as paleoshoreline indicators, each barrier bar has a shoreline trending northwest to southeast. However, each successive barrier bar feature trends slightly more east-to-west than the previous barrier bar feature. This suggests that shoreline orientation changed slightly during the transgression responsible for barrier bar deposition.

At the base of the reservoir, a relatively sharp transition from the siltstones below are overlain by the lower, laterally continuous, prograding sand. Within the barrier bar complex geobody (Figure A-3), the lower sand is usually overlain by 1 to 3 feet of mudstone, separating the lower sand from the overlying transgressive deposits of the barrier bar. The seaward side of the barrier bar contains relatively thick, clean, bar front deposits that were exposed to a higher degree of wave energy and tidal influence. The landward side of the barrier bar contains back bar deposits that were deposited as finer-grained material was washed over the bar. These back bar deposits are shown on the well log by an increase in gamma ray signature, a decrease in sonic travel time, and a decrease in shallow and deep resistivity.

Lagoon Geobody

Contemporaneous with barrier bar development, lagoons (Figure A-4) formed on the landward side of the bar in restricted, relatively still water, resulting in the deposition of fine-grained material. The boundary of this geobody is easily picked on well logs by an increase in gamma ray response at the top of the reservoir. The fine-grained deposits contained within this geobody show slow sonic velocity, create destructive interference in the seismic data, and consequently appear as very low amplitude features.

Within the lagoon geobody, the base of the reservoir shows a sharp transition from the siltstones below. The lower, prograding sand can be overlain by a mudstone facies which separates it from the upper, retrograding sand. The retrograding sand facies within the lagoon geobody is often relatively thin (<5 feet) and, based on increased gamma ray and decreased resistivity response, does not appear to be as clean as in other geobodies. At the top of the reservoir are fine-grained lagoonal deposits.

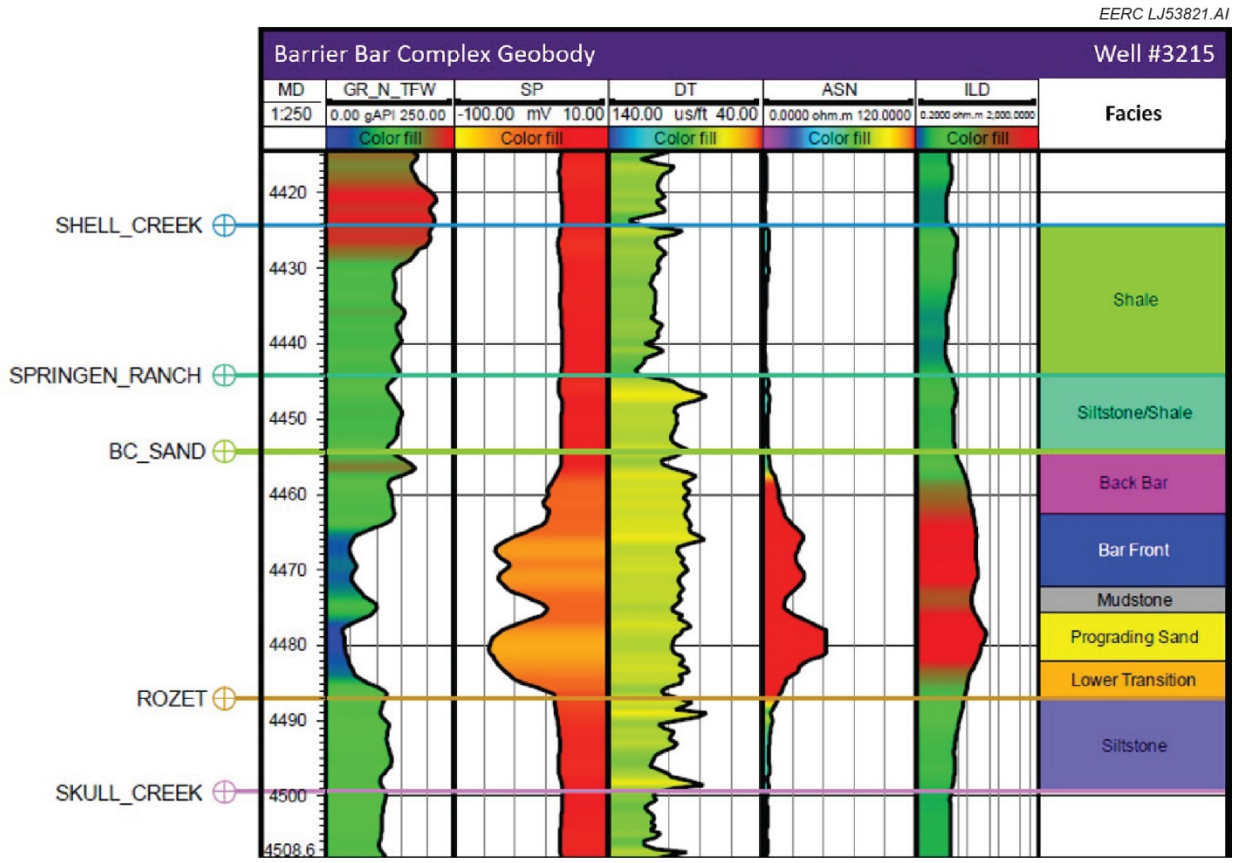

Figure A-3. Type log of the barrier bar complex geobody.

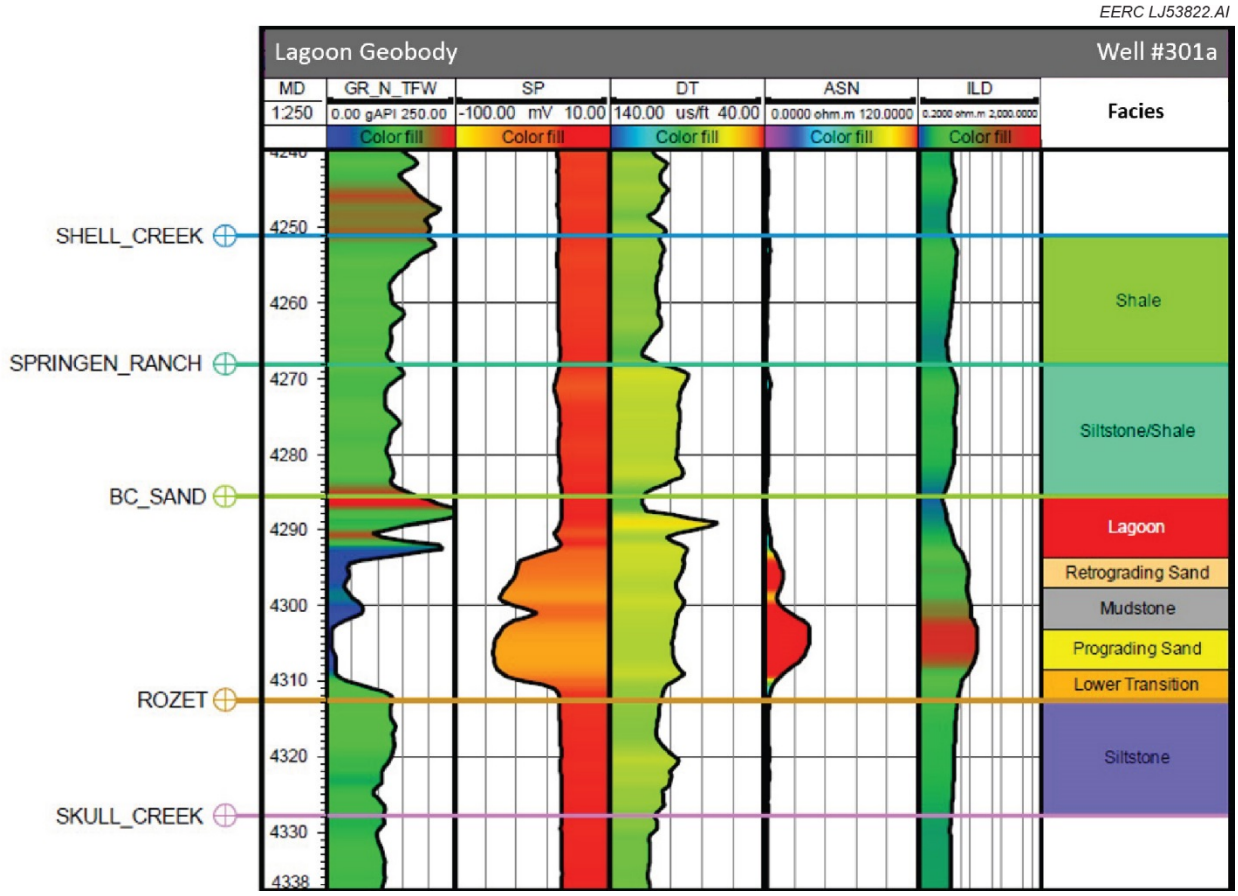

Figure A-4. Type log of the lagoon geobody.

The lagoon geobody can create a permeability barrier to the adjacent geobodies (Bosshart and others, 2015; Jin and others, 2016). This is likely due to the large presence of mudstone between the regressive and transgressive deposits, overall siltier composition of the retrograding sand, and the presence of fine-grained lagoonal deposits.

To the southwest of the lagoon geobody found at the boundaries of Phases 1 and 3 and Phases 2 and 4 (Bosshart and others, 2015; Jin and others, 2016), similar lagoonal material was deposited on the landward side of a previously developed barrier bar (southwest lagoon geobody, Phase 1; Figure A-5). This geobody closely resembles the lagoon geobody discussed above, apart from the transgressive sand deposits appearing on well logs to be more representative of the cleaner bar front deposits found within the barrier bar complex.

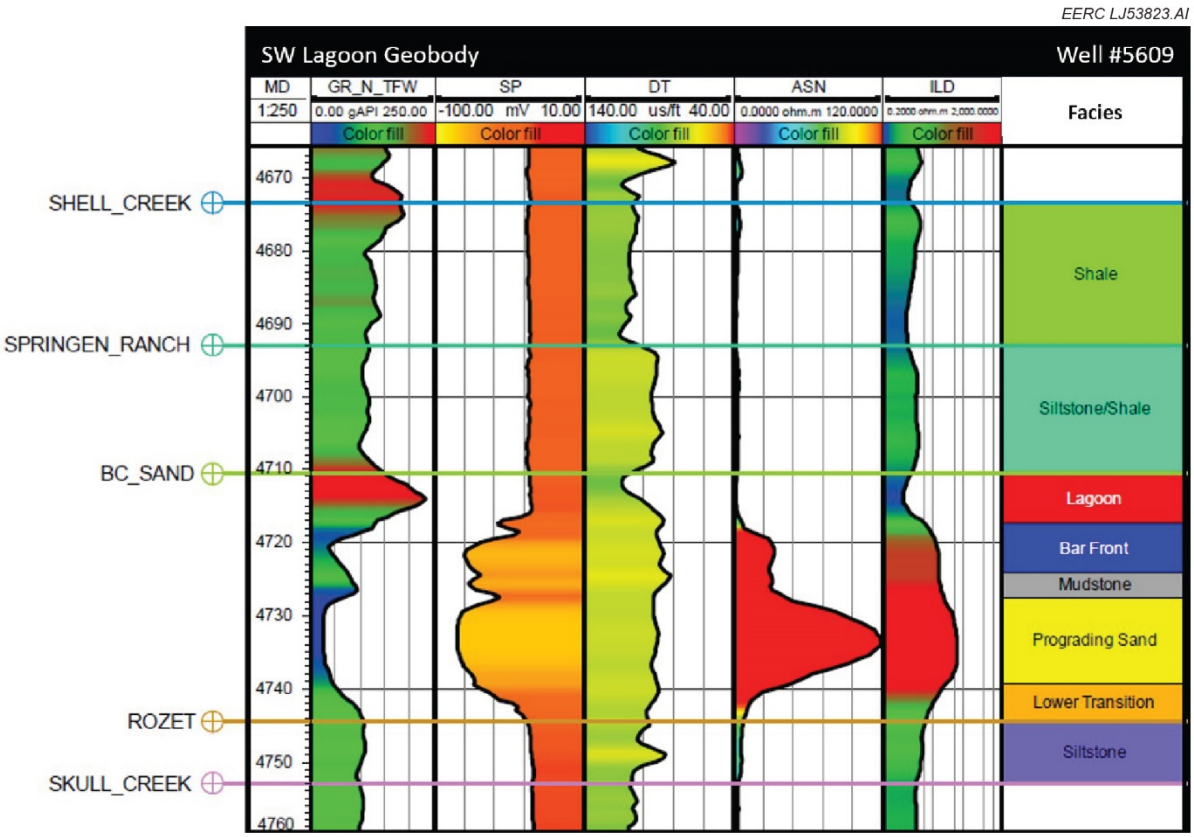

Figure A-5. Type log of the southwest lagoon geobody.

Sheet Sands Geobody

During a brief still stand that was responsible for the deposition of the furthest northeast barrier bar and lagoon deposits in Phases 1 and 2, transgressive sheet sands (Figure A-6) were deposited landward of the barrier bar complex, to the northeast of the lagoonal deposits, by onlapping retrogradion. These transgressive sheet sands of the upper Bell Creek Sand facies are mostly continuous in the northeastern region of the Bell Creek Field and can range in thickness from 5 to 10 feet.

Within the sheet sands geobody, at the base of the reservoir, there is a sharp transition from the siltstones below. The lower, prograding sand can be overlain by a very laterally discontinuous mudstone and can also contain another relatively thin mudstone layer approximately 3 to 5 feet from the top of the prograding sand facies. These mudstones vary in stratigraphic position from the middle of the reservoir to approximately 5 feet from the top of the reservoir. Overlying the mudstone facies (where present) is the retrograding sand facies which transitions into the confining siltstones and shales above.

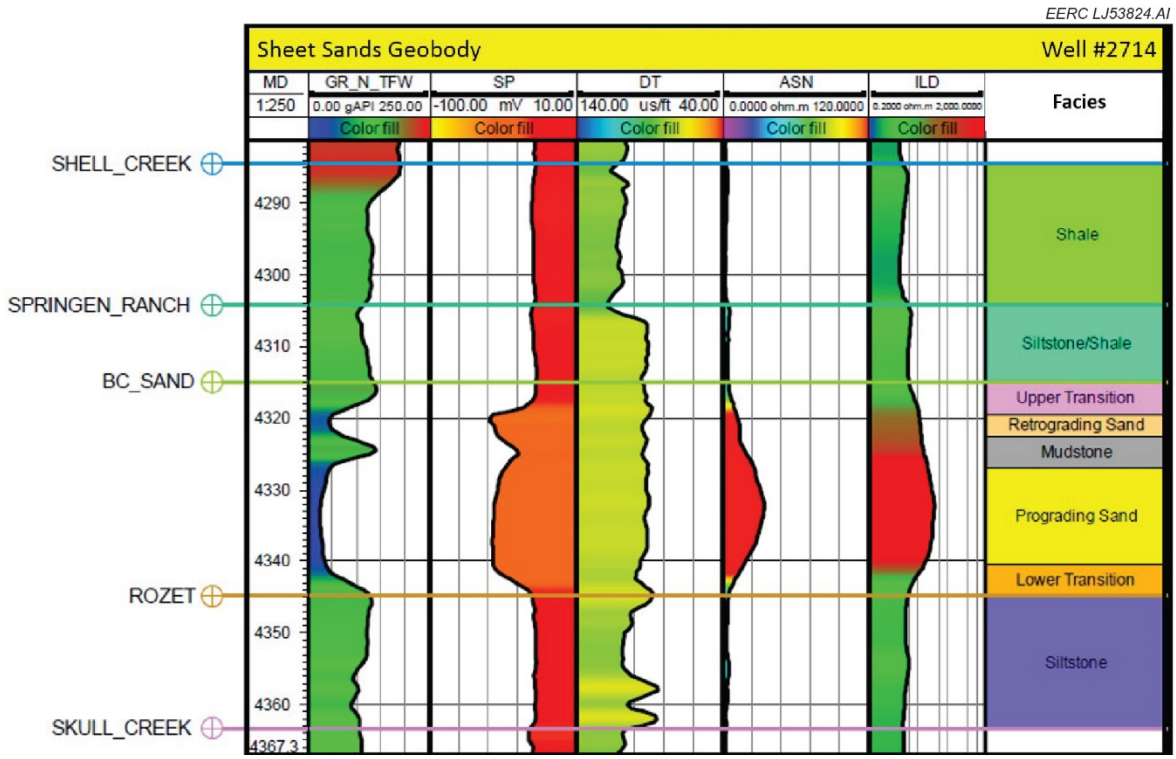

Figure A-6. Type log of the sheet sands geobody.

North/South Trending Channel Geobody

Contemporaneous to the transgressive sheet sands being deposited, a fluvial incised valley (north-south channel geobody, Figure A-7) developed along a path that has created the eastern margin of Phase 3 and the border between the Phase 1 and 2 areas. The fluvial incised valley continues south, forming the eastern margin of Phase 8 where it becomes more difficult to track because of the lack of well control and seismic data. The incision of this channel feature has removed all appreciable thicknesses of reservoir quality sand, leaving behind only a very thin layer of lag deposits. As the sea transgressed, this channel feature was filled with the siltstones and shales of the Springen Ranch Member, creating a lateral permeability barrier to all adjacent geobodies (Farnham and Haddenhorst, 1972; Molnar, 1990; Bosshart and others, 2015; Jin and others, 2016).

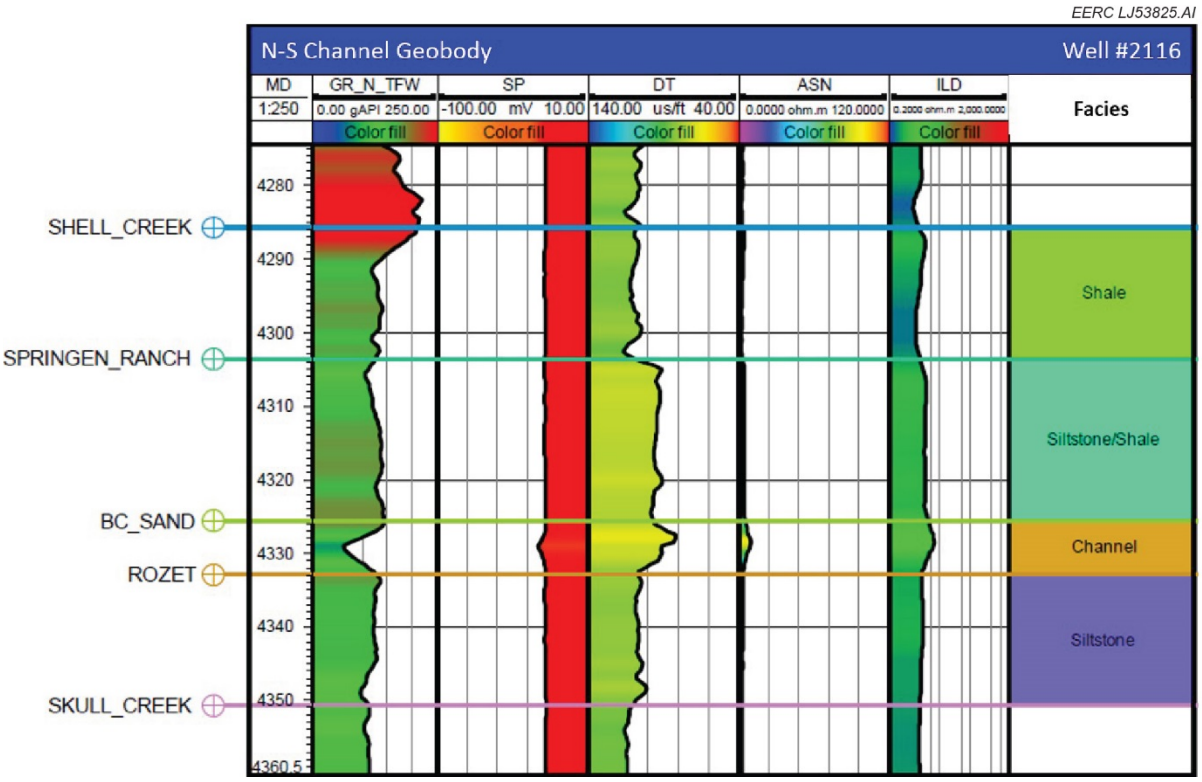

Figure A-7. Type log of the north to south trending channel geobody.

Tidal Channel Geobody

As the sea transgressed, tidal channels formed in the southwest part of the field. These channels developed as the surrounding barrier bar deposits were cut by the ebb and flow of the tidal current. Figure A-1 shows the main tidal channel trending approximately north to south with smaller, dendritic, tributary channels trending approximately parallel with the interpreted depositional dip (northeast to southwest).

Within this geobody, the lower, regressive deposits show similar log response to the surrounding geology but can be much thinner (<5 feet thick). Overlying the regressive deposits, there are one or two distinct sand-to-silt/shale cyclothems (Figure A-8) that can produce coarser-grained sand near the base of each of the cyclothems. Previous studies have speculated that a lateral shift in tidal channels should deposit a distinct sediment package that is analogous to a point-bar sequence (fining-upward sequence) left by a meandering stream channel (Kumar and Sanders, 1974). Here the basal sand grades into finer-grained material and is generally capped by a highly radioactive, low-density shale. In areas where the basal sand of the fining upward sequence is thin and the lower, prograding sand deposits are also thin, it appears from 4-D seismic data that this geobody may be causing a lateral permeability barrier.

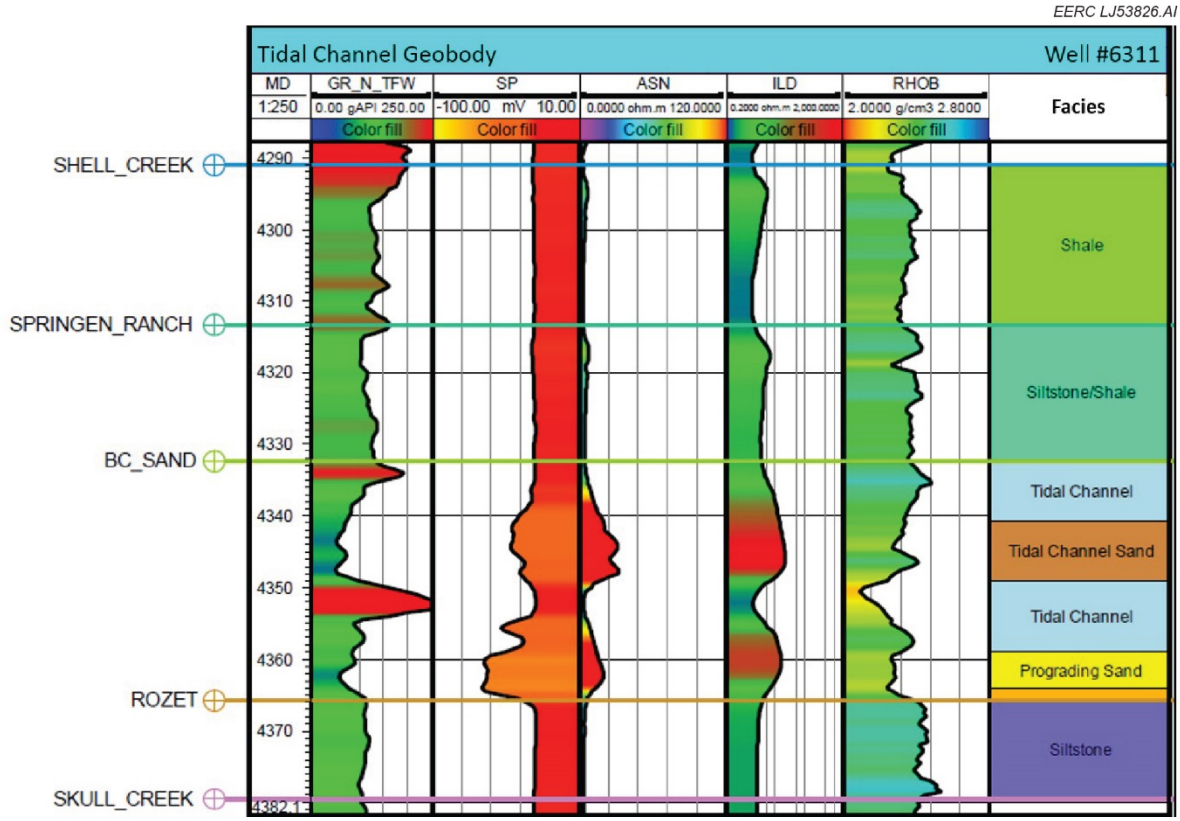

Figure A-8. Type log of the tidal channel geobody.

REFERENCES

Bosshart, N.W., Jin, L., Dotzenrod, N.W., Burnison, S.A., Ge, J., He, J., Burton-Kelly, M.E., Ayash, S.C., Gorecki, C.D., Hamling, J.A., Steadman, E.N., and Harju, J.A., 2015, Bell Creek test site – simulation report: Plains CO_2 Reduction (PCOR) Partnership Phase III Task 9 Deliverable D66 (Update 4) for U.S. Department of Energy National Energy Technology Laboratory Cooperative Agreement No. DE-FC26-05NT42592, EERC Publication—EERC-10-09, Grand Forks, North Dakota, Energy & Environmental Research Center, August.

Farnham, F.E., and Haddenhorst, F.A., 1972, Four and one-half years—discovery to unitized operation of the major, multi-reservoir Bell Creek field, *in* SPE Rocky Mountain Regional Meeting: Society of Petroleum Engineers, January 1.

Jin, L., Bosshart, N.W., Oster, B.S., Hawthorne, S.B., Peterson, K.J., Burton-Kelly, M.E., Feole, I.K., Jiang, T., Pekot, L.J., Peck, W.D., Ayash, S.C., and Gorecki, C.D., 2016, Bell Creek test site – simulation report: Plains CO_2 Reduction (PCOR) Partnership Phase III draft Task 9 Deliverable D66 (Update 5) executive summary for U.S. Department of Energy National Energy Technology Laboratory Cooperative Agreement No. DE-FC26-05NT42592, Grand Forks, North Dakota, Energy & Environmental Research Center, August.

Kumar, N., and Sanders, J.E., 1974, Inlet sequence—a vertical succession of sedimentary structures and textures created by the lateral migration of tidal inlets: Sedimentology, v. 21, no. 4, p. 491–532.

Molnar, P.S., 1990, Geologic reservoir study of the Bell Creek Field, Carter and Powder River Counties, Montana: Midland, Texas, Exxon Company.